2020

Synthesis and reactivity of transition metal complexes supported by oxazolinyl borato ligands and the functionalization of silica surface

Abhranil Biswas
Iowa State University

Synthesis and reactivity of transition metal complexes supported by oxazolinyl borato ligands and the functionalization of silica surface

by

Abhranil Biswas

A dissertation submitted to the graduate faculty

in partial fulfillment of the requirements for the degree of

DOCTOR OF PHILOSOPHY

Major: Organic Chemistry

Program of Study Committee:
Aaron D Sadow, Major Professor
Marek Pruski
Igor I. Slowing
Levi M. Stanley
Wenyu Huang

The student author, whose presentation of the scholarship herein was approved by the program of study committee, is solely responsible for the content of this dissertation. The Graduate College will ensure this dissertation is globally accessible and will not permit alterations after a degree is conferred.

Iowa State University

Ames, Iowa

2020

DEDICATION

To my family and friends

TABLE OF CONTENTS

ACKNOWLEDGMENTS

I deeply appreciate many individuals who have supported and continually encouraged me throughout my Ph.D. life at Iowa State University. Without their time, attention, encouragement, and patience, I would not have been able to see it through.

First, I would like to thank my advisor, Prof. Aaron D. Sadow, for giving me an opportunity to work in his research group under his guidance, with suggestions throughout all my years of graduate school. You have set an example of excellence as a researcher, mentor, instructor and role model. I am also very grateful to Aaron for his scientific advice, knowledge and many insightful discussions and suggestions. His guidance helped me in all the time of research and writing this thesis. I could not have imagined having a better advisor and mentor for my Ph.D. study.

Besides my advisor, I would like to thank all of my POS committee members Prof. Marek Pruski, Prof. Igor Slowing, Prof. Keith Woo, Prof. Levi Stanley, and Prof. Wenyu Huang for their valuable support, advice and time.

I would also like to thank my past and present group members in the Sadow group: Especially, I am grateful to Songchen for training me to use glovebox and Regina for teaching me how to use the Schlenk line and for her assistance in helping perform my first and successful reaction in the Sadow Group. My fellow travelers, Smita and Kasuni who have been on this journey with me and provided much needed encouragement and support. I thank undergraduate student Jacob Brunton, who had conducted research with me in Sadow lab.

I would like to thank Dr. Igor I. Slowing and the Slowing group members for our collaboration for the synthesis of functionalized silica material. Thanks to Dr. Takeshi Kobayashi and Dr. Zhuoran Wang for their valuable time spent collecting solid-state NMR data for my samples for our collaboration project. I also thank Prof. Marek Pruski for our collaboration.

I thank all the chemical instrument services, glass shop, Chemistry Stores and machine shop in the chemistry department. Thanks to Dr. Shu Xu and Dr. Sarah Cady for helping me with several NMR experiments for my research. I would like to thank the Ames Laboratory and Iowa State University for funding and support of my research.

I'd also like to thank my Ames family who have been there for me during my ups and downs. I'd like to thank Naresh, Abhishek, Raghu, Aleem, Avipsa, Kalyan, Subhrajit, Judhajit and Saheli for their friendships that helped me immensely in this journey. Special thanks to Ishani for her support and help over that last to two years. It would have been impossible to survive without you.

Lastly, I'd like to thank my family (Maa, Baba and brother, Mriganka) for their enormous support and encouragement throughout my life and my graduate school journey. It would not have been possible without you guys.

ABSTRACT

Oxidative addition of a nonpolar Si–H bond to the rhodium dicarbonyl $\{PhB(Ox^{Me2})_2Im^{Mes}\}Rh(CO)_2$ is an unusual example of this kind, as it is accompanied by thermal dissociation of CO. The reaction was found to be reversible, and kinetic measurements model the approach to equilibrium. The oxidative addition is first-order in both $\{PhB(Ox^{Me2})_2Im^{Mes}\}Rh(CO)_2$ and primary silane, with rate constants for oxidative addition of $PhSiH_3$ and $PhSiD_3$ revealing $k_H/k_D \sim 1$. The reaction is significantly inhibited in the presence of externally added CO. The reverse reaction, reductive elimination of Si–H from $\{PhB(Ox^{Me2})_2Im^{Mes}\}RhH(SiH_2R)CO$, also follows a second-order rate law (first-order in both the reactants). Equilibrium constants are measured from equilibrium concentrations of all the species in the reaction mixture over a 30° C temperature range, provide $\Delta H° = -5.5 \pm 0.2$ kcal/mol and $\Delta S° = -16 \pm 1$ cal·mol^{-1}K^{-1}. Activation entropy for both forward and reverse reaction are negative ($\Delta S^{‡} = -26 \pm 3$ cal·mol^{-1}·K^{-1} and $\Delta S^{‡} = -10 \pm 3$ cal·mol^{-1}·K^{-1} respectively), suggests a highly associated transition state containing $\{PhB(Ox^{Me2})_2Im^{Mes}\}Rh(CO)_2$ and $RSiH_3$.

$RuHCl(PPh_3)_3$ catalyzes cross-dehydrogenative coupling between various silane-alcohol and silane-amine pairs in homogeneous reaction conditions under ambient temperature and low catalyst loading (1 mol%). Catalysis was further extended to functionalize silica material. Surface silanol (≡SiOH) successfully reacts with hydrosilanes (primary, secondary and tertiary) in presence of a catalytic amount of $RuHCl(PPh_3)_3$ under ambient reaction conditions to produce $\equiv SiOSiR_3$. Infra-red spectroscopy measurement confirmed the disappearance of isolated ≡SiOH (3747 cm^{-1}) and the appearance of new Si–H stretching in the case of primary and secondary hydrosilanes. The amount of silane grafted was measured via elemental analysis, ^{29}Si DPMAS

study and titration of the remaining ≡SiOH with $Mg(CH_2Ph)_2(O_2C_4H_8)_2$. Newly created Si–H bonds further successfully reacted with N–H of amines in the presence of $RuHCl(PPh_3)_3$ to produce unique ≡Si–O–Si–N– bonded functionalized materials. Notably, the synthesis of surface silazanes from silica material was successfully achieved in a one-pot technique.

A new ruthenium tris(oxazolinyl)borato complex is synthesized by stirring $TlTo^M$ and $Ru(NCPh)_4Cl_2$ at 80° C. Resulting complex shows a C_s symmetric geometry around the ruthenium center. Further, the ruthenium complex efficiently catalyzes cycloisomerization of diethyl diallylmalonate to produce *exo*-methylenecyclopentane isomer selectively. A significant solvent effect was observed as the only cycloisomerization occurred in protic solvent (*i*PrOH) and a side product resulting from olefin isomerization was found in CH_2Cl_2. In addition, a range of different 1,6-heptadienes with different functional groups was tested to successfully produce cycloisomerization products in high yield.

CHAPTER 1. INTRODUCTION

General Introduction

A specific class of chemical compounds containing both metal and organic moieties with at least one bonding interaction between them are called organometallic compounds. Even though the first organometallic compound was synthesized in 1760,[1] world had to wait for another 70 years to get its first structurally recognized organometallic compound made by W.C Zeiss in 1827. Later, at the beginning of the 20th century, starting with Grignard several organometallic reagents were developed that have been highly useful in organic synthesis since then. In addition, organometallic compounds have been known to effectively catalyze reactions in both homogeneous and heterogeneous conditions. Historically, the word '*catalyst*' was synonymous with heterogeneously catalyzed reactions as opposed to the literal definition. Later, since the mid 20th-century, homogeneous catalysis has been established and has been a useful tool in catalytic organic transformations.

One of the most studied catalytically active class of organometallic compounds is transition metal complexes. Over the last few decades, transition metal catalysis has been well developed and is nowadays applied in both bulk and fine chemical industries. One of earliest examples of transition metal catalysis was reported by Fujii *et. al*. where catalytic hydrogenation was achieved by a palladium-catalyst.[2] Since then hundreds of different transition metal-based catalytic systems have been developed: metathesis reaction catalyzed by metal alkylidene compounds,[3,4] palladium catalyzed cross-coupling reactions,[5,6] asymmetric hydrogenation reactions,[7-9] etc.

The above-mentioned transition metal-based catalytic systems provide excellent advantages over heterogeneous catalysis in terms of tunability. Small or massive changes made to the coordinating ligand affect catalytic activity in small or moderate amounts. Ligands with

different donor atoms such as N, O, P and C have been studied and developed over the years to achieve a higher level of fine-tuning in reactivity as well as high selectivity. For example, rhodium complexes with simple phosphine ligand (triphenylphosphine) were successful in the hydrogenation of olefins,[10] whereas a modified chiral phosphine ligand (BINAP) based rhodium complex reduced olefins and carbonyls with high enantioselectivity.[11]

Modification of ligand systems has been a keen subject of interest due to its effects on the reactivity of the metal centers. Depending upon the particular reaction of interest, the electronic and steric properties of the ligand system can be modified to increase the reactivity. One of the most useful reactions in organometallic chemistry is oxidative addition.[12] The process involves breaking of a σ-bond (preferably a less polar and strong bond like H–H, C–H, Si–H, etc.)

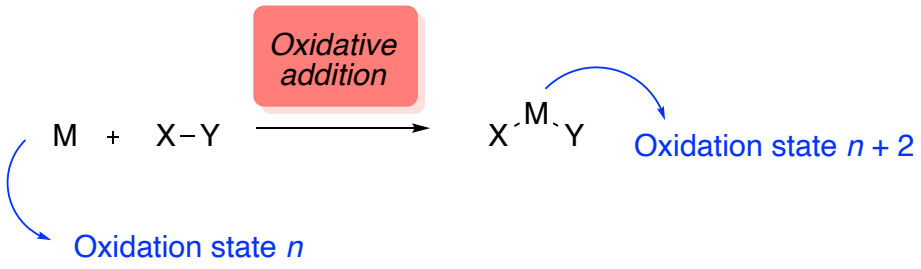

Figure 1-1. General oxidative addition reaction.

along with increasing the oxidation state of the metal center by +2 (Figure 1-1). Oxidative addition has been established as a key step in several transition metal-catalyzed reactions. For example, the oxidative addition of Si–H was found to be a key-step in hydrosilylation and silane dehydrogenative coupling reactions.[13] Similarly, H–H bond cleavage is enrooted within different hydrogenation reactions. Reactivity of any metal towards oxidative addition reaction can be directly corelated to the electronic configuration and electronic density of the corresponding metal center. Metal centers with high electron density and low coordination number tend to undergo

oxidative addition more frequently. In addition, an important way to tune the electron density of the active metal center is by introducing different donor atoms as the coordinating ligand system.

Nitrogen donor-based ligand system has been widely studied due to its strong donating ability as well as powerful coordinating capabilities. Initially, coordinating organic molecules like amines as found to be effective. For example, rich literature could be found based on pyridine coordinated transition metal chemistry. Strong σ-donation as well as π-accepting abilities favors strong coordination bonds between pyridine and transition metals. Further, bipyridines and pyrrole-based ligands were developed to synthesize metal complexes and to study their catalytic activities. Later, Trofimenko designed the first generation of tris(pyrazolyl)borato ligands (Tp) as well as its metal complexes involving Mo, Fe and W.[14] Presence of three strongly donating pyrazole rings elevates the catalytic activities. Mantovani *et. al*. reported a highly efficient catalytic polymerization of ethylene in the presence of Tp-palladium complexes.[15] Also, Graham reported an efficient C–H activation with a tris(pyrazolyl)borato rhodium compound. However, unsymmetrically substituted Tp derivatives (like 5-mesitylpyrazolyl) are susceptible to isomerization processes, giving a mixture of Tp complexes (3- and 5- substituted tris(pyrazolyl)borato). In addition, ligand decomposition (in zirconium-based Tp complexes) through B–N cleavage hinders possible utility in catalysis. A possible alternate of these ligand systems was thought to be achieved by changing the individual pyrazolyl rings with a different heterocycle.

Oxazoline and its derivatives have been widely used over the years as a coordinating ligand unit in various substituted bis-oxazoline based ligands. Further, a range of bis-oxazoline ligands

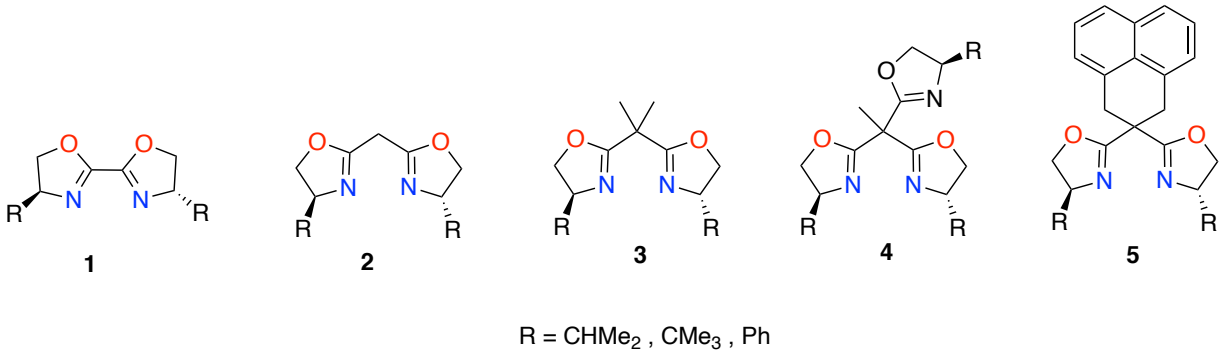

Figure 1-2. Evolution of bis-oxazoline ligands.

was reported having various substitution on methylene (–CH_2–) backbone. Also, metal complexes with various chiral bis-oxazolines are widely used as chiral catalyst to achieve high enantioselectivity (Figure 1-2). For example, Nishiyama was able to improve iron-catalyzed asymmetric hydrosilylation by introducing bulky substituents on the oxazoline rings.[16] To avail the advantages of excellent reactivity of oxazoline rings and to avoid decomposition mechanisms faced by Tp ligand, an analogue of the ligand was synthesized where the pyrazolyl rings were replaced by three oxazoline rings to produce anionic tris(oxazolinyl)borato ligand.[17]

Metal complexes of tris(oxazolinyl)borato ligand with metals like rhodium, iridium, and magnesium were found to be active catalysts for C–H bond activation and intramolecular hydroamination.[18, 19] Also, chiral versions of the ligand were synthesized with ^{i}Pr and ^{t}Bu substitutions on the oxazoline rings.[20] In addition, metal complexes (magnesium, calcium, and zinc)[21,22] of chiral tris(oxazolinyl)borato ligands are also catalytically active species. In order to further tune the electronic properties of the oxazolinyl(borato)ligand system, one of the oxazoline rings was replaced by an imidazole ring with a B–N bonding connectivity, producing a neutral ligand. Upon deprotonation followed by salt metathesis reaction, rhodium and iridium complexes

of the ligand containing a imidazole C–Metal bond were synthesized. Further, these complexes were successfully able to undergo oxidative addition of Si–H bond under thermal conditions which was a unique reactivity compared to its analogues (Tp and To^M).[23]

Also, ruthenium complexes of tris(pyrazolyl)borato ligand and its derivatives were synthesized by Trofimenko et al in form of ruthenium hydrido compounds.[14] Later, a comparative study of reactivities was done between cyclopentadienyl ruthenium complexes and tri(pyrazolyl)borato ruthenium complexes. The study found Cp coordinated ruthenium carbyne complexes to stabilize Ru(II) metal center at a higher extent than the Tp system.[24] Although, ruthenium complexes of various Tp derived ligands had catalytic activities, in a lot of cases these complexes failed to show any significant reactivities. Therefore, it is of great interest to see if the presence of an oxazoline ring in the supporting ligand system makes any difference.

Applications of different homogeneous catalytic systems can be also applied to functionalize solid materials such as silica. Modified silica with the functionalized surface has great importance in analytical chemistry, pharmaceutical industry and semiconductor industry.[25] While common methods to synthesize these functionalized materials are efficient, most of them involve harsh reaction conditions (high temperature and strong basic conditions) and highly sensitive precursors. Also, these pathways produce chemically hazardous side products. Therefore, a new efficient and atom economic pathway is necessary.

This thesis contributes to the synthesis and characterization of a range of rhodium hydrido silyl complex supported by a bis(oxazolinyl)imidazole borato ligand via oxidative addition of Si–H bond to a Rh(I) metal center. A detailed study was done to understand different parameters of the reaction and to propose a plausible mechanism. In addition, a new ruthenium tris(oxazolinyl)borato ligand was synthesized and its catalytic activity was measured in

cycloisomerization of 1,6-dienes. Finally, a novel catalytic method was developed to synthesize functionalized silica material using hydrosilanes to obtain chemically active Si–H bonds on the surface.

Thesis organization

This thesis contains five chapters that include published manuscript as well as unpublished work. Chapter 1 provides a general introduction to organometallic chemistry, development of coordinating ligand systems, transition metal complexes and their application in different homogeneous and heterogeneous catalysis for different transformations. Chapter 2 presents work from a published manuscript whereas chapters 3 and 4 consists of unpublished works. Chapter 5 provides general conclusions.

Chapter 2 consists of a published manuscript in Inorganic Chemistry titled "CO displacement in an Oxidative Addition of Primary Silane to Rhodium(I)". This work focuses on a detailed kinetic study of an unusual oxidative addition of the Si–H bond, accompanied by CO dissociation under thermal conditions. The X-ray structures were solved by Dr. Ellern.

Chapters 3 and 4 consists of unpublished works and thus are manuscripts in progress. In chapter 3 a new catalytic route has been developed to efficiently functionalize silica materials using various silanes. This work also extends the route to synthesize new surface silazane materials. The silica material (SBA-15) used in the study was provided by Younghun Park. Solid-state NMR was measured by Dr. Zhuoran Wang and Dr. Takeshi Kobayashi.

Chapter 4 describes the synthesis and characterization of a new ruthenium tris(oxazolnyl)borato complex and demonstrates its catalytic activity in selective cycloisomerization of 1,6-dienes. Several dienes required for the study were synthesized by Jacob Brunton.

References

1. Rothenberg, G., *Catalysis: Concepts and Green Applications*. 2017.

2. Akabori, S.; Sakurai, S.; Izumi, Y.; Fujii, Y., An Asymmetric Catalyst. *Nature* **1956,** *178* (4528), 323-324.

3. Grubbs, R. H.; Trnka, T. M., Ruthenium-Catalyzed Olefin Metathesis. *Ruthenium in Organic Synthesis* **2004**, 153-177.

4. Trnka, T. M.; Grubbs, R. H., The Development of L2X2RuCHR Olefin Metathesis Catalysts: An Organometallic Success Story. *Accounts of Chemical Research* **2001,** *34* (1), 18-29.

5. Miyaura, N.; Suzuki, A., Palladium-Catalyzed Cross-Coupling Reactions of Organoboron Compounds. *Chemical Reviews* **1995,** *95* (7), 2457-2483.

6. Nicolaou, K. C.; Bulger, P. G.; Sarlah, D., Palladium-Catalyzed Cross-Coupling Reactions in Total Synthesis. *Angewandte Chemie International Edition* **2005,** *44* (29), 4442-4489.

7. Noyori, R.; Ohkuma, T.; Kitamura, M.; Takaya, H.; Sayo, N.; Kumobayashi, H.; Akutagawa, S., Asymmetric hydrogenation of .beta.-keto carboxylic esters. A practical, purely chemical access to .beta.-hydroxy esters in high enantiomeric purity. *Journal of the American Chemical Society* **1987,** *109* (19), 5856-5858.

8. Nishi, T.; Kitamura, M.; Ohkuma, T.; Noyori, R., Synthesis of statine and its analogues by homogeneous asymmetric hydrogenation. *Tetrahedron Letters* **1988,** *29* (48), 6327-6330.

9. Kitamura, M.; Ohkuma, T.; Takaya, H.; Noyori, R., A practical asymmetric synthesis of carnitine. *Tetrahedron Letters* **1988,** *29* (13), 1555-1556.

10. Hallman, P. S.; Evans, D.; Osborn, J. A.; Wilkinson, G., Selective catalytic homogeneous hydrogenation of terminal olefins using tris(triphenylphosphine)hydridochlororuthenium(II); hydrogen transfer in exchange and isomerisation reactions of olefins. *Chemical Communications (London)* **1967,** (7), 305-306.

11. Noyori, R.; Takaya, H., BINAP: an efficient chiral element for asymmetric catalysis. *Accounts of Chemical Research* **1990,** *23* (10), 345-350.

12. Labinger, J. A., Tutorial on Oxidative Addition. *Organometallics* **2015,** *34* (20), 4784-4795.

13. Zhao, L.; Nakatani, N.; Sunada, Y.; Nagashima, H.; Hasegawa, J.-y., Theoretical Study on the Rhodium-Catalyzed Hydrosilylation of C═C and C═O Double Bonds with Tertiary Silane. *The Journal of Organic Chemistry* **2019,** *84* (13), 8552-8561.

14. Moreno, B.; Sabo-Etienne, S.; Chaudret, B.; Rodriguez-Fernandez, A.; Jalon, F.; Trofimenko, S., Synthesis and Reactivity of a Stable Hydrido Bis(dihydrogen) Derivative in a Nitrogen Donor Environment LRuH(H2)2 (L = HB(3,5-Me2-pz), HB(3-iPr,4-Br-pz)). *Journal of the American Chemical Society* **1994,** *116* (6), 2635-2636.

15. Santi, R.; Romano, A. M.; Sommazzi, A.; Grande, M.; Bianchini, C.; Mantovani, G., Catalytic polymerisation of ethylene with tris(pyrazolyl)borate complexes of late transition metals. *Journal of Molecular Catalysis A: Chemical* **2005,** *229* (1), 191-197.

16. Inagaki, T.; Phong, L. T.; Furuta, A.; Ito, J.-i.; Nishiyama, H., Iron- and Cobalt-Catalyzed Asymmetric Hydrosilylation of Ketones and Enones with Bis(oxazolinylphenyl)amine Ligands. *Chemistry – A European Journal* **2010,** *16* (10), 3090-3096.

17. Dunne, J. F.; Su, J.; Ellern, A.; Sadow, A. D., A New Scorpionate Ligand: Tris(4,4-dimethyl-2-oxazolinyl)borate and Its Zirconium(IV) Complexes. *Organometallics* **2008,** *27* (11), 2399-2401.

18. Dunne, J. F.; Fulton, D. B.; Ellern, A.; Sadow, A. D., Concerted C−N and C−H Bond Formation in a Magnesium-Catalyzed Hydroamination. *Journal of the American Chemical Society* **2010,** *132* (50), 17680-17683.

19. Ho, H.-A.; Manna, K.; Sadow, A. D., Acceptorless Photocatalytic Dehydrogenation for Alcohol Decarbonylation and Imine Synthesis. *Angewandte Chemie International Edition* **2012,** *51* (34), 8607-8610.

20. Baird, B.; Pawlikowski, A. V.; Su, J.; Wiench, J. W.; Pruski, M.; Sadow, A. D., Easily Prepared Chiral Scorpionates: Tris(2-oxazolinyl)boratoiridium(I) Compounds and Their Interactions with MeOTf. *Inorganic Chemistry* **2008,** *47* (22), 10208-10210.

21. Xu, S.; Magoon, Y.; Reinig, R. R.; Schmidt, B. M.; Ellern, A.; Sadow, A. D., Organometallic Complexes of Bulky, Optically Active, C3-Symmetric Tris(4S-isopropyl-5,5-dimethyl-2-oxazolinyl)phenylborate (ToP*). *Organometallics* **2015,** *34* (14), 3508-3519.

22. Neal, S. R.; Ellern, A.; Sadow, A. D., Optically active, bulky tris(oxazolinyl)borato magnesium and calcium compounds for asymmetric hydroamination/cyclization. *Journal of Organometallic Chemistry* **2011,** *696* (1), 228-234.

23. Xu, S.; Manna, K.; Ellern, A.; Sadow, A. D., Mixed N-Heterocyclic Carbene–Bis(oxazolinyl)borato Rhodium and Iridium Complexes in Photochemical and Thermal Oxidative Addition Reactions. *Organometallics* **2014,** *33* (23), 6840-6860.

24. Beach, N. J.; Williamson, A. E.; Spivak, G. J., A comparison of Cp*- and Tp-ruthenium carbyne complexes prepared via site selective electrophilic addition to neutral ruthenium vinylidenes. *Journal of Organometallic Chemistry* **2005,** *690* (21), 4640-4647.

25. Moitra, N.; Ichii, S.; Kamei, T.; Kanamori, K.; Zhu, Y.; Takeda, K.; Nakanishi, K.; Shimada, T., Surface Functionalization of Silica by Si–H Activation of Hydrosilanes. *Journal of the American Chemical Society* **2014,** *136* (33), 11570-11573.

CHAPTER 2. CO DISPLACEMENT IN AN OXIDATIVE ADDITION OF PRIMARY SILANES TO RHODIUM(I)

Modified from a manuscript published in *Inorganic Chemistry* **2019**, 58, *6*, 3815-3824

Abhranil Biswas, Arkady Ellern, Aaron D. Sadow

Abstract

The rhodium dicarbonyl {PhB(Ox^{Me2})$_2$Im^{Mes}}Rh(CO)$_2$ (**1**) and primary silanes react by oxidative addition of a nonpolar Si–H bond, uniquely, in concert with a thermal dissociation of CO. These reactions are reversible, and kinetic measurements model the approach to equilibrium. Thus, **1** and RSiH$_3$ react by oxidative addition at room temperature in the dark, even in CO-saturated solutions. The oxidative addition reaction is first-order in both **1** and RSiH$_3$, with rate constants for oxidative addition of PhSiH$_3$ and PhSiD$_3$ revealing k_H/k_D ~1. The reverse reaction, reductive elimination of Si–H from {PhB(Ox^{Me2})$_2$Im^{Mes}}RhH(SiH$_2$R)CO (**2**), also follows a second-order rate law (first-order in both [**2**] and [CO]). The equilibrium concentrations, determined over a 30 °C temperature range, provide $\Delta H°$ = –5.5 ± 0.2 kcal/mol and $\Delta S°$ = –16 ± 1 cal·mol^{-1}K^{-1}. The rate laws and activation parameters for oxidative addition ($\Delta H^‡$ = 11 ± 1 kcal·mol^{-1} and $\Delta S^‡$ = –26 ± 3 cal·mol^{-1}·K^{-1}) and reductive elimination ($\Delta H^‡$ = 17 ± 1 kcal·mol^{-1} and $\Delta S^‡$ = –10 ± 3 cal·mol^{-1}K^{-1}), particularly the negative activation entropy for both forward and reverse reactions, suggest a highly associated transition state containing {PhB(Ox^{Me2})$_2$Im^{Mes}}Rh(CO)$_2$ and RSiH$_3$. Comparison of a series of primary silanes reveals that oxidative addition of arylsilanes is ca. 5× faster than alkylsilanes, whereas reductive elimination of Rh–Si/Rh–H from alkylsilyl and arylsilyl rhodium(III) occur with similar rate constants. Thus, the equilibrium constant K_e for oxidative addition of arylsilanes is greater than 1, whereas reductive elimination is favored for alkylsilanes.

Introduction

Oxidative addition of nonpolar bonds (H–H, C–H, Si–H) to low valent rhodium and iridium metal complexes has been widely studied because this elementary step, and the resulting metal hydride, alkyl, or silyl species, are invoked in many catalytic reactions including hydroformylation,[2, 3] hydrosilylation,[4-8] and silane dehydrocoupling.[9-15] Such transformations often involve carbon monoxide directly or metal carbonyls as catalysts, but catalytic steps involving CO dissociation are notably absent in their proposed mechanistic cycles. Instead, open coordination sites for oxidative addition are generated via product-forming reductive elimination steps, and CO itself is frequently an inhibitor in many catalytic reactions. For example, the catalytic hydroformylation of 1-hexene with $HRhCO(PPh_3)_3$, a reaction in which CO is consumed as a reactant, shows inverse dependence of the rate on CO pressure.[2, 3, 16-18] This inhibition is attributed to the strong binding affinity and π-acidity of CO to the rhodium(I) species, which decreases its reactivity.

The strong coordination of CO must also be overcome to affect catalytic decarbonylation chemistry. Stoichiometric reactions of aldehydes and esters typically provide metal-carbonyl compounds (e.g., Ni–CO or Rh–CO),[19-22] and in fact, oxidative addition of polar C–O bonds of esters to Ni(0) is reversible upon addition of CO.[22] Catalytic processes involving decarbonylation of aldehydes,[23, 24] ketones,[25, 26] acyl halides,[21, 27-30] esters,[31-35] and amides[36] require high temperatures or photochemical activation. Key intermediates proposed in catalytic cycles for these decarbonylative transformation include oxidized metal carbonyls, resulting from de-insertion of metal acyl species, and low valent, electron-rich metal sites that react with polar substrates by oxidative addition. Likely, low valent metal carbonyl compounds are present, considering that low valent metal species readily bind CO, formed from the decarbonylation process. Ancillary ligand

effects in these systems are, as expected, significant. For example, bidentate trialkyl phosphines give decarbonylation in palladium-catalyzed reductions of acyl fluorides and in nickel-catalyzed cross-coupling of aryl esters and aryl boronate esters, while monodentate trialkyl phosphines give carbonyl-containing products.[29, 35] However, the diarylphosphine PPh_2Me is more effective than the trialkylphosphine PCy_3 in acylfluoride cross-coupling, as well as in the rate of decarbonylation to nickel(0)-carbonyl.[21] Likely, trends are obscured by changing reaction conditions (reagents, temperatures, reactants) and complex, multistep mechanisms.

In contrast, the active species are well defined in photochemically activated oxidative additions of nonpolar bonds. Photolytic dissociation of CO is a prerequisite for reactions of $Cp^*Rh(CO)_2$ or $Tp^*Rh(CO)_2$ ($Cp^* = C_5Me_5$; Tp* = tris(3,5-dimethyl-1-pyrazolyl)borate) with C–H or Si–H bonds.[37-44] For example, $Tp^*Rh(CO)_2$ and Et_3SiH react under photochemical conditions to give $Tp^*RhH(SiEt_3)CO$ and CO (Figure 1).[45] A sequence of photolytic CO dissociation followed by C–H cleavage is invoked here, as well as in rhodium- or iridium-catalyzed carbonylations of benzene, which occur under continuous irradiation.[46, 47] Detailed time-resolved spectroscopic and computational studies of the mechanism of C–H and Si–H bond activation by CpRh(CO),[48-51] Cp*Rh(CO),[41, 42, 52] TpRh(CO),[53] Tp*Rh(CO),[50, 54-57] and Tp*Rh(CNR),[44] formed via photolytic ligand dissociation, reveal details and lifetimes of the activation process. Interestingly, bidentate and tridentate coordination of pyrazolylborate ligands modulate the electronic structure of rhodium to affect C–H bond oxidative cleavage.

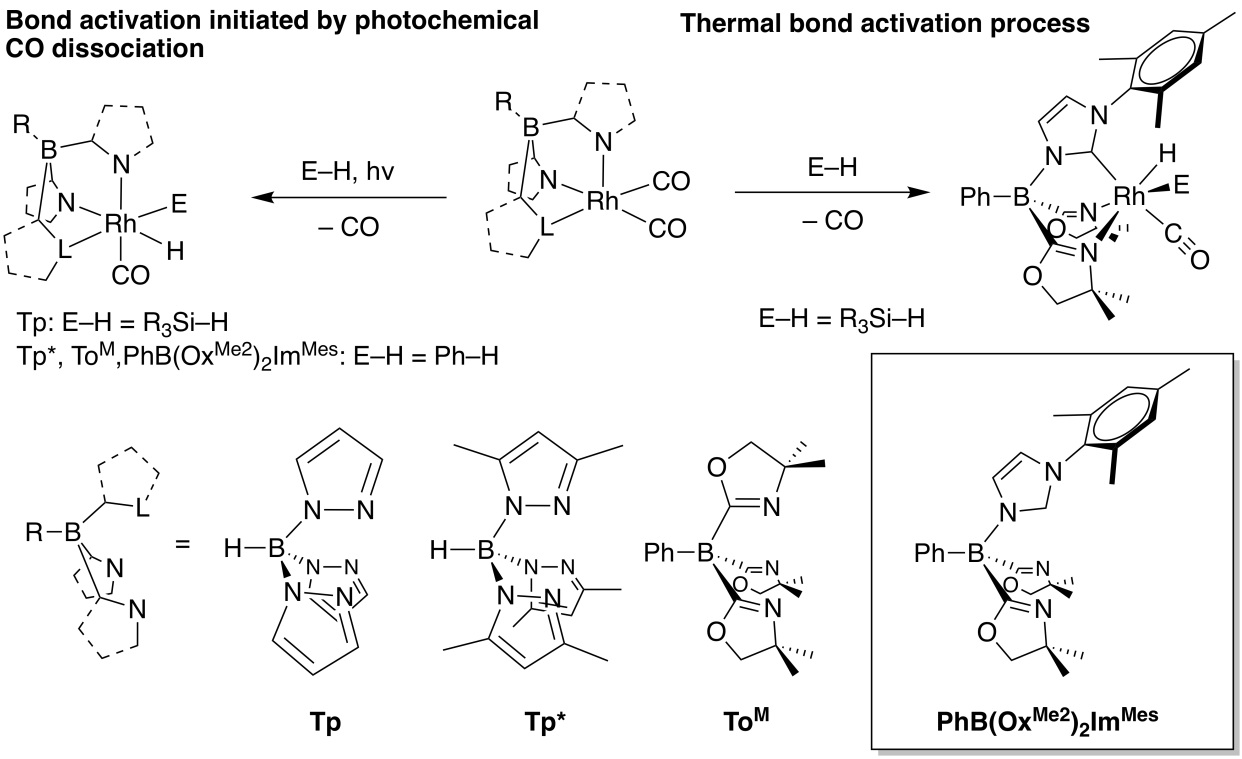

Figure 2-1. Photochemical and thermal pathways for oxidative addition of C–H and Si–H bonds to rhodium(I).

In addition, competition studies of the bond activation processes mediated by the low-coordinate photo-dissociated species provide valuable insight into relative Rh–C bond dissociation energies.[58, 59] Experimental studies probing the overall thermodynamic constraints imposed by the rhodium(I) dicarbonyl species, however, are limited. A recent study compares {κ^3-Tp}Rh(CNR)(η^2-RNCNR) and hydrocarbons to the (photochemically-mediated) oxidative addition products and the carbodiimide byproduct, showing the process is unfavorable by ca. 13-15 kcal/mol (for cyclopentane).[44]

Although these studies elucidate the influence of ancillary ligands on C–H bond oxidative addition steps, new strategies are needed to affect both the bond activation and CO displacement for development of new, thermal conversions. Oxidized or electron-poor metal centers that are poorly π-back-donating disfavor CO binding; however, such species are also less likely to react by

oxidative addition. Alternatively, a nucleophilic metal complex could interact with the E–H bond, and σ-coordination might reduce the π-back donating ability to CO and promote its dissociation. This idea implies, perhaps counter-intuitively, that a strongly σ-donating ligand that generates an electron-rich, nucleophilic rhodium species, even when coordinated by CO, could be reactive in thermal oxidative additions and accelerate the dissociation of CO.

The trend in electron-donating ability for tridentate, *fac*-coordinating ligands in rhodium dicarbonyl compounds, based on CO stretching frequencies, is Tp < Tp* < To^M (To^M = tris(4,4-dimethyl-2-oxazolinyl)phenylborate, Figure 1);[60, 61] however $To^MRh(CO)_2$ does not appear to react with hydrocarbons or silanes under thermal conditions, and we concluded that the tris(oxazolinyl)borate ligand was not sufficiently electron donating to test this idea. In order to further increase the electron-donating ability of the *fac*-coordinating ligand system, we replaced one oxazoline in To^M with a *N*-heterocyclic carbene to give the bis(oxazolinyl)(NHC)borate ligand $PhB(Ox^{Me2})_2Im^{Mes}$ (Figure 1, Ox^{Me2} = 4,4-dimethyl-2-oxazolinyl, Im^{Mes} = 1-(2,4,6-trimethylphenyl)imidazole).[62] In fact, $PhSiH_3$ and $\{PhB(Ox^{Me2})_2Im^{Mes}\}Rh(CO)_2$ (**1**) react in the dark to give $\{PhB(Ox^{Me2})_2Im^{Mes}\}RhH(SiH_2Ph)CO$ (**2a**) and CO.[63]

Tp*$Rh(CO)_2$, $To^MRh(CO)_2$, and **1** all contain monoanionic, multidentate ligands, which coordinate either in fluxional bidentate or tridentate modes. The carbonyls are photochemical labile, and all undergo C–H bond oxidative addition upon photolysis. Both four- and five-coordinate ground state structures contain photolabile carbonyl ligands and access states needed for C–H bond activation. For example, the related square-planar tris(pyrazolyl)borate rhodium di(isocyanide) mediate C–H bond activation upon photolysis,[64] giving six-coordinate rhodium(III) products.

Here we study the kinetic and thermodynamic features of Si–H bond oxidative addition to **1** and Rh–Si/Rh–H bond reductive elimination from **2a**. These investigations of the thermal processes provide contrast with photochemical-promoted Si–H and C–H bond oxidative additions.[37-40]

Results and Discussion

Synthesis of rhodium silyl compounds

The reaction of **1** and 3 equiv. of $PhSiH_3$ gives **2a** over 18 h in benzene at room temperature in 94% isolated yield.[63] Similarly, **1** and primary alkylsilanes (R = C_6H_{13}, $C_{12}H_{25}$) or arylsilanes $RSiH_3$ (R = *p*-MeC_6H_4, *p*-$MeOC_6H_4$) react to give {PhB(Ox^{Me2})$_2$$Im^{Mes}$}RhH($SiH_2R$)CO (R = C_6H_{13} (**2b**), $C_{12}H_{25}$ (**2c**), *p*-MeC_6H_4 (**2d**), *p*-$MeOC_6H_4$ (**2e**); Scheme 1). The reactions of alkylsilanes and **1** are slower than the corresponding reactions of arylsilanes under equivalent reaction conditions. For example, the reaction of **1** and hexylsilane (10 equiv) in benzene requires 1 d at room temperature to form **2b** quantitatively, whereas the reaction of $PhSiH_3$ under equivalent conditions affords **2a** quantitatively after 6 h.

Scheme 2-1. Thermal reactions of {PhB(Ox^{Me2})$_2$$Im^{Mes}$}Rh(CO)$_2$ (1) and primary silanes.

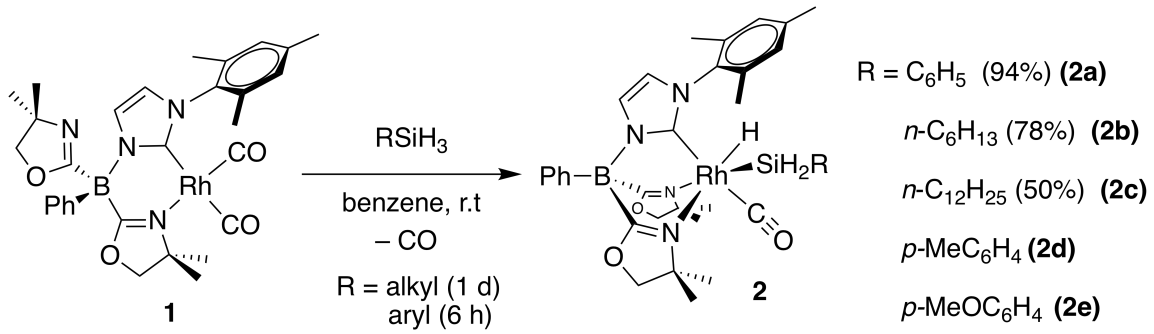

In the solid-state structure of **2d** (Figure 2), the Rh1–N1 interatomic distance *trans* to the hydride is shorter by 0.05 Å than that of the oxazoline *trans* to the silyl group. The CO ligand and

the NHC group are *trans*. This configuration and the shorter Rh–N interatomic distance *trans* to H are consistent across the solid-state structures of **2a**[63] and **2b** (see Figure S17). In contrast, the reaction of $\{PhB(Ox^{Me2})_2Im^{Mes}\}Ir(CO)_2$ and benzene, which occurs under photochemical conditions, results in CO *trans* to an oxazoline and the phenyl *trans* to the NHC.[63] These distinct configurations of the two products suggest distinct mechanisms for thermal and photochemical processes.

Contamination by residual arylsilane hinders reproducible isolation of **2d** and **2e** as pure species. These compounds are instead spectroscopically characterized in the presence of $RSiH_3$. Attempts to increase the rate of oxidative addition of *p*-$MeC_6H_4SiH_3$ or *p*-$MeOC_6H_4SiH_3$, by performing the reactions at 60 °C, result in organosilane rearrangement to give (*p*-$MeC_6H_4)_2SiH_2$ or (*p*-$MeOC_6H_4)_2SiH_2$. Neither triarylsilanes nor the SiH_4 product expected from redistribution were detected by NMR spectroscopy or GC-MS; however, additional SiH and RhH signals suggest that these species, if formed, might have undergone further reaction. The majority of redistribution products appear in the latter stages of the reaction after almost all of **1** is consumed, suggesting that **2d** and **2e** are involved in redistribution. This process is faster for *p*-$MeOC_6H_4SiH_3$ than for *p*-$MeC_6H_4SiH_3$, and only the oxidative addition pathway is observed at room temperature. Interestingly, neither $PhSiH_3$ nor the alkylsilanes appear to undergo rearrangement to Ph_2SiH_2 or R_2SiH_2 at 60 °C, instead giving the desired rhodium silyl hydride product selectively.

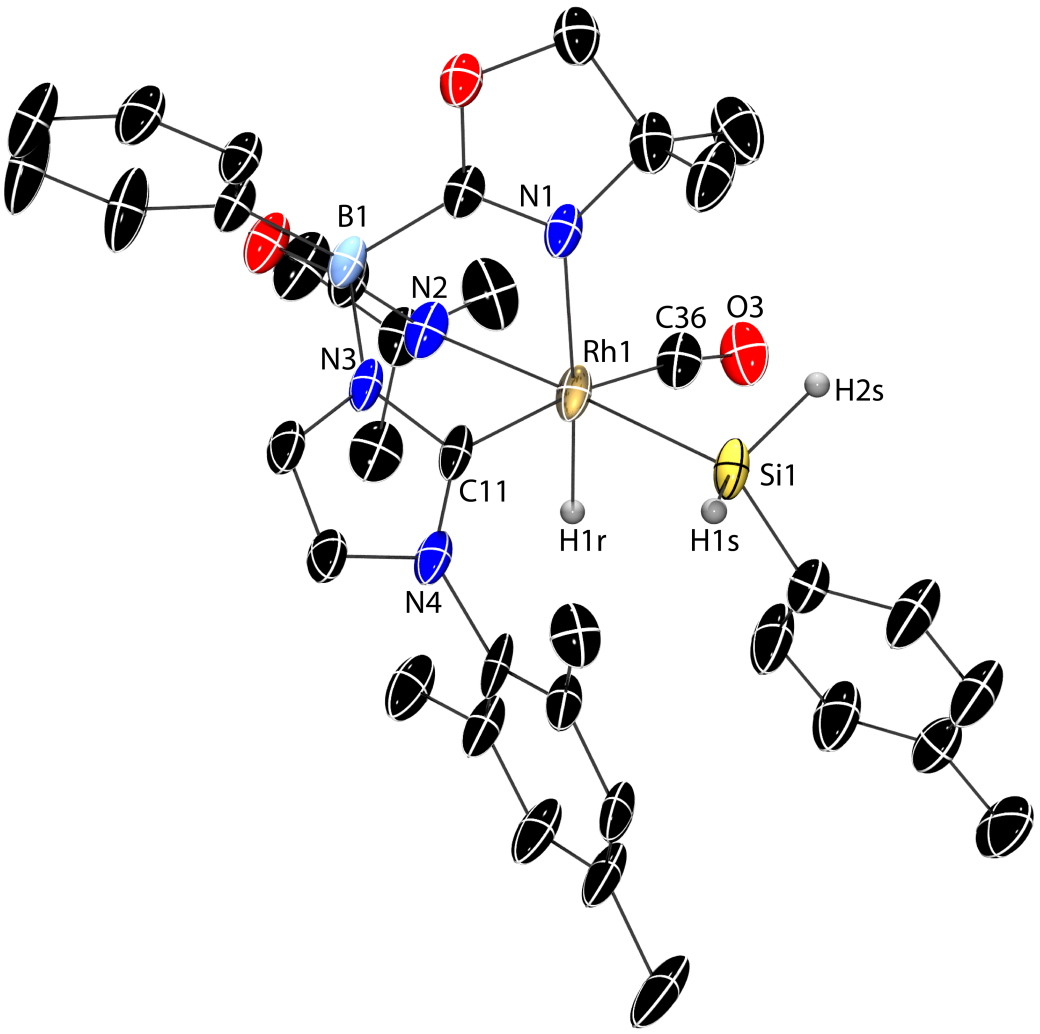

Figure 2-2. Thermal ellipsoid plot of {PhB(Ox^{Me2})$_2$Im^{Mes}}RhH(SiH$_2$C$_6$H$_4$Me)CO (2d) at 35% probability. One of two positions of the disordered tolyl group is shown. H atoms bonded to Rh1 and Si1 were located objectively in the difference Fourier map, refined isotropically, and were included in the representation. Selected interatomic distances (Å): Rh1–Si1, 2.336(1); Rh1–C11, 2.070(4); Rh1–C36, 1.888(3); Rh1–H1r, 1.58(4); Rh1–N1, 2.197(3); Rh1–N2, 2.242(3).

Kinetic studies of oxidative addition. Initial kinetic studies, in which concentrations of PhSiH$_3$ and **1** were monitored by ^{1}H NMR spectroscopy, suggested first order dependence of reaction rate on [PhSiH$_3$] and [**1**]. Unfortunately, reactions in sealed NMR tubes do not result in complete conversion, even with excess PhSiH$_3$. For example, 15 equiv. of PhSiH$_3$ (140 mM) vs **1** (9 mM) gives 92% yield of **2a** after 70 min. (**1**:**2a** = 0.085:1). Although the concentration of **1** follows an

exponential decay over the first few half-lives, the composition of the reaction mixture changes more slowly in the later stages of the reaction than expected for a pseudo-first order reaction. Moreover, a plot of pseudo-first order rate constants vs [$PhSiH_3$] provides only a rough trend, and considerable scatter suggests additional factors influenced the rate.

A unimolecular decomposition via reductive elimination of the rhodium silyl hydride is ruled out because compound **2a** is isolable and persistent in pure form. In contrast, the reaction of **2a** and CO (1 atm) results in ca. 30% conversion to **1** and $PhSiH_3$ at room temperature after 1 d. This observation indicates that oxidative addition of Si–H to **1** is reversible in the presence of CO. Thus, the reproducible kinetics for reactions of **1** might be complicated by slow and variable loss of CO into the NMR tube headspace. An addition complication to studying the CO-promoted reductive elimination from **2a** involves the formation of $PhB(Ox^{Me2})_2Im^{Mes}H$ as a side product under conditions with higher CO pressures or high temperature (>60 °C). In contrast, the reaction produces only **1** and $PhSiH_3$ under ambient conditions. Apparently, the number of CO ligands coordinated to Rh increases at higher pressure, leading to reductive elimination of C–H rather than Si–H. Note that the harsher conditions required for C–H reductive elimination indicate that the Si–H reductive elimination is kinetically preferred.

Solution-phase IR and UV-vis spectroscopies were tested as alternative methods to study the reactions, with the latter method appearing to be most promising. UV-vis spectroscopy provides the advantage that the disappearance of **1** could be monitored in sealed cuvettes with negligible headspaces, eliminating one of the issues associated with the NMR kinetic studies. In a first experiment, spectra (250 – 700 nm) of a reaction mixture of **1** and $PhSiH_3$ were acquired at 15 min. intervals over the reaction (Figure 3). The signal at 385.5 nm systematically decreased, while the center of the band at 301 nm blue-shifted and appeared non-Gaussian in the final

spectrum of **2a**. Subsequent kinetic experiments monitored the absorption at 385.5 nm. While photolysis of **1** in benzene affords the cyclometalated $\{\kappa^4\text{-PhB(Ox}^{Me2})_2\text{Im}^{Mes'}\text{CH}_2\}\text{RhH(CO)}$,[63] that process was not observed in the spectrophotometer. That is, a series of UV-vis spectra for **1** acquired under otherwise equivalent conditions, but without $PhSiH_3$, were all identical to the first spectrum.

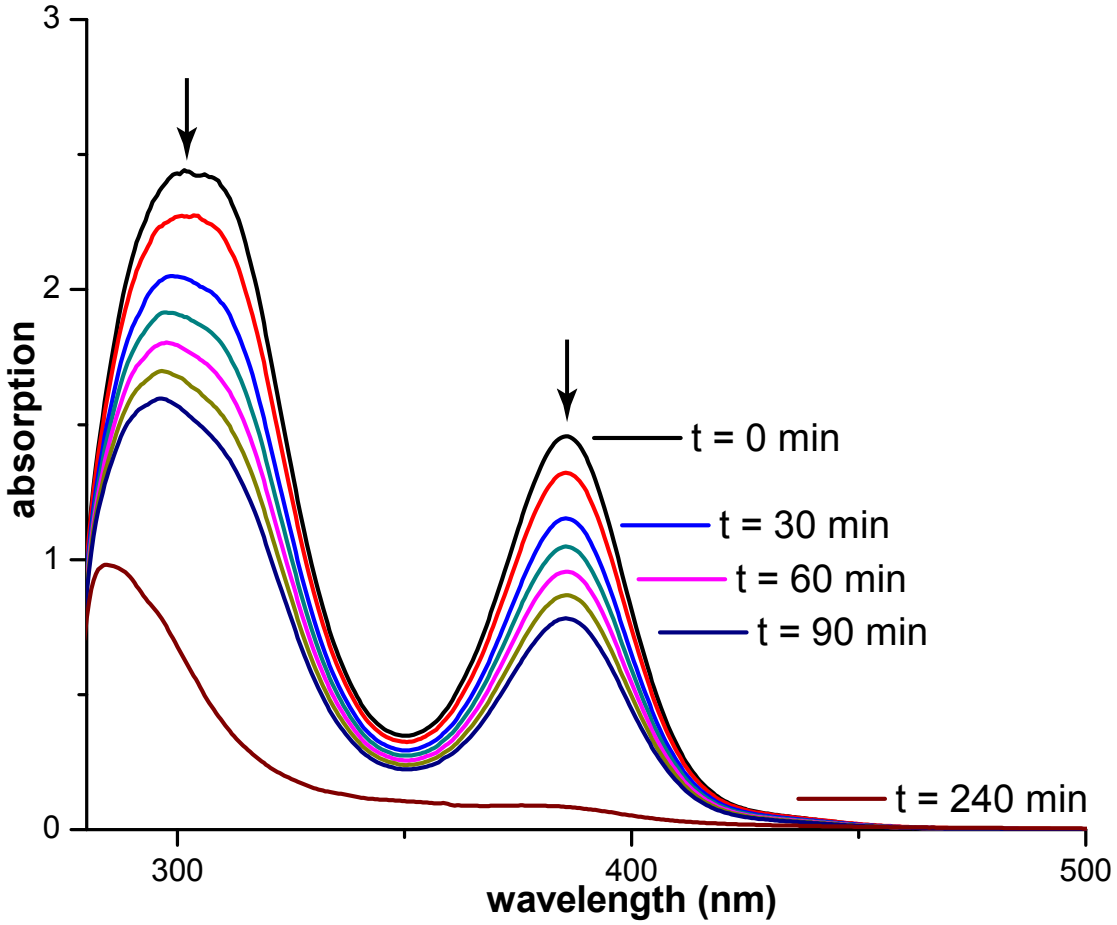

Figure 2-3. Electronic absorption spectra of 1 ($[1]_{ini} = 2.7 \times 10^{-4}$ M) during its reaction with $PhSiH_3$ (1.1×10^{-3} M) at room temperature in benzene acquired at 15 min. intervals. $PhSiH_3$ does not absorb at >250 nm.

Under conditions employing large excesses of $PhSiH_3$ (ranging from 25 to 140 equiv vs **1**) for reactions monitored at 296 K, plots of [**1**] vs time followed an exponential decay for 3 half-lives, indicating first-order dependence on [**1**]. Under the conditions of these experiments, particularly

with dilute [**1**] and high [$PhSiH_3$], the final concentration of **1** approach zero (Figure 4). Non-linear least-squares fits were superior for experiments with higher concentrations of $PhSiH_3$, while some deviation was observed at longer reaction times with lower $[PhSiH_3]_{ini}$. This observation suggests that at longer reaction times, [CO] increases and the reverse reaction contributes to the observed rate constant (see below for studies with non-zero initial CO concentrations). Thus, the initial portion of the time course approximates the reaction as irreversible under conditions where $[CO]_{ini}$ = 0 M.

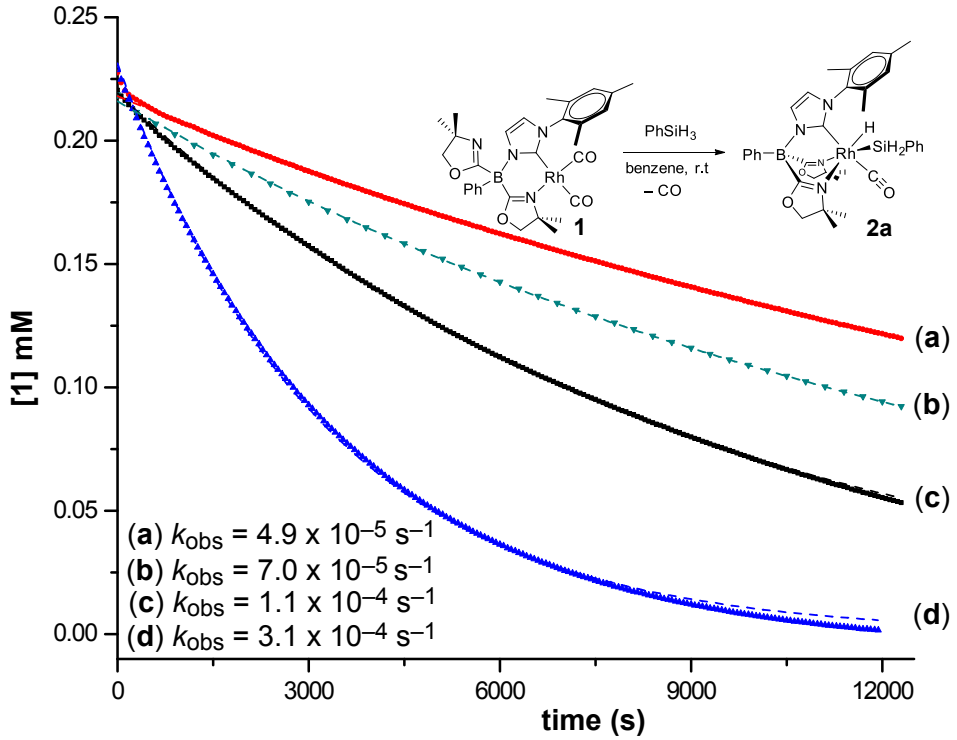

Figure 2-4. Plots of [1] vs time in its reaction with $PhSiH_3$ in benzene at 296 K, monitored at 385.5 nm, with [$PhSiH_3$] = (a) 4.0, (b) 5.8, (c) 10.0, and (d) 25.5 mM. Non-linear least-squares regression fits to exponential decay curves $[Rh]_t = [Rh]_{ini}\, e^{-kt}$ confirm first-order dependence.

Plots of k_{obs} vs [$PhSiH_3$] provide a forward rate constant k^{app} (given in Figure S21, constrained by the approximation that the rate of reductive elimination is negligible at $[CO]_{ini}$ = 0 M). In addition, a plot of log[$PhSiH_3$] vs. log(k_{obs}) is linear with a slope of 1 (Figure S23),

indicating first-order dependence on phenylsilane concentration. The rate constants were measured over five temperatures (up to 322 K, Table 1) to determine the activation parameters of $\Delta H^{\ddagger H\text{-}app}$ = 11 ± 1 kcal·mol^{-1} and $\Delta S^{\ddagger H\text{-}app}$ = –30 ± 3 cal·mol^{-1}K^{-1} (Figure S24). For comparison, the $\Delta S^{\ddagger}$ for oxidative addition of Si–H bonds in tertiary silanes to photolytically-generated $CpMn(CO)_2$ range from –6 to –10 cal·mol^{-1}K^{-1};[65] however, these values vary considerably with the cyclopentadiene-based ancillary ligand.[66]

The same approach provides the second-order rate constants for the addition of **1** and $PhSiD_3$. The activation parameters, determined from an Eyring plot, are $\Delta H^{\ddagger D\text{-}app}$ = 10 ± 1 kcal·mol^{-1} and $\Delta S^{\ddagger D\text{-}app}$ = –34 ± 4 cal·mol^{-1}K^{-1}. These two sets of values are experimentally indistinguishable, thus $k_H/k_D \sim 1$ for all accessible reaction temperatures.

Table 2-1. Second-order rate constants k1app from pseudo-first order kinetic studies

Temp. (K)	k_H^{app} M^{-1}s^{-1} (×10^{-2})	k_D^{app} M^{-1}s^{-1} (×10^{-2})	k_H/k_D
296.0	1.1 ± 0.1	1.1 [b]	1
297.4	1.2 [b]	1.3 ± 0.1	0.9
308.3	2.0 ± 0.1	2.3 ± 0.1	0.9 ± 0.1
312.3	2.9 ± 0.3	3.0 ± 0.1	1.0 ± 0.1
316.8	3.7 ± 0.1	3.7 ± 0.3	0.99 ± 0.02
322.3	4.2 ± 0.4	5.0 ± 0.1	0.9 ± 0.1

[a] k_1^{app} is the rate constant for the forward, oxidative addition of $PhSiH_3$ to **1**, determined at $[CO]_{ini}$ = 0. [b] Calculated from corresponding Eyring plots.

Equilibrium kinetic studies. Additional evidence that oxidative addition of phenylsilane is reversible in the presence of CO comes from the reaction with $PhSiH_3$ in a CO-saturated benzene solution (7.3 mM).[67] Under otherwise equivalent conditions, the reaction shows an apparent decrease in rate and final concentration (Figure 5).

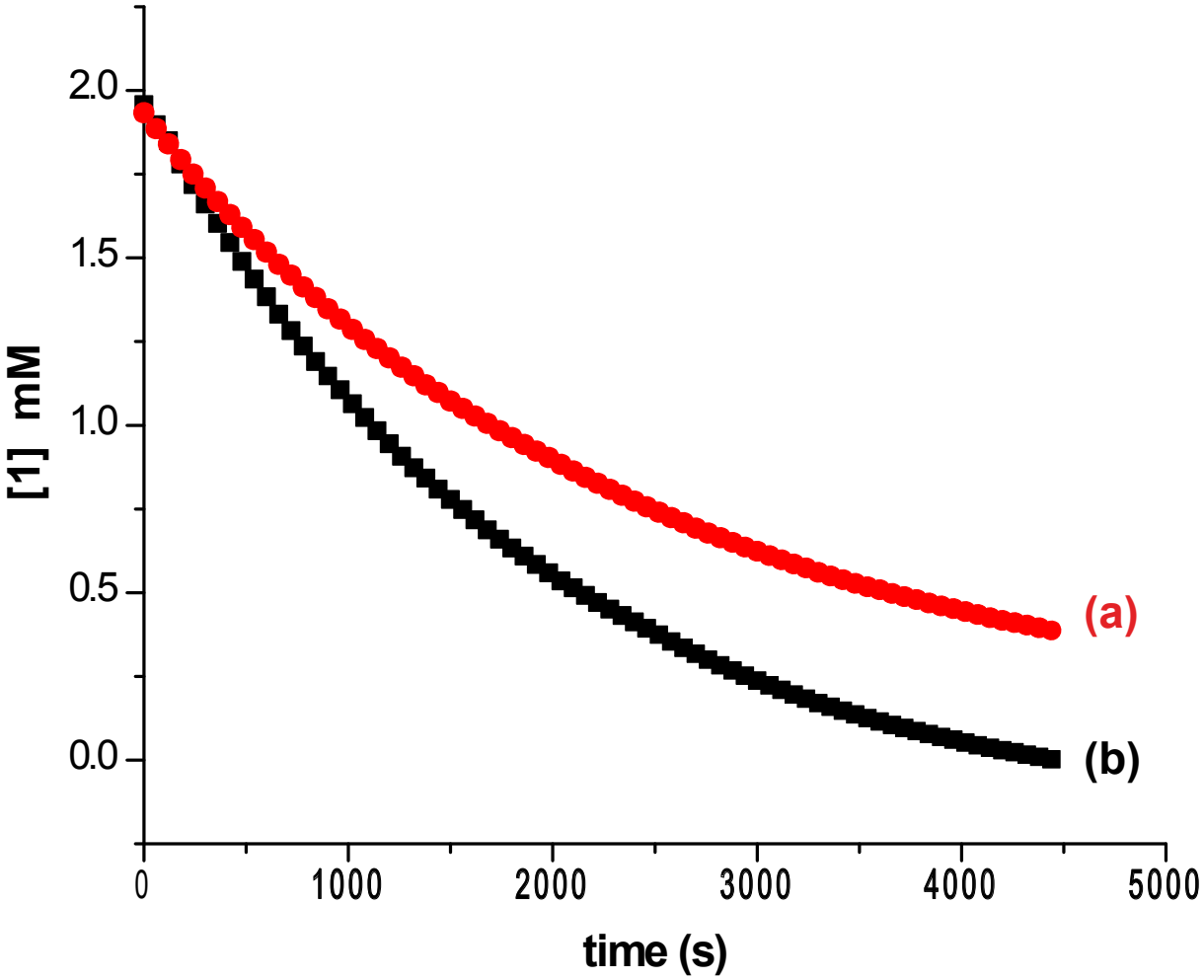

Figure 2-5. Plots of [1] vs time for its reaction with $PhSiH_3$ (260 equiv.) in benzene saturated with (a) ca. 35 equiv. of CO and (b) without CO at 296 K, measured by UV-Vis spectroscopy at 385.5 nm. $[CO]_{ini}$ = 7.3 mM, $[1]_{ini}$ = 0.2 mM, $[PhSiH_3]_{ini}$ = 52.0 mM.

Clearly, mechanisms of both forward and reverse reactions are of interest. Note that the observed rate constant for a first-order reaction that approaches equilibrium is the sum of forward and reverse rate constants ($k_e = k_1 + k_{-1}$).[68] In the present case, the observed pseudo-first order rate constant (k_e) is equal to the sum of the oxidative addition and reduction elimination rate constants, multiplied by concentrations of flooded reagents, respectively (eq. 1).

$$k_e = k_1[\mathrm{PhSiH_3}]_e[\mathbf{1}]_e\left\{\frac{1}{[\mathrm{PhSiH_3}]_e}+\frac{1}{[\mathbf{1}]_e}\right\}+k_{-1}[\mathrm{CO}]_e[\mathbf{2a}]_e\left\{\frac{1}{[\mathrm{CO}]_e}+\frac{1}{[\mathbf{2a}]_e}\right\} \quad (1)$$

Under high [$PhSiH_3$] and [CO] (flooding conditions), eq. 1 simplifies into eq. 2, where the observed rate constant k_e depends on both $[PhSiH_3]_e$ and $[CO]_e$ (which are defined by their initial concentrations). The forward and reverse rate constants are related to the equilibrium constant $K_e = k_1/k_{-1}$.

$$k_e = k_1[\mathrm{PhSiH_3}]_e + k_{-1}[\mathrm{CO}]_e = k_1[\mathrm{PhSiH_3}]_e + \frac{k_1}{K_e}[\mathrm{CO}]_e \quad (2)$$

To determine K_e, **1** (0.1 – 0.2 mM) and $PhSiH_3$ (4.8 – 8 mM) are allowed to react in CO-saturated benzene solution (7.3 mM) over 1 – 2 days, until the absorbance of **1** becomes static and corresponds to $[\mathbf{1}]_e$. $[\mathbf{2a}]_e$ is determined from the relationship $[\mathbf{1}]_{ini} - [\mathbf{1}]_e$. At 297 K, K_e is 2.8 ± 0.2 (from four independent measurements). The equilibrium constants were measured from 297 to 328 K, and a van't Hoff plot provides $\Delta H° = -5.5 \pm 0.2$ kcal/mol and $\Delta S° = -16 \pm 1$ cal·mol^{-1}K^{-1} (Figure S25). The van't Hoff plot also allows the prediction of equilibrium constants for other temperatures.

The concentration of **1** vs. time was measured under conditions of excess $PhSiH_3$ and excess CO (7.3 mM). Non-linear least-squares regression of the data to eq. 3 provides k_e.

$$[\mathbf{1}] = [\mathbf{1}]_e + ([\mathbf{1}]_o - [\mathbf{1}]_e)e^{-k_e t} \quad (3)$$

The rate constants k_1 and k_{-1} are determined using eq. 2 and k_e, K_e, $[PhSiH_3]_e$ and $[CO]_e$ values. Measurements of [**1**] vs time from 297 to 328 K (four measurements at each temperature) provide temperature-dependent k_e (Table S1). These rate constants, combined with the K_e from the van't Hoff analysis, provide k_1 and k_{-1} over a 30 K range. Here, we note that the rate constant $k_1^{296\ K}$ of 0.01 M^{-1}s^{-1} (calculated from the Eyring equation and van't Hoff plot for a reaction occurring at 296 K) and the k^{app} (0.012 M^{-1}s^{-1}, measured experimentally at 296 K) are in good agreement, indicating that the approximate rate constant at $[CO]_{ini} = 0$ is a reasonable estimate of k_1.

The activation parameters for oxidative addition of **1** and $PhSiH_3$ are determined to be $\Delta H^{\ddagger}$ = 11 ± 1 kcal·mol^{-1} and $\Delta S^{\ddagger}$ = –26 ± 3 cal·mol^{-1}·K^{-1} (Figure 6). These values are also equivalent to those determined above from rate constants k_{app} in which the reverse direction is neglected at $[CO]_{ini}$ = 0. The second-order rate law indicates that **1** and $PhSiH_3$ are present in that transition state, while this negative entropy of activation suggests that CO is not dissociating from the rhodium complex as the rate-controlling step occurs. The reverse reaction also features a negative entropy of activation ($\Delta H^{\ddagger}$ = 17 ± 1 kcal·mol^{-1} and $\Delta S^{\ddagger}$ = –10 ± 3 cal·mol^{-1}K^{-1}), and the rate law is also second-order (∝ [**2a**][CO]). These data, and the principle of microscopic reversibility, indicate that the composition of the transition state for forward and reverse processes is [{$PhB(Ox^{Me2})_2Im^{Mes}$}$Rh(CO)_2$·$PhSiH_3$]. Thus, the reverse pathway involves associative coordination of CO to **2a**, as expected because **2a** persists in the absence of CO.

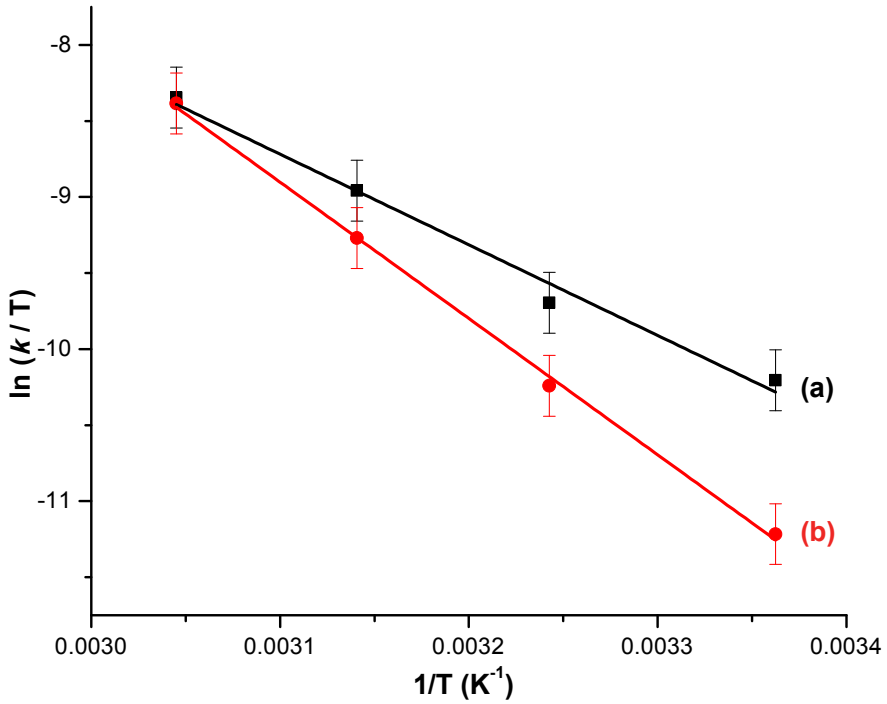

Figure 2-6. Eyring plots (ln(k/T) vs 1/T) for (a) k_1 representing oxidative addition and (b) k_{-1} representing reductive elimination.

Rates and equilibrium constants for organosilane addition. The equilibrium constant K_e, forward rate constant k_1, and reverse rate constant k_{-1} are determined for the reaction of **1** and four primary silanes (Table 2). Comparison of K_e values reveals that oxidative addition of arylsilanes is more favorable than alkylsilanes. The forward rate constant (k_1) is nearly five times faster for arylsilanes than for alkylsilanes, whereas the rate constants for the reverse reaction are similar across all silanes. Because the reverse rate constants are relatively similar, the difference in equilibrium constant between alkylsilanes and arylsilanes results from the difference in forward rate constant.

The rate constant for oxidative addition of alkylsilanes is smaller than that for reductive elimination, whereas reductive elimination of arylsilanes occurs with a lower rate constant than the oxidative addition. Even though this thermodynamic assessment predicts that compounds **2d** and **2e** would be stable while **2b** and **2c** would be unstable, somewhat ironically, the latter compounds are the isolable species. Clearly, the unfavorable thermodynamic bias may be overcome under synthetic conditions by removing CO from the system.

Table 2-2. K_e, k_1, k_{-1} for reaction of 1 and $RSiH_3$ measured at 297 °C.

$RSiH_3$	**K_e**	**k_1 ($M^{-1}s^{-1}$) ($\times 10^{-2}$)**	**k_{-1} ($M^{-1}s^{-1}$) ($\times 10^{-2}$)**
n-hexylsilane	0.53 ± 0.01	0.23 ± 0.01	0.43 ± 0.01
n-dodecylsilane	0.48 ± 0.01	0.25 ± 0.02	0.53 ± 0.05
phenylsilane	2.8 ± 0.3	1.25	0.49
p-methoxyphenylsilane	2.1 ± 0.1	1.34 ± 0.02	0.64 ± 0.01
p-tolylsilane	4.5 ± 0.1	1.4 ± 0.1	0.32 ± 0.02

Conclusion

The equilibrium between **1** and **2** allows an experimental determination of the thermodynamic constraints in a transformation that dissociates a metal-carbonyl and breaks an Si–H bond. First, we note that the $\Delta H°$ is –5.5 ± 0.2 kcal/mol for oxidative addition of the Si–H of $PhSiH_3$ and dissociation of CO. The bond dissociation enthalpy (BDE) for an Si–H bond in $PhSiH_3$ is ca. 88 kcal/mol, whereas the value in $MeSiH_3$ is ca. 90 kcal/mol.[69] Jones has shown that Rh–C BDEs vary only a small amount relative to the corresponding differences in C–H BDE.[58] Assuming the small variation of M–X BDEs, in comparison to Si–H BDEs, extends to Rh–Si bonds for the series of silyls, the difference in equilibrium constants for the two sets of silanes may be attributed to stronger Si–H bond in alkylsilanes.

The BDE for the benzylic C–H in toluene is also ca. 88 kcal/mol.[69] If Rh–C and Rh–Si BDE values are equal, then compound **1** should be thermodynamically competent for C–H bond oxidative addition of toluene; however, this reaction is not observed. It is likely that the Rh–Si bond is stronger than the Rh–C bond in a benzylic organometallic, and that the equilibrium for toluene oxidative addition in the presence of CO would strongly favor **1**. This conclusion is further supported by thermal rearrangement of $CpRhH(CH_2CH_2SiHEt_2)CO$, generated under ultrafast UV-pump conditions, into $CpRhH(SiEt_3)CO$.[57]

Comparison of the forward and reverse rate constants between reaction of arylsilanes and alkylsilanes, as well as the rate laws and activation parameters for $PhSiH_3$ oxidative addition and reductive elimination, provide considerable insight into the pathway and mechanisms. First, reductive elimination follows a second-order rate law. The rate law is first-order in [CO], and the reaction does not occur in the absence of CO. Thus, two CO groups are present in the transition state of the rate-limiting step on the pathway for reductive elimination (eq. 6 of Scheme 2, in

reverse). Alternative mechanisms, in which one oxazoline dissociates from **2** to give a high energy 16-electron rhodium(III) species that is trapped by CO or undergoes Si–H bond reductive elimination, are ruled out by the dependence on CO in the rate law.

Two additional observations suggest that coordination of CO to **2** is the rate-limiting step of the reductive elimination process. In this reaction, $\Delta S^{\ddagger}$ is negative (-10 ± 3 cal·mol^{-1}K^{-1}), which is consistent with an ordered transition state. Loss of the H–SiH_2R group during or prior to the rate-limiting step would result in a positive entropy term. In addition, the rate constants are similar for the reductive elimination reactions of **2a-e**, where the alkylsilyl and arylsilyl ligand is varied. A rate-determining step involving either Rh–Si bond cleavage, and especially Si–H bond formation, would be expected to vary significantly with the silyl substituent. On the basis of these ideas, we conclude that the rate-limiting step for the reductive elimination pathway involves CO coordination to give a high-energy, 20-electron species {κ^3-$PhB(Ox^{Me2})_2Im^{Mes}$}$RhH(SiH_2R)(CO)_2$. This step is the first step in the overall pathway from **2** back to **1**.

This interpretation limits the possible mechanisms of the oxidative addition (forward) pathway (Scheme 2). In oxidative addition of Si–H to **1**, two CO ligands are present up to the rate-limiting step, at which point CO dissociates from rhodium, as required by the principle of microscopic reversibility. Thus, low coordinate species, analogous to photochemically generated κ^2-Tp*RhL or κ^3-Tp*RhL (L = CO, CNR), are never accessed in this transformation.

Scheme 2-2. Proposed pathway for oxidative addition of Si–H bonds under thermal conditions.

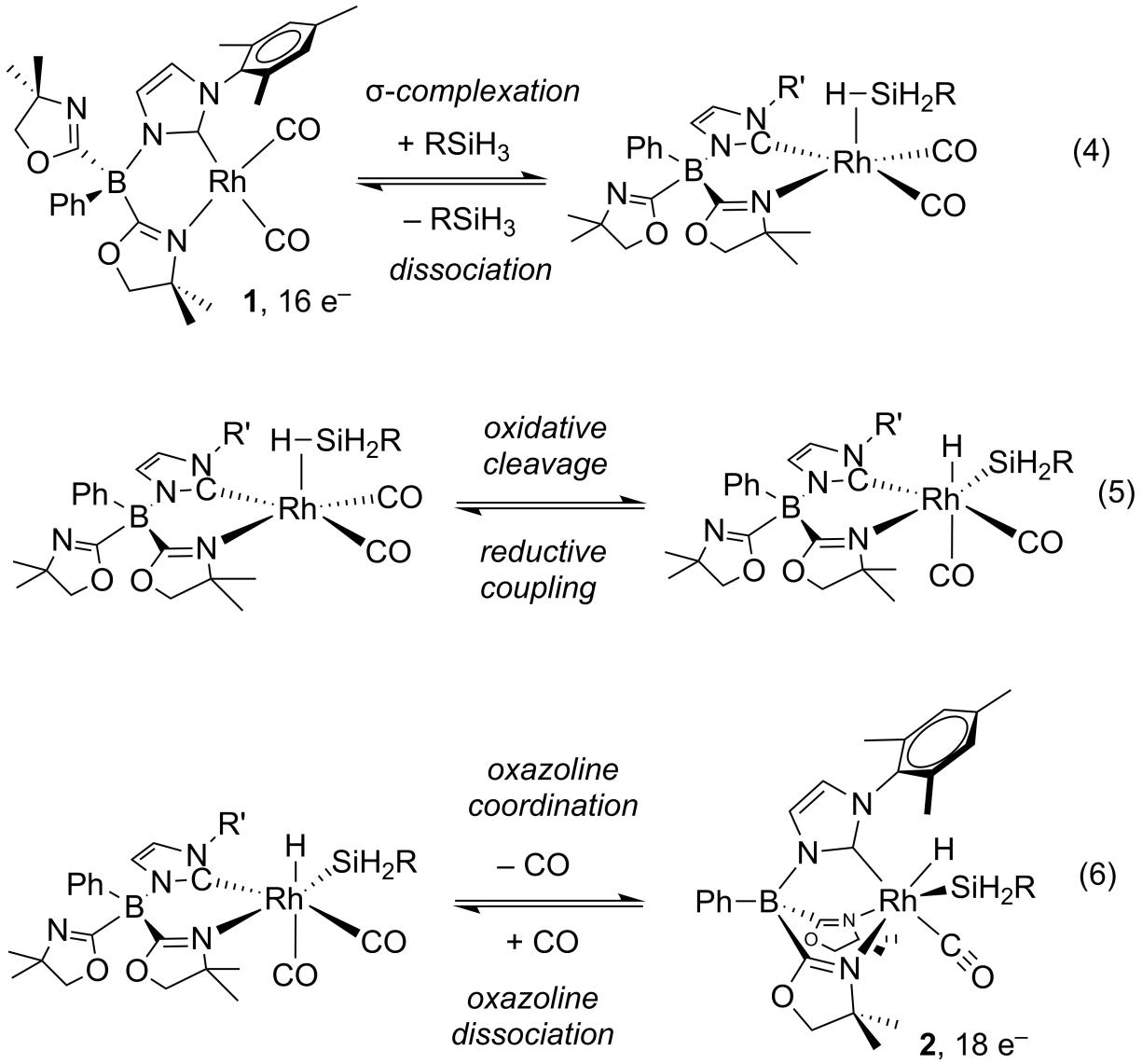

In addition, the Si–H bond is cleaved during or prior to the rate-limiting step in the reaction of **1** and silanes. The evidence for this aspect of the mechanism includes the second-order rate law which contains first-order dependence on silane concentration. The activation entropy ($\Delta S^{\ddagger}$ = –26 ± 3 cal·mol^{-1}·K^{-1}) is more negative than for the reverse direction, which is consistent with the loss of entropy resulting from creation of the rhodium-silane interaction. Finally, the rate constants for oxidative addition to **1** are 5× greater with arylsilanes than alkylsilanes, indicating that the relative

energy of the starting material vs. that of the rate-determining transitions state is affected by the nature of the silane. Thus, we attribute the change in rate of oxidative addition for **1** and silanes to large changes in the energy of the silane (variation in the ground state). This interpretation is consistent with the similar rates for reductive elimination over the series **2a-e**, which indicates the energies difference between **2** and the rate-limiting transition for reductive elimination are similar.

In contrast, we note that k_H/k_D is ~1. The most straightforward interpretation of these data is that the Si–H is broken prior to the rate-determining step. A second possibility is that Si–H bond cleavage occurs during the rate-determining step, and an inverse equilibrium isotope effect from the formation of a silane-rhodium σ-complex balances a normal kinetic isotope effect for Si–H oxidative cleavage.[70] The data cannot unambiguously distinguish these alternatives, but we favor the former pathway of Scheme 2 because the observed kinetic isotope effect is unity over a range of temperatures and this scheme provides the simplest kinetically consistent mechanism.

The thermodynamic and kinetic data are entirely inconsistent with a mechanism resembling the photochemical activation and E–H bond oxidative addition chemistry of the classical cyclopentadienyl and tris(pyrazolyl)borato rhodium and iridium species. The newly proposed mechanism invokes associative steps to access the trivalent rhodium intermediate, which is then susceptible to displacement of CO by a chelating oxazoline. This work shows that thermal pathways for catalytic functionalization are plausible, even in the presence of CO, but such reactions still face considerable challenges due to kinetic and thermodynamic constraints on bond activation. Moreover, CO dissociation from a low valent metal complex is not a necessary pre-requisite for oxidative addition. The presence of coordinating groups, either as part of polar substrates, may also facilitate coordination, oxidative addition, and CO dissociation during catalytic conversions.

Experimental Section

General. All reactions were performed under a dry argon atmosphere using standard Schlenk techniques or under a nitrogen atmosphere in a glovebox. Benzene, toluene, methylene chloride, pentane, and tetrahydrofuran were dried and deoxygenated using an IT PureSolv system. Benzene-d_6 was heated to reflux over Na/K alloy and vacuum transferred. $[Rh(\mu\text{-}Cl)(CO)_2]_2$,[71] $\{PhB(Ox^{Me2})_2Im^{Mes}\}Rh(CO)_2$ (**1**), $\{PhB(Ox^{Me2})_2Im^{Mes}\}RhH(SiH_2Ph)CO$,[63] and *p*-methoxyphenylsilane were synthesized according to the literature procedure.[72] Phenylsilane, *n*-hexylsilane, *n*-dodecylsilane and *p*-tolylsilane were synthesized by reducing corresponding trichlorosilanes with $LiAlH_4$. $PhSiD_3$ was synthesized from $PhSiCl_3$ and $LiAlD_4$. Potassium benzyl was synthesized by reacting potassium *tert*-butoxide with *n*-BuLi in toluene.[73]

^1H, $^{13}C\{^1H\}$, ^{11}B and ^{15}N spectra were collected on Bruker Avance III 600 or AVNEO 400 MHz NMR spectrometers. NMR signals (^1H, ^{13}C, and ^{15}N) were assigned based on COSY, HMQC, and HMBC experiments. ^{15}N chemical shifts were determined by ^1H–^{15}N HMBC experiments. ^{15}N chemical shifts were initially referenced to NH_3 and recalibrated to the CH_3NO_2 chemical shift scale by adding −381.9 ppm. Infrared spectra were recorded on a Bruker Vertex spectrometer. Elemental analyses were performed using a PerkinElmer 2400 Series II CHN/S in the Iowa State Chemical Instrumentation Facility.

$\{PhB(Ox^{Me2})_2Im^{Mes}\}RhH(SiH_2C_6H_{13})CO$ (2b). *n*-Hexylsilane (185 mg, 1.6 mmol) was added to a solution of **1** (100 mg, 0.158 mmol) in benzene to give a pale-yellow solution. The resulting solution was allowed to stir for 24 h. The volatile materials were evaporated in vacuo giving $\{PhB(Ox^{Me2})_2Im^{Mes}\}RhH(SiH_2C_6H_{13})CO$ (88 mg, 0.123 mmol, 78%). ^1H NMR (benzene-d_6, 600 MHz): δ 8.40 (d, $^3J_{HH}$ = 7.8 Hz, 2 H, *o*-BC_6H_5), 7.54 (t, $^3J_{HH}$ = 7.8 Hz, 2 H, *m*-BC_6H_5), 7.39 (t, $^3J_{HH}$ = 7.3 Hz, 1 H, *p*-BC_6H_5), 6.83 (s, 1 H, *m*-$C_6H_2Me_3$), 6.78 (s, 1 H, *m*-$C_6H_2Me_3$), 6.53 (d, $^3J_{HH}$ = 1.6 Hz, 1 H, $N_2C_3H_2Mes$), 5.94 (d, $^3J_{HH}$ = 1.6 Hz, 1 H, $N_2C_3H_2Mes$), 4.91 (t, $^2J_{HH}$ = 6.8 Hz, $^1J_{SiH}$

= 168 Hz, 1 H, SiH), 4.43 (t, $^{2}J_{HH}$ = 6.8 Hz, $^{1}J_{SiH}$ = 180 Hz, 1 H, SiH), 3.60 (m, 3 H, CNCMe$_2$C*H*$_2$O), 3.36 (d, $^{2}J_{HH}$ = 8.3 Hz, 1 H, CNCMe$_2$C*H*$_2$O), 2.23 (s, 3 H, *p*-C$_6$H$_2$*Me*$_3$), 2.09 (s, 3 H, *o*-C$_6$H$_2$*Me*$_3$), 2.02 (s, 3 H, *o*-C$_6$H$_2$*Me*$_3$), 1.55 (br, 2 H, SiCH$_2$C*H*$_2$), 1.33-1.40 (br, 6 H, CH$_2$C*H*$_2$CH$_2$), 1.23 (s, 3 H, CNC*Me*$_2$CH$_2$O trans to H), 1.16 (s, 3 H, CNC*Me*$_2$CH$_2$O trans to H), 1.10 (s, 3 H, CNC*Me*$_2$CH$_2$O trans to Si), 0.99 (s, 3 H, CNC*Me*$_2$CH$_2$O trans to Si), 0.95 (t, $^{3}J_{HH}$ = 7 Hz, 3 H, CH$_2$C*H*$_3$), 0.41 (m, 1 H, SiH$_2$C*H*$_2$), −0.12 (m, 1 H, SiH$_2$C*H*$_2$), −13.70 (dd, $^{1}J_{RhH}$ = 22.4 Hz, $^{3}J_{HH}$ = 1.5 Hz, 1 H, RhH). ^{13}C{^{1}H} NMR (benzene-*d*$_6$, 150 MHz): δ 195.05 (d, $^{1}J_{RhC}$ = 51.9 Hz, 2*C*-N$_2$C$_3$H$_2$Mes), 179.24 (d, $^{1}J_{RhC}$ = 40.5 Hz, CO), 138.49 (br, *ipso*-BC$_6$H$_5$), 137.58 (*p*-*C*$_6$H$_2$Me$_3$), 136.70 (*o*-*C*$_6$H$_2$Me$_3$), 136.64 (*o*-BC$_6$H$_5$), 136.36 (*o*-*C*$_6$H$_2$Me$_3$), 129.58 (*m*-*C*$_6$H$_2$Me$_3$), 129.51 (*m*-*C*$_6$H$_2$Me$_3$), 127.50 (*m*-BC$_6$H$_5$),127.03 (*p*-BC$_6$H$_5$), 124.60 (4,5C-N$_2$*C*$_3$H$_2$Mes), 121.12 (4,5C-N$_2$*C*$_3$H$_2$Mes), 80.40 (CNCMe$_2$*C*H$_2$O), 80.39 (CNCMe$_2$*C*H$_2$O), 68.79 (CN*C*Me$_2$CH$_2$O), 66.64 (CN*C*Me$_2$CH$_2$O), 33.64 (CH$_2$), 32.32 (CH$_2$), 29.88 (CNC*Me*$_2$CH$_2$O), 28.37 (CNC*Me*$_2$CH$_2$O), 28.08 (CNC*Me*$_2$CH$_2$O), 27.03 (CNC*Me*$_2$CH$_2$O), 23.29 (CH$_2$), 21.16 (*p*-C$_6$H$_2$*Me*$_3$), 19.52 (*o*-C$_6$H$_2$*Me*$_3$), 19.37(*o*-C$_6$H$_2$*Me*$_3$), 18.01 (CH$_2$), 17.99 (CH$_2$), 14.50 (*C*H$_3$). ^{15}N{^{1}H} NMR (benzene-*d*$_6$, 61 MHz): δ −160 (CNCMe$_2$CH$_2$O trans to Si), −172 (CNCMe$_2$CH$_2$O trans to H), −188 (N$_2$C$_3$H$_2$Mes). ^{11}B NMR (benzene-*d*$_6$, 192 MHz): δ −9.7. IR (KBr, cm^{-1}): 3135, 3043, 2959, 2923, 2733, 2359, 2279, 2041, 2011, 1652, 1595, 1458, 1275, 967, 820. Anal. Calcd for C$_{35}$H$_{50}$BN$_4$O$_3$RhSi: C, 58.66; H, 7.03; N, 7.82. Found: C, 58.68; H, 7.21; N, 7.61

{PhB(Ox^{Me2})$_2$Im^{Mes}}RhH(SiH$_2$C$_{12}$H$_{25}$)CO (2c). *n*-dodecylsilane (318 mg, 1.59 mmol) was added to a solution of **1** (100 mg, 0.159 mmol) in benzene to give a pale yellow solution. The resulting solution was allowed to stir for 24 h. The volatile materials were evaporated in vacuo resulting a white solid which was washed with pentane to give pure {PhB(Ox^{Me2})$_2$Im^{Mes}}RhH(SiH$_2$C$_{12}$H$_{25}$)CO (65 mg, 0.08 mmol, 50%). ^{1}H NMR (benzene-*d*$_6$, 600

MHz): δ 8.41 (d, $^{3}J_{HH}$ = 7.8 Hz, 2 H, *o*-BC_6H_5), 7.54 (t, $^{3}J_{HH}$ = 7.2 Hz, 2 H, *m*-BC_6H_5), 7.4 (t, $^{3}J_{HH}$ = 7.2 Hz, 1 H, *p*-BC_6H_5), 6.84 (s, 1 H, *m*-$C_6H_2Me_3$), 6.80 (s, 1 H, *m*-$C_6H_2Me_3$), 6.54 (d, $^{3}J_{HH}$ = 1.6 Hz, 1 H, $N_2C_3H_2Mes$), 5.94 (d, $^{3}J_{HH}$ = 1.8 Hz, 1 H, $N_2C_3H_2Mes$), 4.26 (t, $^{2}J_{HH}$ = 7.2 Hz, $^{1}J_{SiH}$ = 160 Hz, 1 H, SiH), 3.81 (t, $^{2}J_{HH}$ = 6.6 Hz, $^{1}J_{SiH}$ = 180 Hz, 1 H, SiH), 3.64-3.57(m, 3 H, $CNCMe_2CH_2O$), 3.35 (d, $^{2}J_{HH}$ = 8.4 Hz, 1 H, $CNCMe_2CH_2O$), 2.26 (s, 3 H, *p*-$C_6H_2Me_3$), 2.09 (s, 3 H, *o*-$C_6H_2Me_3$), 2.03 (s, 3 H, *o*-C6H2Me3), 1.58 (br, 2 H, $SiCH_2CH_2$), 1.33-1.29 (br, 21 H, $CH_2CH_2CH_2$), 1.23 (s, 3 H, $CNCMe_2CH_2O$ trans to H), 1.16 (s, 3 H, $CNCMe_2CH_2O$ trans to H), 1.10 (s, 3 H, $CNCMe_2CH_2O$ trans to Si), 0.99 (s, 3 H, $CNCMe_2CH_2O$ trans to Si), 0.93 (t, $^{3}J_{HH}$ = 7.2 Hz, 3 H, CH_2CH_3), 0.44 (m, 1 H, SiH_2CH_2), –0.07 (m, 1 H, SiH_2CH_2), –13.68 (dd, $^{1}J_{RhH}$ = 22.2 Hz, $^{3}J_{HH}$ = 1.8 Hz, 1 H, RhH). $^{13}C\{^{1}H\}$ NMR (benzene-d_6, 150 MHz): δ 195.06 (d, $^{1}J_{RhC}$ = 52.8 Hz, 2C-$N_2C_3H_2Mes$), 185.79 (br, $CNCMe_2CH_2O$), 179.23 (d, $^{1}J_{RhC}$ = 40.7 Hz, CO), 138.49 (*p*-$C_6H_2Me_3$), 137.60 (*ipso*-$C_6H_2Me_3$), 136.70 (*o*-$C_6H_2Me_3$), 136.66 (*o*-$C_6H_2Me_3$), 136.39 (*o*-BC_6H_5), 129.59 (*m*-$C_6H_2Me_3$), 129.52 (*m*-$C_6H_2Me_3$) 127.51 (*m*-BC_6H_5), 127.04 (*p*-BC_6H_5), 124.61 (4,5-$CN_2C_3H_2Mes$), 121.12 (4,5-$CN_2C_3H_2Mes$), 80.40 ($CNCMe_2CH_2O$), 80.39 ($CNCMe_2CH_2O$), 68.79 ($CNCMe_2CH_2O$), 66.64 ($CNCMe_2CH_2O$), 34.00 (CH_2), 32.38 (CH_2), 30.37 (CH_2), 30.31 (CH_2), 30.26 (CH_2), 30.19 (CH_2), 29.94 (CH_2), 29.87 (CH_2), 28.37 ($CNCMe_2CH_2O$), 28.08 ($CNCMe_2CH_2O$), 28.02 ($CNCMe_2CH_2O$), 27.03 ($CNCMe_2CH_2O$), 23.16 (CH_2), 21.18 (*p*-$C_6H_2Me_3$), 19.53 (*o*-$C_6H_2Me_3$), 19.38 (*o*-$C_6H_2Me_3$), 18.02 (CH_2), 18.01 (CH_2), 14.41 (CH_3). $^{15}N\{^{1}H\}$ NMR (benzene-d_6, 61 MHz): δ −160 ($CNCMe_2CH_2O$ trans to Si), –172 ($CNCMe_2CH_2O$ trans to H), −175 ($N_2C_3H_{12}Mes$), −188 ($N_2C_3H_2Mes$). ^{11}B NMR (benzene-d_6, 192 MHz): δ −9.9. IR (KBr, cm^{-1}): 2957, 2922, 2852, 2149, 2044, 2013, 1595, 1463, 1365, 1316, 1183, 1160, 968.

{PhB(Ox^{Me2})$_2$Im^{Mes}}RhH(SiH$_2$C$_6$H$_4$Me)CO (2d). *p*-tolylsilane (195 mg, 1.6 mmol) was added to a solution of **1** (100 mg, 0.158 mmol) in benzene to give a pale yellow solution. The resulting

solution was allowed to stir for 24 h. The volatile materials were evaporated in vacuo giving {PhB(Ox^{Me2})$_2$$Im^{Mes}$}RhH($SiH_2C_6H_4Me$)CO with some residual *p*-tolylsilane. This mixture was characterized by NMR and IR spectroscopy; the residual silane hindered $^{13}C\{^1H\}$ NMR assignments in the aryl region. An X-ray quality crystal was obtained from a pentane solution; however, this approach was not reliable for purification from residual p-tolylsilane. ^1H NMR (benzene-d_6, 600 MHz): δ 8.43 (d, $^3J_{HH}$ = 7.8 Hz, 2 H, o-BC_6H_5), 7.56 (t, $^3J_{HH}$ = 7.2 Hz, 2 H, *m*-BC_6H_5), 7.52 (d, $^3J_{HH}$ = 7.8 Hz, 2 H, *o*-C_6H_4Me), 7.41 (t, $^3J_{HH}$ = 7.2 Hz, 1 H, *p*-BC_6H_5), 6.95 (d, $^3J_{HH}$ = 7.8 Hz, 2 H, *m*-C_6H_4Me), 6.55 (d, $^3J_{HH}$ = 1.8 Hz, 1 H, $N_2C_3H_2$Mes), 6.54 (s, 1 H, *m*-$C_6H_2Me_3$), 6.41 (s, 1 H, *m*-$C_6H_2Me_3$), 5.94 (d, $^3J_{HH}$ = 1.8 Hz, 1 H, $N_2C_3H_2$Mes), 4.91 (t, $^2J_{HH}$ = 4.8 Hz, $^1J_{SiH}$ = 170 Hz, 1 H, SiH), 4.45 (t, $^2J_{HH}$ = 4.8 Hz, $^1J_{SiH}$ = 186 Hz, 1 H, SiH*)*, 3.57-3.65 (m, 3 H, $CNCMe_2CH_2O$), 3.37 (d, $^2J_{HH}$ = 8.4 Hz, 1 H, $CNCMe_2CH_2O$), 2.18 (s, 3 H, *p*-$C_6H_2Me_3$), 2.03 (s, 3 H, *o*-$C_6H_2Me_3$), 2.00 (s, 3 H, *o*-$C_6H_2Me_3$), 1.90 (s, 3 H, *p*-C_6H_4Me), 1.16 (3 H, $CNCMe_2CH_2O$), 1.16 (3 H, $CNCMe_2CH_2O$), 1.08 (3 H, $CNCMe_2CH_2O$), 1.02 (3 H, $CNCMe_2CH_2O$), –13.22 (dd, $^1J_{RhH}$ = 21.6 Hz, $^3J_{HH}$ = 2.4 Hz, 1 H, RhH). $^{13}C\{^1H\}$ NMR (benzene-d_6, 150 MHz): δ 194.48 (d, $^1J_{RhC}$ = 52.9 Hz, 2*C*-$N_2C_3H_2$Mes), 178.40 (d, $^1J_{RhC}$ = 40.8 Hz, CO), 138.29 (*ipso*-SiC_6H_4Me), 136.96 (*p*-$C_6H_2Me_3$), 136.68 (*ipso*-$C_6H_2Me_3$), 136.67 (*o*-BC_6H_5), 129.34 (*o*-SiC_6H_4Me), 129.31 (*m*-SiC_6H_4Me), 127.54 (*m*-$C_6H_2Me_3$), 127.07 (*m*-$C_6H_2Me_3$), 124.60 (4,5C-$N_2C_3H_2$Mes), 121.50 (4,5C-$N_2C_3H_2$Mes), 80.49 ($CNCMe_2CH_2O$), 80.31 ($CNCMe_2CH_2O$), 68.80 ($CNCMe_2CH_2O$), 66.70 ($CNCMe_2CH_2O$), 28.38 ($CNCMe_2CH_2O$), 28.07 ($CNCMe_2CH_2O$), 27.78 ($CNCMe_2CH_2O$), 27.03 ($CNCMe_2CH_2O$), 21.48 (*p*-$C_6H_2Me_3$), 21.04 (*p*-SiC_6H_4Me), 19.49 (*o*-$C_6H_2Me_3$), 19.08 (*o*-$C_6H_2Me_3$). $^{15}N\{^1H\}$ NMR (benzene-d_6, 61 MHz): δ −161 ($CNCMe_2CH_2O$ trans to Si), –172, ($CNCMe_2CH_2O$ trans to H), −174 ($N_2C_3H_2$Mes), −188 ($N_2C_3H_2$Mes). ^{11}B NMR

(benzene-d_6, 192 MHz): δ −9.8. IR (KBr, cm^{-1}): 2962, 2923, 2855, 2279, 2104, 2016, 1917, 1652, 1605.

{PhB(Ox^{Me2})$_2$Im^{Mes}}RhH(SiH$_2$C$_6$H$_4$OMe)CO (2e). *p*-methoxyphenylsilane (220 mg, 1.6 mmol) was added to a solution of **1** (100 mg, 0.158 mmol) in benzene to give a pale yellow solution. The resulting solution was allowed to stir for 24 h. The volatile materials were evaporated in vacuo giving {PhB(Ox^{Me2})$_2$Im^{Mes}}RhH(SiH$_2$C$_6$H$_4$OMe)CO with some residual *p*-methoxyphenylsilane. This mixture was characterized by NMR and IR spectroscopy; the residual silane and its slow catalyzed redistribution hindered $^{13}C\{^1H\}$ NMR assignments in the aryl region. ^1H NMR (benzene-d_6, 600 MHz): δ 8.42 (d, $^3J_{HH}$ = 7.2 Hz, 2 H, *o*-BC_6H_5), 7.55 (t, $^3J_{HH}$ = 7.2 Hz, 2 H, *m*-BC_6H_5), 7.50 (d, $^3J_{HH}$ = 8.4 Hz, 2 H, *o*-C_6H_5OMe), 7.40 (t, $^3J_{HH}$ = 7.2 Hz, 1 H, *p*-BC_6H_5), 6.74 (d, $^3J_{HH}$ = 8.4 Hz, 2 H, *m*-C_6H_5OMe), 6.57-6.54 (2 H, *m*-$C_6H_2Me_3$ + $N_2C_3H_2Mes$), 6.43 (s, 1 H, *m*-$C_6H_2Me_3$), 5.94 (d, $^3J_{HH}$ = 1.2 Hz, 1 H, $N_2C_3H_2Mes$), 4.93 (t, $^2J_{HH}$ = 6 Hz, $^1J_{SiH}$ = 172 Hz, 1 H, SiH), 4.45 (t, $^2J_{HH}$ = 6 Hz, $^1J_{SiH}$ = 180 Hz, 1 H, SiH), 3.65-3.57 (m, 3 H, $CNCMe_2CH_2O$), 3.39 (s, 3 H, C_6H_6OMe), 3.38 (d, $^3J_{HH}$ = 8.4 Hz, 1 H, $CNCMe_2CH_2O$), 2.02 (s, 3 H, *p*-$C_6H_2Me_3$), 2.01 (s, 3 H, *o*-$C_6H_2Me_3$), 1.96 (s, 3 H, *o*-$C_6H_2Me_3$), 1.17 (s, 3 H, $CNCMe_2CH_2O$), 1.16 (s, 3 H, $CNCMe_2CH_2O$), 1.09 (s, 3 H, $CNCMe_2CH_2O$), 1.04 (s, 3 H, $CNCMe_2CH_2O$), −13.24 (dd, $^1J_{RhH}$ = 18 Hz, $^3J_{HH}$ = 2 Hz, 1 H, RhH). $^{13}C\{^1H\}$ NMR (benzene-d_6, 150 MHz): δ 194.23 (d, $^1J_{RhC}$ = 76.5 Hz, 2*C*-$N_2C_3H_2Mes$), 178.12 (d, $^1J_{RhC}$ = 60 Hz, CO), 80.11 ($CNCMe_2CH_2O$), 79.95 ($CNCMe_2CH_2O$), 68.42 ($CNCMe_2CH_2O$), 66.33 ($CNCMe_2CH_2O$), 54.50 (*p*-C_6H_4OMe), 28.01 ($CNCMe_2CH_2O$), 27.72 ($CNCMe_2CH_2O$), 27.41 ($CNCMe_2CH_2O$), 26.65 ($CNCMe_2CH_2O$), 20.70 (*p*-$C_6H_2Me_3$), 19.12 (*o*-$C_6H_2Me_3$), 18.74 (*o*-$C_6H_2Me_3$). ^{15}N NMR (benzene-d_6, 61 MHz): δ –161 ($CNCMe_2CH_2O$ trans to Si), –172 ($CNCMe_2CH_2O$ trans to H), –176 ($N_2C_3H_2Mes$), –188

($N_2C_3H_2Mes$). ^{11}B NMR (benzene-d_6, 192 MHz): δ −9.9. IR (KBr, cm^{-1}): 2961, 2933, 2836. 2562, 2531, 2170, 2016, 1903.

NMR kinetic study. A stock solution of **1** (0.011 M) and $Si(SiMe_3)_4$ (0.097 M) as an internal standard in benzene was prepared. Portions of this solution were placed in an NMR tube, and the initial concentration of [**1**] was verified by the integrated spectrum. Excess $PhSiH_3$ (to give concentrations greater than 0.1 M) was added by syringe through the septum of the NMR tube. The NMR tube was placed in the NMR probe, which had been pre-heated and calibrated to the desired temperature for the reaction. ^1H NMR spectra were acquired at regular programmed intervals, and concentrations were determined by integrating appropriate signals in each spectrum. Plots of [**1**] versus time were fit using non-linear least-squares regression to an exponential decay curve based on the equation $[\mathbf{1}] = [\mathbf{1}]_o\, e^{-kt}$ for the analysis.

UV-vis kinetic experiments: (a) Pseudo-irreversible conditions, (b) CO-saturated approach to equilibrium, and (c) equilibrium constant measurements.

(a) Pseudo-irreversible conditions. Four UV-Vis cuvettes, completely filled with phenylsilane dissolved in benzene at four concentrations (0.0192, 0.0238, 0.0291, 0.0348 M), were capped in the glovebox. The temperature of the UV-Vis chamber was set to 308.3 K, and the sample was placed in the cavity and allowed to reach the preset temperature. Approximately 20 μL of a solution of **1** (40 mM) was added to the cuvette through a syringe. The absorption of the reaction mixture was measured at 385.5 nm at programmed time intervals, and [**1**] was calculated using Beer's law. A plot of [**1**] versus time was fit to the equation $[\mathbf{1}] = [\mathbf{1}]_o\, e^{-kt}$ using non-linear least-squares regression analysis, to determine pseudo first-order rate constants. Subsequent experiments varied [$PhSiH_3$], a plot of k_{obs} versus [$PhSiH_3$] was linear, and the slope provided the second-order rate

constant k_1^{app}. This procedure, performed over a range of temperatures from 296 K to 322.3 K, provided the temperature-dependent second-order rate constants for an Eyring plot.

(b) CO-saturated approach to equilibrium. Solution of $PhSiH_3$ (14 mM, 15 mM, 18 mM, 19 mM) in benzene were degassed by three freeze-pump-thaw cycles, and then saturated with CO by stirring under a CO atmosphere (298 K, 1 atm). The solutions were transferred to nitrogen-flushed and dried UV-Vis cuvettes using air-free syringe technique. These samples were used for the kinetic study, following the procedure above, to determine k_e by non-linear least-squares analysis. The series of experiments, combined with K_e (determined below) provide forward (k_1) and reverse (k_{-1}) rate constants. This procedure was repeated for the three other temperatures (308.4, 318.4, 328.4 K). For the silane p-tolylsilane, p-methoxysilane, hexylsilane, and dodecylsilane, this procedure was applied at room temperature to determine forward and reverse rate constants.

(c) Equilibrium constant measurement. Reactions of **1** and $PhSiH_3$ (3.2 mM, 3.8 mM, 4 mM, 11.9 mM), in CO-saturated benzene solution, were monitored by UV-Vis, as described above, until the reaction mixture reached equilibrium. [**1**] was determined from Beer's law, $[\mathbf{2a}]_e$ was determined from difference between $[Rh]_{total}$ and $[\mathbf{1}]_e$, and $[PhSiH_3]_e$ and $[CO]_e$ were approximated to be equal to their initial concentration (in large excess of $[Rh]_{total}$). This procedure was repeated for other temperatures (296, 301.5, 318.4, 328.4 K) to provide data for a van't Hoff plot to determine ΔH and ΔS.

References

(1) Van Leeuwen, P. W. N. M.; Clarver, C.: *Rhodium Catalyzed Hydroformylation*; Springer: Dordrecht, Netherlands, 2002.

(2) Wiese, K.-D.; Obst, D.: Hydroformylation. In *Catalytic Carbonylation Reactions*; Beller, M., Ed.; Springer: Berlin, 2006; pp 1-33.

(3) Ojima, I.; Donovan, R. J.; Clos, N. Rhodium and Cobalt Carbonyl Clusters $Rh_4(CO)_{12}$, $Co_2Rh_2(CO)_{12}$, and $Co_3Rh(CO)_{12}$ as Effective Catalysts for Hydrosilylation of Isoprene, Cyclohexanone, and Cyclohexenone. *Organometallics* **1991**, *10*, 2606-2610.

(4) Bellachioma, G.; Cardaci, G.; Colomer, E.; Corriu, R. J. P.; Vioux, A. Reactivity of $Fe(CO)_4(H)MPh_3$ (M = Si, Ge) and Mechanism of Substitution by Two-Electron-Donor Ligands: Implications for the Mechanism of Hydrosilylation of Olefins Catalyzed by Iron Pentacarbonyl. *Inorg. Chem.* **1989**, *28*, 519-525.

(5) Marciniec, B.: *Hydrosilylation: A Comprehensive Review on Recent Advances*; Springer: Berlin, 2009.

(6) Schneider, N.; Finger, M.; Haferkemper, C.; Bellemin-Laponnaz, S.; Hofmann, P.; Gade, L. H. Metal Silylenes Generated by Double Silicon–Hydrogen Activation: Key Intermediates in the Rhodium-Catalyzed Hydrosilylation of Ketones. *Angew. Chem.* **2009**, *121*, 1637-1641.

(7) Schneider, N.; Finger, M.; Haferkemper, C.; Bellemin-Laponnaz, S.; Hofmann, P.; Gade, L. H. Multiple Reaction Pathways in Rhodium-Catalyzed Hydrosilylations of Ketones. *Chem. Eur. J.* **2009**, *15*, 11515-11529.

(8) Ojima, I.; Inaba, S.-I.; Kogure, T.; Nagai, Y. The Action of Tris(triphenylphosphine)chlororhodium on Polyhydromonosilanes. *J. Organomet. Chem.* **1973**, *55*, C7-C8.

(9) Brown-Wensley, K. A. Formation of Si-Si Bonds from Si-H Bonds in the Presence of Hydrosilation Catalysts. *Organometallics* **1987**, *6*, 1590-1591.

(10) Ojima, I.; Clos, N.; Donovan, R. J.; Ingallina, P. Hydrosilylation of 1-Hexyne Catalyzed by Rhodium and Cobalt-Rhodium Mixed-Metal Complexes. Mechanism of Apparent Trans Addition. *Organometallics* **1990**, *9*, 3127-3133.

(11) Rosenberg, L.; Fryzuk, M. D.; Rettig, S. J. Dimeric Rhodium μ-Silylene and μ-η2-Silyl Complexes: Catalytic Silicon−Silicon Bond Formation and X-ray Structures of $[\{i\text{Pr}_2\text{PCH}_2\text{CH}_2\text{P}i\text{Pr}_2\}\text{Rh}]_2(\mu\text{-SiRR}')_2$ (R = R' = Ph and R = Me, R' = Ph) and $[\{i\text{Pr}_2\text{PCH}_2\text{CH}_2\text{P}i\text{Pr}_2\}\text{Rh(H)}]_2(\mu\text{-}\eta^2\text{-H}-\text{SiMe}_2)_2$. *Organometallics* **1999**, *18*, 958-969.

(12) Rosenberg, L.; Davis, C. W.; Yao, J. Catalytic Dehydrogenative Coupling of Secondary Silanes Using Wilkinson's Catalyst. *J. Am. Chem. Soc.* **2001**, *123*, 5120-5121.

(13) Rosenberg, L.; Kobus, D. N. Dehydrogenative Coupling of Primary Alkyl Silanes Using Wilkinson's Catalyst. *J. Organomet. Chem.* **2003**, *685*, 107-112.

(14) Azpeitia, S.; Fernández, B.; Garralda, M. A.; Huertos, M. A. Dehydrogenative Coupling of a Tertiary Silane Using Wilkinson's Catalyst. *Eur. J. Inorg. Chem.* **2016**, *2016*, 2891-2895.

(15) Evans, D.; Osborn, J. A.; Wilkinson, G. Hydroformylation of Alkenes by Use of Rhodium Complex Catalysts. *J. Chem. Soc. A* **1968**, 3133-3142.

(16) Moser, W. R.; Papile, C. J.; Brannon, D. A.; Duwell, R. A.; Weininger, S. J. The Mechanism of Phosphine-Modified Rhodium-Catalyzed Hydroformylation Studied by CIR-FTIR. *J. Mol. Catal.* **1987**, *41*, 271-292.

(17) Horváth, I. T.; Kastrup, R. V.; Oswald, A. A.; Mozeleski, E. J. High-Pressure NMR Studies of the Water Soluble Rhodium Hydroformylation System. *Catal. Lett.* **1989**, *2*, 85-90.

(18) Baird, M. C.; Nyman, C. J.; Wilkinson, G. The Decarbonylation of Aldehydes by Tris(triphenylphosphine)chlororhodium(I). *J. Chem. Soc. A* **1968**, 348-351.

(19) Graham, P. M.; Mocella, C. J.; Sabat, M.; Harman, W. D. Dihapto-Coordinated Amide, Ester, and Aldehyde Complexes and Their Role in Decarbonylation. *Organometallics* **2005**, *24*, 911-919.

(20) Malapit, C. A.; Bour, J. R.; Brigham, C. E.; Sanford, M. S. Base-Free Nickel-Catalysed Decarbonylative Suzuki–Miyaura Coupling of Acid Fluorides. *Nature* **2018**, *563*, 100-104.

(21) Yamamoto, T.; Ishizu, J.; Kohara, T.; Komiya, S.; Yamamoto, A. Oxidative addition of aryl carboxylates to nickel(0) complexes involving cleavage of the acyl-oxygen bond. *J. Am. Chem. Soc.* **1980**, *102*, 3758-3764.

(22) Doughty, D. H.; Pignolet, L. H. Catalytic Decarbonylation of Aldehydes. *J. Am. Chem. Soc.* **1978**, *100*, 7083-7085.

(23) Ho, H.-A.; Manna, K.; Sadow, A. D. Acceptorless Photocatalytic Dehydrogenation for Alcohol Decarbonylation and Imine Synthesis. *Angew. Chem. Int. Ed.* **2012**, *51*, 8607-8610.

(24) Lei, Z.-Q.; Li, H.; Li, Y.; Zhang, X.-S.; Chen, K.; Wang, X.; Sun, J.; Shi, Z.-J. Extrusion of CO from Aryl Ketones: Rhodium(I)-Catalyzed C–C Bond Cleavage Directed by a Pyridine Group. *Angew. Chem. Int. Ed.* **2012**, *51*, 2690-2694.

(25) Zeng, R.; Dong, G. Rh-Catalyzed Decarbonylative Coupling with Alkynes via C–C Activation of Isatins. *J. Am. Chem. Soc.* **2015**, *137*, 1408-1411.

(26) Blum, J.; Oppenheimer, E.; Bergmann, E. D. Decarbonylation of Aromatic Carbonyl Compounds Catalyzed by Rhodium Complexes. *J. Am. Chem. Soc.* **1967**, *89*, 2338-2341.

(27) Malapit, C. A.; Ichiishi, N.; Sanford, M. S. Pd-Catalyzed Decarbonylative Cross-Couplings of Aroyl Chlorides. *Org. Lett.* **2017**, *19*, 4142-4145.

(28) Ogiwara, Y.; Sakurai, Y.; Hattori, H.; Sakai, N. Palladium-Catalyzed Reductive Conversion of Acyl Fluorides via Ligand-Controlled Decarbonylation. *Org. Lett.* **2018**, *20*, 4204-4208.

(29) Keaveney, S. T.; Schoenebeck, F. Palladium-Catalyzed Decarbonylative Trifluoromethylation of Acid Fluorides. *Angew. Chem. Int. Ed.* **2018**, *57*, 4073-4077.

(30) Zahalka, H. A.; Alper, H.; Sasson, Y. Homogeneous Decarbonylation of Formate Esters Catalyzed by Vaska's Compound. *Organometallics* **1986**, *5*, 2497-2499.

(31) Gooßen, L. J.; Paetzold, J. New Synthesis of Biaryls via Rh-Catalyzed Decarbonylative Suzuki-Coupling of Carboxylic Anhydrides with Arylboroxines. *Adv. Synth. Catal.* **2004**, *346*, 1665-1668.

(32) Muto, K.; Yamaguchi, J.; Musaev, D. G.; Itami, K. Decarbonylative Organoboron Cross-Coupling of Esters by Nickel Catalysis. *Nature Communications* **2015**, *6*, 7508.

(33) Guo, L.; Rueping, M. Decarbonylative Cross-Couplings: Nickel Catalyzed Functional Group Interconversion Strategies for the Construction of Complex Organic Molecules. *Acc. Chem. Res.* **2018**, *51*, 1185-1195.

(34) Chatupheeraphat, A.; Liao, H.-H.; Srimontree, W.; Guo, L.; Minenkov, Y.; Poater, A.; Cavallo, L.; Rueping, M. Ligand-Controlled Chemoselective C(acyl)–O Bond vs C(aryl)–C Bond Activation of Aromatic Esters in Nickel Catalyzed C(sp^2)–C(sp^3) Cross-Couplings. *J. Am. Chem. Soc.* **2018**, *140*, 3724-3735.

(35) Hu, J.; Zhao, Y.; Liu, J.; Zhang, Y.; Shi, Z. Nickel-Catalyzed Decarbonylative Borylation of Amides: Evidence for Acyl C−N Bond Activation. *Angew. Chem. Int. Ed.* **2016**, *55*, 8718-8722.

(36) Hoyano, J. K.; Graham, W. A. G. Oxidative Addition of the Carbon-Hydrogen Bonds of Neopentane and Cyclohexane to a Photochemically Generated Iridium(I) Complex. *J. Am. Chem. Soc.* **1982**, *104*, 3723-3725.

(37) Hoyano, J. K.; McMaster, A. D.; Graham, W. A. G. Activation of Methane by Iridium Complexes. *J. Am. Chem. Soc.* **1983**, *105*, 7190-7191.

(38) Rest, A. J.; Whitwell, I.; Graham, W. A. G.; Hoyano, J. K.; McMaster, A. D. Photo-Activation of Methane at 12 K by (η^5-Cyclopentadienyl)- and (η^5-Pentamethylcyclopentadienyl)-Dicarbonyl-Rhodium and -Iridium Complexes. *J. Chem. Soc., Chem. Commun.* **1984**, 624-626.

(39) Ghosh, C. K.; Graham, W. A. G. Efficient and Selective Carbon-Hydrogen Activation by a Tris(Pyrazolyl)Borate Rhodium Complex. *J. Am. Chem. Soc.* **1987**, *109*, 4726-4727.

(40) George, M. W.; Hall, M. B.; Jina, O. S.; Portius, P.; Sun, X.-Z.; Towrie, M.; Wu, H.; Yang, X.; Zaric, S. D. Understanding the Factors Affecting the Activation of Alkane by Cp'Rh(CO)$_2$ (Cp' = Cp or Cp*). *Pro. Natl. Acad. Sci. U.S.A.* **2010**, *107*, 20178-20183.

(41) George, M. W.; Hall, M. B.; Portius, P.; Renz, A. L.; Sun, X.-Z.; Towrie, M.; Yang, X. Combined Experimental and Theoretical Investigation into C–H Activation of Cyclic Alkanes by Cp′Rh(CO)$_2$ (Cp′ = η^5-C_5H_5 or η^5-C_5Me_5). *Dalton Trans.* **2011**, *40*, 1751-1757.

(42) McKeown, B. A.; Lee, J. P.; Mei, J.; Cundari, T. R.; Gunnoe, T. B. Transition Metal Mediated C–H Activation and Functionalization: The Role of Poly(pyrazolyl)borate and Poly(pyrazolyl)alkane Ligands. *Eur. J. Inorg. Chem.* **2016**, 2296-2311.

(43) Guan, J.; Wriglesworth, A.; Sun, X. Z.; Brothers, E. N.; Zarić, S. D.; Evans, M. E.; Jones, W. D.; Towrie, M.; Hall, M. B.; George, M. W. Probing the Carbon–Hydrogen Activation of Alkanes Following Photolysis of Tp′Rh(CNR)(carbodiimide): A Computational and Time-Resolved Infrared Spectroscopic Study. *J. Am. Chem. Soc.* **2018**, *140*, 1842-1854.

(44) Purwoko, A. A.; Lees, A. J. Photochemical C–H Bond Activation Reactivity of (HBPz*$_3$)Rh(CO)$_2$ (Pz* = 3,5-Dimethylpyrazolyl) in Alkane Solutions. *Inorg. Chem.* **1996**, *35*, 675-682.

(45) Kunin, A. J.; Eisenberg, R. Photochemical Carbonylation of Benzene by Iridium(I) and Rhodium(I) Square-Planar Complexes. *J. Am. Chem. Soc.* **1986**, *108*, 535-536.

(46) Sakakura, T.; Tanaka, M. Efficiently Catalytic C–H Activation. Direct and Mild Carbonylation of Benzene and Cyclohexane by RhCl(CO)(PMe$_3$)$_2$ under Irradiation. *Chem. Lett.* **1987**, *16*, 249-252.

(47) Wasserman, E. P.; Moore, C. B.; Bergman, R. G. Gas-Phase Rates of Alkane C-H Oxidative Addition to a Transient CpRh(CO) Complex. *Science* **1992**, *255*, 315.

(48) Song, J.; Hall, M. B. Theoretical Studies of Inorganic and Organometallic Reaction Mechanisms. 6. Methane Activation on Transient Cyclopentadienylcarbonylrhodium. *Organometallics* **1993**, *12*, 3118-3126.

(49) Yang, H.; Kotz, K. T.; Asplund, M. C.; Wilkens, M. J.; Harris, C. B. Ultrafast Infrared Studies of Bond Activation in Organometallic Complexes. *Acc. Chem. Res.* **1999**, *32*, 551-560.

(50) Snee, P. T.; Payne, C. K.; Kotz, K. T.; Yang, H.; Harris, C. B. Triplet Organometallic Reactivity under Ambient Conditions: An Ultrafast UV Pump/IR Probe Study. *J. Am. Chem. Soc.* **2001**, *123*, 2255-2264.

(51) Pitts, A. L.; Wriglesworth, A.; Sun, X.-Z.; Calladine, J. A.; Zarić, S. D.; George, M. W.; Hall, M. B. Carbon–Hydrogen Activation of Cycloalkanes by

Cyclopentadienylcarbonylrhodium—A Lifetime Enigma. *J. Am. Chem. Soc.* **2014**, *136*, 8614-8625.

(52) Zarić, S.; Hall, M. B. Prediction of the Reactive Intermediates in Alkane Activation by Tris(pyrazolyl borate)rhodium Carbonyl. *J. Phys. Chem. A* **1998**, *102*, 1963-1964.

(53) Lian, T.; Bromberg, S. E.; Yang, H.; Proulx, G.; Bergman, R. G.; Harris, C. B. Femtosecond IR Studies of Alkane C−H Bond Activation by Organometallic Compounds: Direct Observation of Reactive Intermediates in Room Temperature Solutions. *J. Am. Chem. Soc.* **1996**, *118*, 3769-3770.

(54) Bromberg, S. E.; Yang, H.; Asplund, M. C.; Lian, T.; McNamara, B. K.; Kotz, K. T.; Yeston, J. S.; Wilkens, M.; Frei, H.; Bergman, R. G.; Harris, C. B. The Mechanism of a C-H Bond Activation Reaction in Room-Temperature Alkane Solution. *Science* **1997**, *278*, 260-263.

(55) Blake, A. J.; George, M. W.; Hall, M. B.; McMaster, J.; Portius, P.; Sun, X. Z.; Towrie, M.; Webster, C. E.; Wilson, C.; Zarić, S. D. Probing the Mechanism of Carbon–Hydrogen Bond Activation by Photochemically Generated Hydridotris(pyrazolyl)borato Carbonyl Rhodium Complexes: New Experimental and Theoretical Investigations. *Organometallics* **2008**, *27*, 189-201.

(56) Asplund, M. C.; Snee, P. T.; Yeston, J. S.; Wilkens, M. J.; Payne, C. K.; Yang, H.; Kotz, K. T.; Frei, H.; Bergman, R. G.; Harris, C. B. Ultrafast UV Pump/IR Probe Studies of C−H Activation in Linear, Cyclic, and Aryl Hydrocarbons. *J. Am. Chem. Soc.* **2002**, *124*, 10605-10612.

(57) Jones, W. D. On the Nature of Carbon−Hydrogen Bond Activation at Rhodium and Related Reactions. *Inorg. Chem.* **2005**, *44*, 4475-4484.

(58) Evans, M. E.; Li, T.; Vetter, A. J.; Rieth, R. D.; Jones, W. D. Thermodynamic Trends in Carbon–Hydrogen Bond Activation in Nitriles and Chloroalkanes at Rhodium. *J. Org. Chem.* **2009**, *74*, 6907-6914.

(59) Tellers, D. M.; Skoog, S. J.; Bergman, R. G.; Gunnoe, T. B.; Harman, W. D. Comparison of the Relative Electron-Donating Abilities of Hydridotris(pyrazolyl)borate and Cyclopentadienyl Ligands: Different Interactions with Different Transition Metals. *Organometallics* **2000**, *19*, 2428-2432.

(60) Ho, H.-A.; Dunne, J. F.; Ellern, A.; Sadow, A. D. Reactions of Tris(oxazolinyl)phenylborato Rhodium(I) with C–X (X = Cl, Br, OTf) Bonds: Stereoselective Intermolecular Oxidative Addition. *Organometallics* **2010**, *29*, 4105-4114.

(61) Xu, S.; Everett, W. C.; Ellern, A.; Windus, T. L.; Sadow, A. D. Oxygen Insertion Reactions of Mixed N-Heterocyclic Carbene-Oxazolinylborato Zinc Alkyl Complexes. *Dalton Trans.* **2014**, *43*, 14368-14376.

(62) Xu, S.; Manna, K.; Ellern, A.; Sadow, A. D. Mixed N-Heterocyclic Carbene–Bis(oxazolinyl)borato Rhodium and Iridium Complexes in Photochemical and Thermal Oxidative Addition Reactions. *Organometallics* **2014**, *33*, 6840-6860.

(63) Jones, W. D.; Hessell, E. T. Synthesis and Structures of Rhodium Isocyanide Complexes Containing an η^2-Hydrotris(3,5-dimethylpyrazolyl)borate Ligand. *Inorg. Chem.* **1991**, *30*, 778-783.

(64) Hill, R. H.; Wrighton, M. S. Oxidative Addition of Trisubstituted Silanes to Photochemically Generated Coordinatively Unsaturated Species $(\eta^4\text{-}C_4H_4)Fe(CO)_2$, $(\eta^5\text{-}C_5H_5)Mn(CO)_2$, and $(\eta^6\text{-}C_6H_6)Cr(CO)_2$ and Related Molecules. *Organometallics* **1987**, *6*, 632-638.

(65) Young, K. M.; Wrighton, M. S. Temperature Dependence of the Oxidative Addition of Triethylsilane to Photochemically Generated $(\eta^5\text{-}C_5Cl_5)Mn(CO)_2$. *Organometallics* **1989**, *8*, 1063-1066.

(66) Cargill, R. W.; Battino, R.: *Carbon monoxide*; Pergamon: Oxford, 1990.

(67) Espenson, J. H.: *Chemical Kinetics and Reaction Mechanisms*; 2nd ed.; McGraw-Hill: New York, 1995.

(68) Walsh, R. Bond Dissociation Energy Values in Silicon-Containing Compounds and Some of Their Implications. *Acc. Chem. Res.* **1981**, *14*, 246-252.

(69) Parkin, G. Temperature-Dependent Transitions Between Normal and Inverse Isotope Effects Pertaining to the Interaction of H–H and C–H Bonds with Transition Metal Centers. *Acc. Chem. Res.* **2009**, *42*, 315-325.

(70) Powell, J.; Shaw, B. L. Transition metal–carbon bonds. Part XIII. Di-μ-chlorodicarbonyldi-(ethylene)dirhodium(I). *J. Chem. Soc. A* **1968**, 211-212.

(71) Visco, M. D.; Wieting, J. M.; Mattson, A. E. Carbon–Silicon Bond Formation in the Synthesis of Benzylic Silanes. *Org. Lett.* **2016**, *18*, 2883-2885.

(72) Bailey, P. J.; Coxall, R. A.; Dick, C. M.; Fabre, S.; Henderson, L. C.; Herber, C.; Liddle, S. T.; Loroño-González, D.; Parkin, A.; Parsons, S. The First Structural Characterisation of a Group 2 Metal Alkylperoxide Complex: Comments on the Cleavage of Dioxygen by Magnesium Alkyl Complexes. *Chem. Eur. J.* **2003**, *9*, 4820-4828.

Additional Information

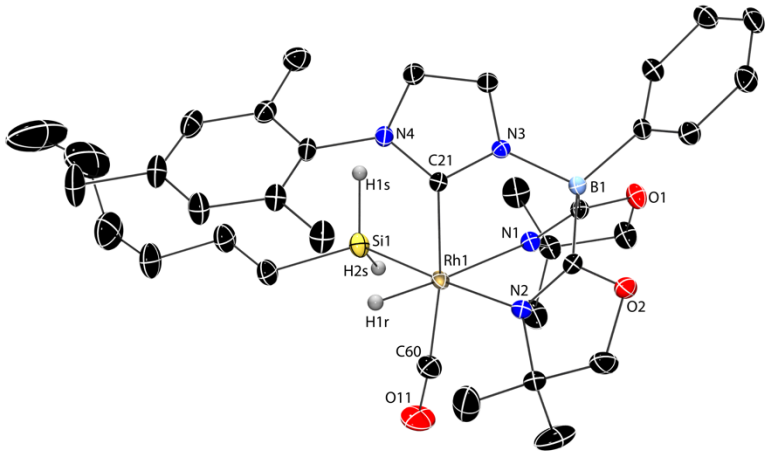

Figure 2-7. Thermal ellipsoid plot of {PhB(Ox^{Me2})$_2$$Im^{Mes}$}RhH($SiH_2C_6H_{13}$)CO (2b) with ellipsoids at 35% probability. H atoms bonded to Si1 and to Rh1 were found objectively in a difference Fourier map and refined using an isotropic approximation. H atoms are not plotted (for clarity) with the exception of H bonded to Rh1 and Si1. Selected interatomic distances (Å): Rh1–Si1, 2.3231(7); Rh1–C21, 2.067(2); Rh1–C60, 1.876(2); Rh1–H1r, 1.50(3); Rh1–N1, 2.190(2); Rh1–N2, 2.230(2).

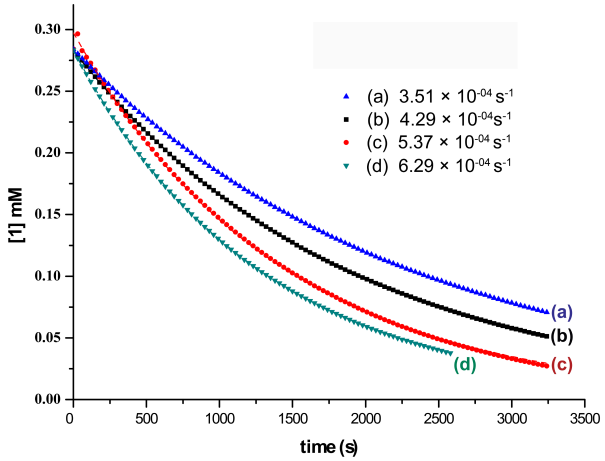

Figure 2-8. Plots of [1] vs. time for a series of [$PhSiH_3$] = (a) 19.2, (b) 23.8, (c) 29.1, and (d) 34.8 mM in benzene at 308.3 K, monitored at 385.5 nm. $[CO]_{ini}$ = 0 mM. k_{obs} values are calculated from a non-linear least-squares regression analysis.

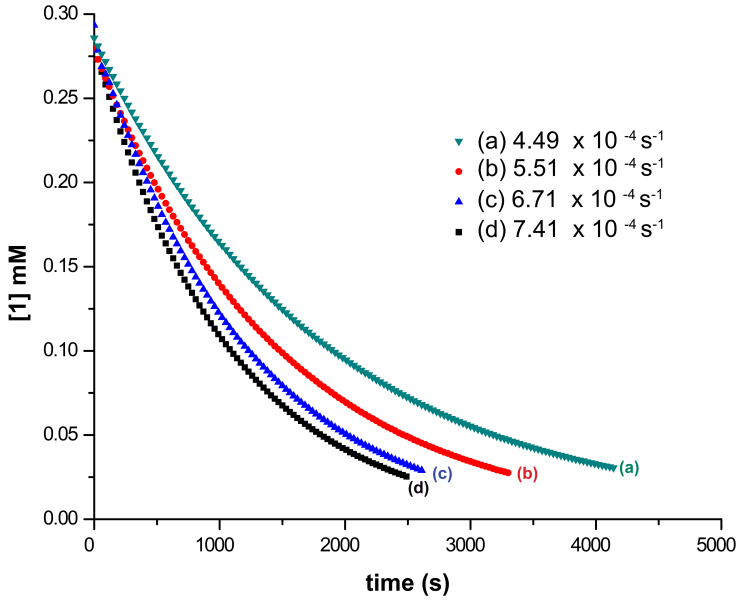

Figure 2-9. Plots of [1] vs. time for [$PhSiH_3$] = (a) 19.2, (b) 23.8, (c) 29.1, and (d) 32.9 mM in benzene at 312.3 K, monitored at 385.5 nm. $[CO]_{ini}$ = 0 mM. k_{obs} values are calculated from a non-linear least-squares regression analysis.

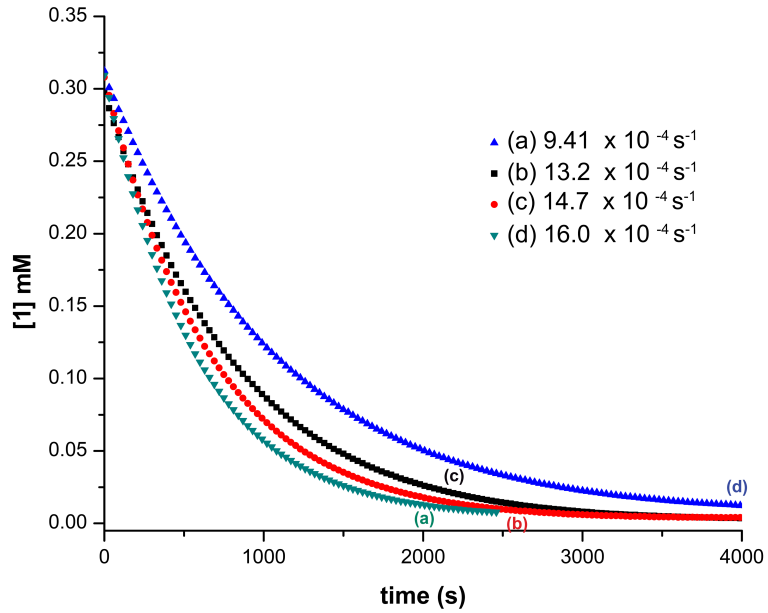

Figure 2-10. Plots of [1] vs. time for [$PhSiH_3$] = (a) 19.2, (b) 23.8, (c) 29.1, (d) 34.8 mM, in benzene at 322.3 K, monitored at 385.5 nm. $[CO]_{ini}$ = 0 mM. kobs values are calculated from a non-linear least-squares regression analysis.

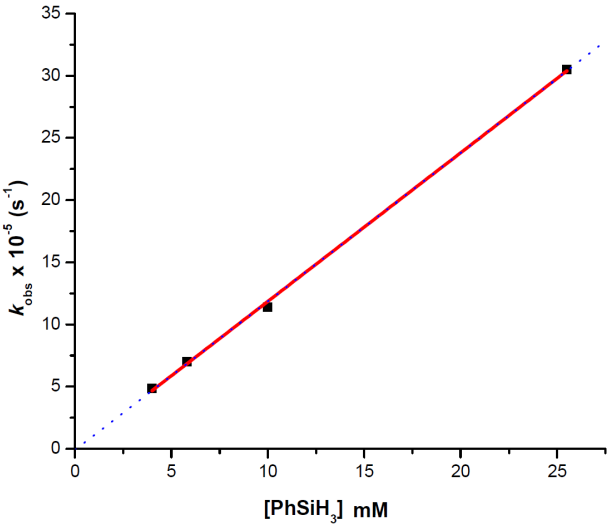

Figure 2-11. Plot of k_{obs} vs. [$PhSiH_3$] (4.0, 5.8, 10.0, 25.5 mM) from reactions performed at 296 K. Values were obtained by non-linear least-squares regression analysis from data given in Figure 2-4.

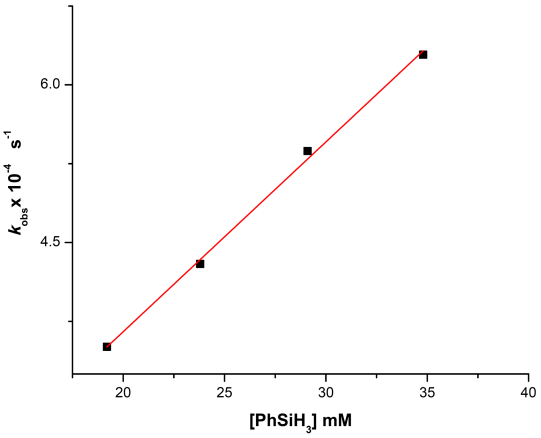

Figure 2-12. Plot of k_{obs} vs. [$PhSiH_3$] (19.2, 23.8, 29.1, 34.8 mM) from reactions performed at 308.3 K. Values were obtained by non-linear least-squares regression analysis from data given in Figure 2-11.

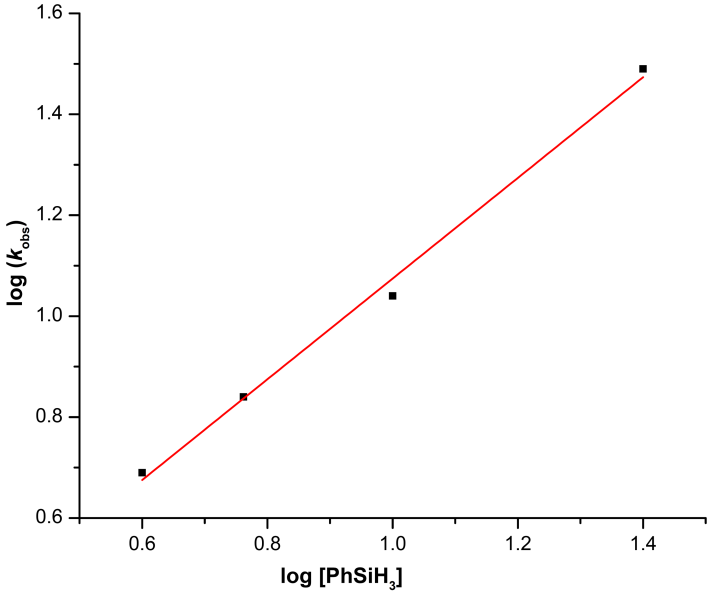

Figure 2-13. Plot of log[$PhSiH_3$] vs. log(k_{obs}) at 296 K. The slope ~ 1 indicates first-order dependence on [$PhSiH_3$].

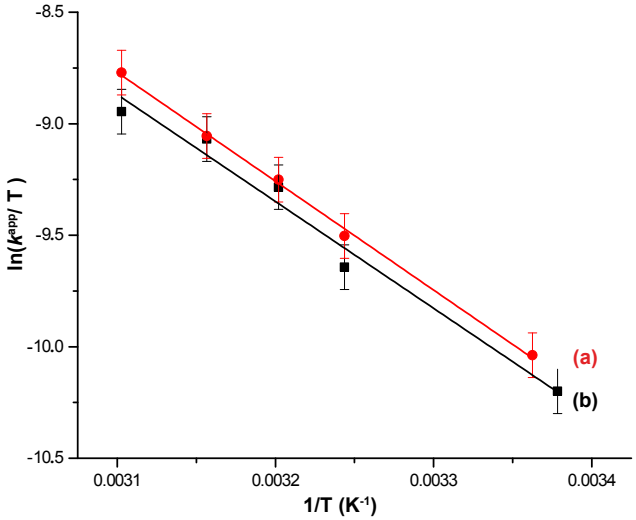

Figure 2-14. Eyring plots (ln(k^{app} /T) vs 1/T) for (a) k_H^{app} from reactions of 1 and $PhSiH_3$ and (b) k_D^{app} from reactions of $PhSiD_3$.

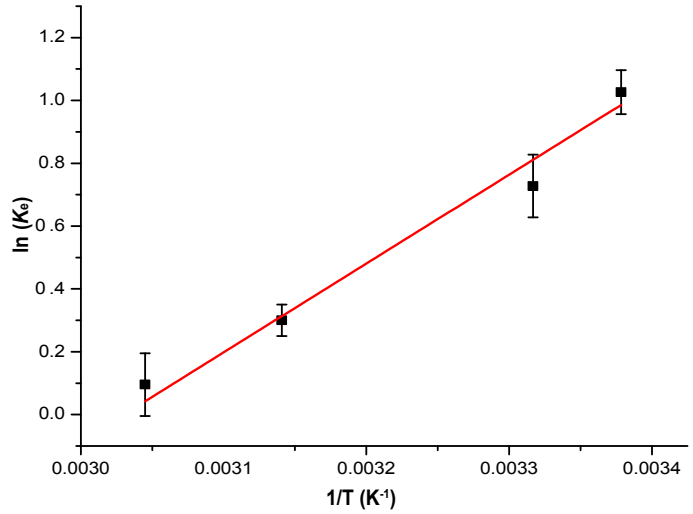

Figure 2-15. van't Hoff plot of the temperature dependence of K_e to derive the free enthalpy ($\Delta H°$) and entropy ($\Delta S°$) from reaction of 1 and $PhSiH_3$ in $[CO]_{ini}$=7.3 mM.

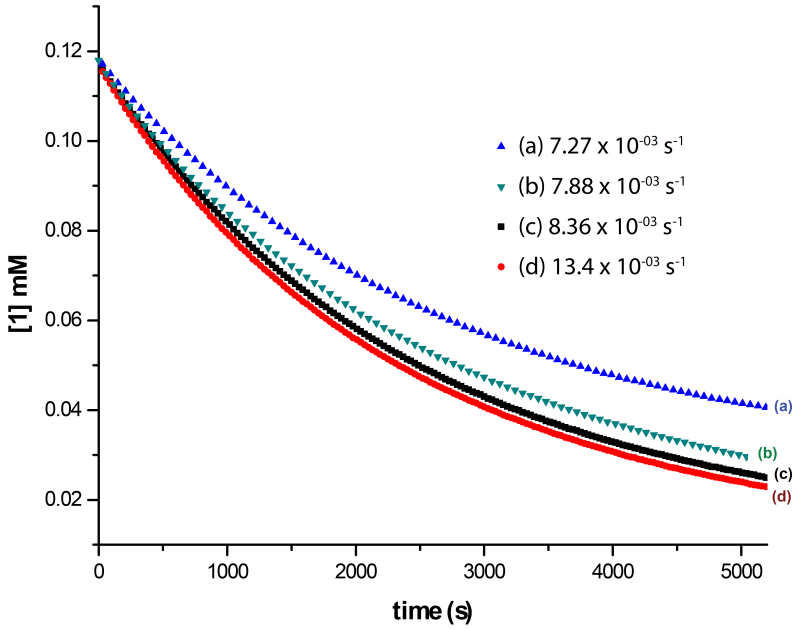

Figure 2-16. Plots of [1] vs. time for $[PhSiH_3]$ = 14.0, 15.0, 15.7, 18.0 mM in presence of [CO] = 7.3 mM, in benzene at 308.3 K, monitored at 385.5 nm.

Table 2-3. K_e, k_1, and k_{-1} values for 1 and $PhSiH_3$ ⇌ 2a and CO; $[CO]_e$ = 7.3 mM.

Temperature (K)	K_e	k_1	k_{-1}
297.4	2.8 ± 0.1	0.011 ± 0.001	0.0040 ±0.0003
301.5	2.1 ± 0.3	0.014 ± 0.001 [b]	0.0058 ± 0.0004 [b]
308.4	1.8 ± 0.2[a]	0.019 ± 0.001	0.011 ± 0.001
318.4	1.4 ± 0.1	0.041 ± 0.002	0.030 ± 0.002
328.4	1.1 ± 0.1	0.078 ± 0.002	0.075 ± 0.002

[a] From van't Hoff analysis. [b] From Eyring analysis

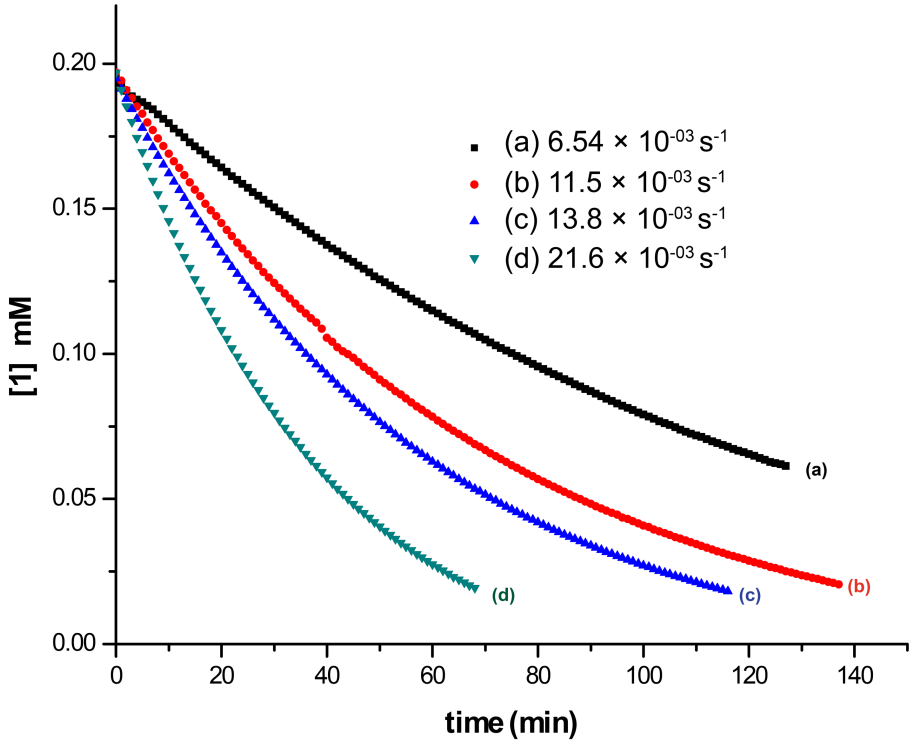

Figure 2-17. Plots of [1] vs. time for $[MeOC_6H_4SiH_3]$ = (a) 12.2, (b) 20.5, (c) 33.3, (d) 40.5 mM, in benzene at 297 K, monitored at 385.5 nm. $[CO]_{ini}$ = 0 mM. k_{obs} values are calculated from a non-linear least-squares regression analysis.

References

1. J. Powell and B. L. Shaw, *J. Chem. Soc. A*, 1968, 211-212.

2. S. Xu, K. Manna, A. Ellern and A. D. Sadow, *Organometallics*, 2014, **33**, 6840-6860.

3. M. D. Visco, J. M. Wieting and A. E. Mattson, *Org. Lett.*, 2016, **18**, 2883-2885.

4. P. J. Bailey, R. A. Coxall, C. M. Dick, S. Fabre, L. C. Henderson, C. Herber, S. T. Liddle, D. Loroño-González, A. Parkin and S. Parsons, *Chem. Eur. J.*, 2003, **9**, 4820-4828.

CHAPTER 3. SILICA SURFACE MODIFICATION VIA A RU CATALYZED DEHYDROCOUPLING REACTION WITH SILANES

Abhranil Biswas, Zhouran Wang, Igor Slowing, Marek Pruski, Aaron Sadow

Abstract

A new silica surface functionalization technique is reported using $RuHCl(PPh_3)_3$ **(1)** catalyzed dehydrocoupling reactions between surface silanols (≡SiOH) and hydrosilanes. **1** efficiently catalyzes the cross-dehydrocoupling reaction between primary- and secondary- hydrosilanes and alcohols in homogeneous conditions with high selectivity towards mono(alkoxy)hydrosilane. Also, **1** can catalyze the cross-dehydrocoupling reaction between hydrosilanes and amines to form selective silazane moieties containing Si–N bonds. The similar method used to modify Si–OH by reacting it to various hydrosilanes in the presence of **1** to produce mostly $Si–O–SiR_3$. The resulting product shows the disappearance of isolated O–H stretching at 3747 cm^{-1} as well as the presence of new Si–H stretching at ~ 2150 cm^{-1}. More conclusive evidence was found by studying solid-state NMR of the grafted material. Si–H bonds on the surface were further reacted with amines in presence of **1** to produce the first surface silazane compound. The product was characterized using DRIFT. Elemental analysis of the material confirms the presence of nitrogen on the surface. Notably, starting from silica material to the silazane synthesis was successfully done in a one-pot technique.

Introduction

Surface modification of predesigned silica has gained great attention in last few decades because of its ubiquitous applications in biosensing,[1, 2] surface chemistry,[3-5] analytical chemistry,[7,8] drug delivery,[9-13] photonics,[14] electronics[15] and optics.[16, 17] The most common technique to achieve these modifications is based on attaching an organic self-assemble monolayer

which gives an excellent control to tune the surface properties.[18] The technique involves the reaction between surface silanol (Si-OH) and a functionalized organosilicon moiety like chlorosilane, resulting in a material with Si–O–Si bonded species via a substitution reaction on the silicon center. The commonly used organosilicon compounds for this process are chlorosilanes,[19] alkoxysilanes,[20] silazanes[21, 22] and other halosilanes[23] (Scheme 3-1). Despite its simplicity, the process involves the formation of undesirable polysiloxanes.[24] In addition, the precursors are often air- and moisture sensitive and difficult to purify.[25]

Scheme 3-1. General synthetic routes for silica functionalization.

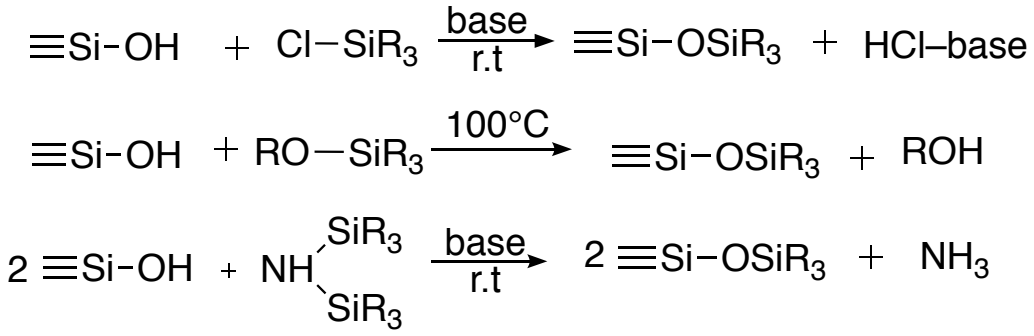

An alternate route to achieve the desired grafted species is via a dehydrogenative coupling with Si–H activation of organosilanes. In one of the earliest examples, Buriak and co-workers have successfully used early transition metal catalysts to couple silicone surface Si–H with heterosilanes,[26] resulting in a new functionalized silicone material. A more recent example was from Veinot where he and his co-workers have used a Rhodium complex as a catalyst to couple organohydrosilanes with H-terminated Si nanoparticles.[27] Even though functionalization of surface Si–H bonds via dehydrogenative coupling with organosilanes have been widely reported, not many studies were found for surface Si–OH bonds (from silica material) functionalization using a similar method. In fact, the only examples of creating Si–H

bonds on silica surface involves reacting the silica material with Hydrogen gas at very high temperature (1273 K)[28] or putting the silica material through multiple chemical reactions also at high temperature (3 steps, 800 K).[29] A new catalytic route was needed to functionalize surface silanols effectively as well as to create Si–H on the silica surface. Moitra and co-workers have shown that $B(C_6H_5)_3$ can be used as an effective catalyst to modify surface silanols via dehydrogenative coupling with tertiary silanes.[30] Not surprisingly the catalyst was only able to activate mostly tertiary silanes and secondary silanes in few cases but was unreactive towards primary silanes.[31, 32]

In this work, we describe a novel catalytic process to functionalize silica via dehydrogenative coupling with primary, secondary and tertiary silanes. We have further demonstrated an efficient route to functionalize surface Si–H bonds via dehydrocoupling with amines to make Si–N bonds on the surface.

Results and discussions

Cross dehydrocoupling reactions of Si–H and O–H bonds are widely studied. A number of transition metal-based catalysts include titanium,[32-34] manganese,[35] zinc,[36] iron,[37] rhenium,[38] copper,[39, 40] rhodium,[41] ruthenium,[42, 43] gold[44] and platinum complexes[45] are known for efficient dehydrocoupling of silane and alcohol to produce siloxanes and hydrogen gas (Scheme 3-2).

Scheme 3-2. General dehydrocoupling reaction of silanes and alcohols.

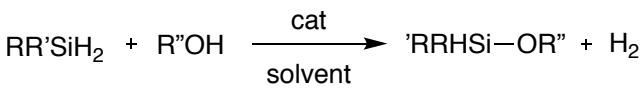

$RuHCl(PPh_3)_3$ (**1**) was found to be most effective in silane-alcohol dehydrocoupling reaction in comparison to a few highly efficient homogeneous catalysts reported in the literature

(Table 3-6). A mixture of $PhSiH_3$ and 2-propanol in presence of 1 mol % **1** at room temperature produces $PhSiH_2O$*i*Pr as the major product (95% selectivity) with 100% conversion within 5 mins (Table 6, Entry 9). For comparison, Cp_2TiCl_2/*n*BuLi system converts all Si–H bonds of primary and secondary silanes into silyl ether linkages in presence of alcohol (Table 6, Entry 1) and a more selective catalyst, To^MZnH need higher temperature and longer reaction time to for the reaction to go to completion (Table 6, Entry 6).

Table 3-1. $RuHCl(PPh_3)_3$ catalyzed cross-dehydrocoupling of hydrosilanes and alcohols.[a]

entry	substrates		cat	time	Product
	alcohol (0.9 eq)	**silane**	(% mol)	(min)	
1	*i*PrOH	$PhSiH_3$	5	<5	$PhSiH_2O$*i*Pr[b]
2	MeOH	$PhMeSiH_2$	5	<5	PhMeSiHOMe
3	*i*PrOH	$PhMeSiH_2$	5	< 5	PhMeSiHO*i*Pr
4	*i*PrOH	$PhMeSiH_2$	1	<5	PhMeSiHO*i*Pr
5	*i*PrOH	$PhMeSiH_2$	0.1	60	PhMeSiHO*i*Pr
6	*t*BuOH	$PhMeSiH_2$	1	20	PhMeSiHO*t*Bu
7	*t*BuOH	$PhMeSiH_2$	1	<5	PhMeSiHO*t*Bu
8	EtOH	$PhMeSiH_2$	1	<5	PhMeSiHOEt

[a] Reaction was monitored using ^1H NMR spectroscopy; [b] produced *i*$PrOSiH_2Ph$ as the major product (95%).

Compound **1** catalyzes dehydrocoupling reaction of phenylmethylsilane with primary, secondary and tertiary alcohols. Initial catalysis was carried out with 5 mol % catalyst, which can be reduced to 1 mol% without affecting the conversion and reaction time (Table 1, Entry 4).

Expectedly in presence of 0.1 mol% **1**, the reaction takes a longer time to achieve high conversion (Table 1, Entry 5). In the case of tertiary alcohol, the reaction appears to be slower at room temperature compared to primary and secondary alcohol (Table 1, Entry 6, 7, 11). Importantly, secondary silanes produced only mono dehydro-coupled product (such as PhMeHSi–OEt) and no di-dehydro-coupled products (e.g., $PhMeSi(OEt)_2$) was detected in the reaction mixture.

Having an excellent catalyst in hand we began to explore grafting experiments. The silica support, in the form of SBA-15 type MSN characterized by a hexagonal array (p6mm) of 9.7 nm diameter pores and a surface area of 782 m^2/g, was produced by hydrolysis−condensation of tetramethyl orthosilicate using the Pluronic P104 template, calcined at 550 °C, washed with water, then heated at 500 °C under vacuum, and subsequently stored in a glovebox away from ambient air and moisture. The SiOH group surface concentration of 1.8 mmol/g was determined by measuring the concentration of toluene produced in a titration $Mg(CH_2Ph)_2(O_2C_4H_8)_2$.[46] The DRIFT spectra showed a sharp absorption at 3747 cm^{-1} assigned to isolated silanol $\nu_{O\text{-}H}$ (Figure 3.1A).

Scheme 3-3. Grafting of hydrosilanes on silica surface via dehydrocoupling reaction.

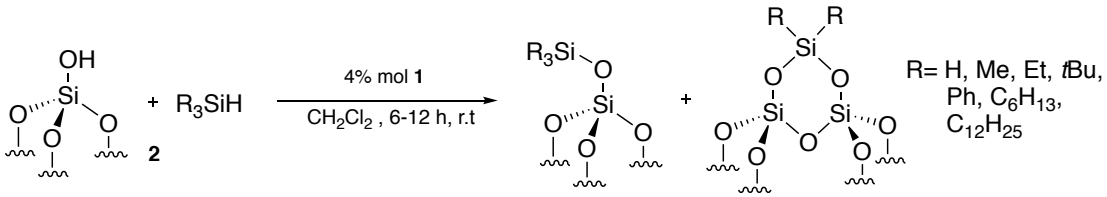

2 **G1-G8**

Thus, prepared silica material (**2**) was reacted in methylene chloride with 10 eq of phenylsilane in presence of **1** (4% mol) for 12 h at room temperature, producing a silane grafted material (**G1**). After the reaction, the material was filtered and was washed vigorously to remove any residual phenylsilane as well as Ru catalyst. ICP-OES measurement confirms the removal of

ruthenium from the material. An IR spectrum of the product contains several new peaks at 3073 cm^{-1}, 3016 cm^{-1} which corresponds to ν_{C-H} of C–H and 2176 cm^{-1} (Figure 3-1B) which can be assigned to Si–H. Significantly the characteristic peak for isolated Si–OH (3747 cm^{-1}) was diminished during this reaction which suggests a successful cross-coupling reaction with phenyl silane.

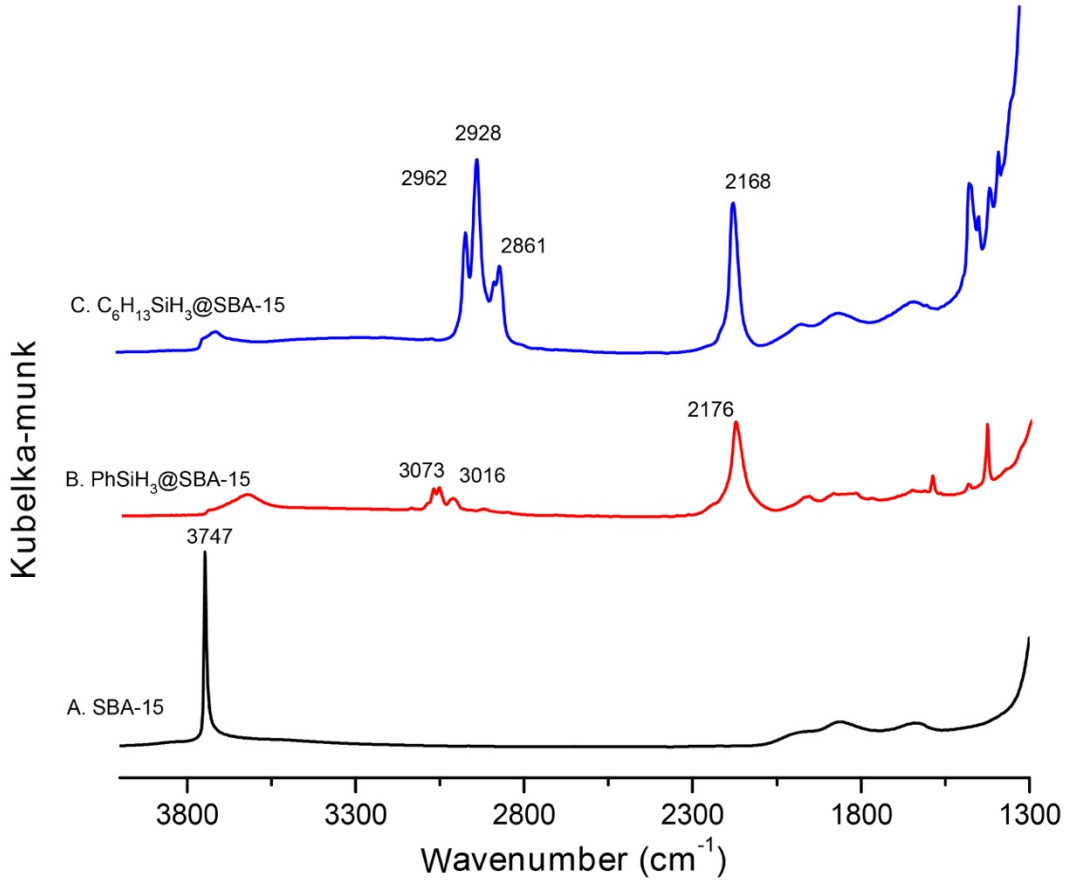

Figure 3-1. Infra-red absorption spectra of (A) SBA-15 heated at 500°C under vacuum for 12 h (**2**), (B) phenylsilane grafted on SBA-15; **G1**, (C) *n*-hexylsilane grafted on SBA-15, **G2.**

The amount of silane grafted on the surface can be determined by measuring the remaining Si–OH on the surface after grafting. The difference in Si–OH concentration between the free silica and grafted silica will give the amount of Si–OH that been grafted with silica. The Si–OH

concentration on the grafted material was measured by titrating it against $Mg(CH_2Ph)_2(O_2C_4H_8)_2$. Maximum silanol covered for **G1** found to be 0.84 mmol/g (Table 4, Entry 1). Also, elemental analysis of **G1** shows carbon weight % of 4.7 which corresponds to organic loading of 0.64 mmol/g. The lower organic loading compared to findings from titration could be attributed to multiple modes of grafting (Scheme 3). Additionally, excess of **2** was added to 15 mg of **1** in 0.6 ml 0.009 M solution of hexamethylbenzene in CD_2Cl_2. The total amount of silane reacted with the silica is 0.01 mmol which gives a silane loading of 0.67 mmol/g.

Grafting process was further studied in different solvents and methylene chloride found to be most effective with 0.84 mmol/g Si–OH covered in 12 h (Table 2, Entry 1). For comparison grafting in benzene with phenylsilane gives 0.48 mmol/g and in diethylether gives 0.68 mmol/g Si–OH covered at the same reaction time (Table 2, Entry 3,4). At reduced catalyst loading (1 mol %) in 12 h, only 0.45 mmol/g silanol was grafted with phenylsilane and IR spectra of the material show the absorption of both isolated silanol (3747 cm^{-1}) as well grafted Si–H (2174 cm^{-1}) confirming a partially grafted species (Figure 3-5).

A number of different primary, secondary and tertiary silanes tested for the silane grafting process (Table 2). To compare, *n*-hexylsilane reacts with **1** in 6 h to get the grafted product (**G2**) compared to phenylsilane which takes 12 h (Table 2, Entry 5). Infra-red spectra of **G2** shows a peak at 2168 cm^{-1} assigned to grafted Si–H bond (Figure 3-1.C). Notably, dodecylsilane gave full conversion in 12 h to form grafted product (**G3**) which could be attributed to the steric bulkiness of the silane. Reaction with secondary and tertiary silanes proved to be slower than primary silanes and produced partially grafted silane material. For example, reaction with diethylsilane resulted in only 0.55 mmol/g Si–OH grafting (**G5**) whereas triethylsilane resulted in 0.27 mmol/g Si–OH grafted (**G6**) (Table 2, Entry 8, 9). Notably absence of Si–H absorbance in

the DRIFT spectra of triethyl silane grafted material confirms that the Si–H bond has reacted with Si–OH (Figure 3-6).

Table 3-2. Catalytic silica surface modification via dehydrogenative coupling of silanols and hydrosilanes using **1** as catalyst.[a]

entry (Product)	silane (10 eq)	solvent	time (h)	Si-OH covered (mmol/g)[b]	ν_{Si-H} stretching (cm^{-1})	C loading (%)	Si-R loading (mmol/g)[c]
1 (**G1**)	$PhSiH_3$	CH_2Cl_2	12	0.82	2174	4.6	0.64
2	$PhSiH_3$	Benzene	12	0.48	-	-	-
3	$PhSiH_3$	Ether	12	0.65	-	-	-
4 [d]	$PhSiH_3$	CH_2Cl_2	12	0.45	-	-	-
5 (**G2**)	*n*-hexylsilane	CH_2Cl_2	6	0.80	2165	4.8	0.70
6 (**G3**)	dodecylsilane	CH_2Cl_2	12	0.78	2166	10.7	0.74
7 (**G4**)	$PhMeSiH_2$	CH_2Cl_2	12	0.82	2157	6.3	0.76
8 (**G5**)	Et_2SiH_2	CH_2Cl_2	12	0.52	2148	2.5	0.52
9 (**G6**)	Et_3SiH	CH_2Cl_2	12	0.27	-	1.8	0.25
10 (**G7**)	Ph_2MeSiH	CH_2Cl_2	12	0.41	-	6.4	0.41
11 (**G8**)	$(t\text{Bu})_3SiH$	CH_2Cl_2	12	0.11	-	1.4	0.09

[a] 4% cat loading, [b] measured from titration, [c] measured from elemental analysis, [d] 1% cat loading.

In order to further characterize the material ^1H solid-state NMR of **G1** was measured. In

Figure 3-2, the peak resonating at 4.6 ppm is assigned to Si–H and the peaks resonating at 7.1 ppm is assigned to protons of Ph- group. The ^{29}Si CPMAS spectra of **G1** (Figure 3-3A) shows that the silane was grafted in both mono-podal and bipodal ways (M site and D site respectively) with a predominant presence of mono-podal species. The four carbon peaks in ^{13}C CPMAS resonating in the range of 120 ppm – 140 ppm (Figure 3-3B) agree well with the four types of carbons in phenylsilyl ($C_6H_5SiH_n$–) groups. However, there is another weak and broad carbon peak resonating around 152 ppm. This may indicate a minor amount of phenyl groups attached to the silica surface through an oxygen link.

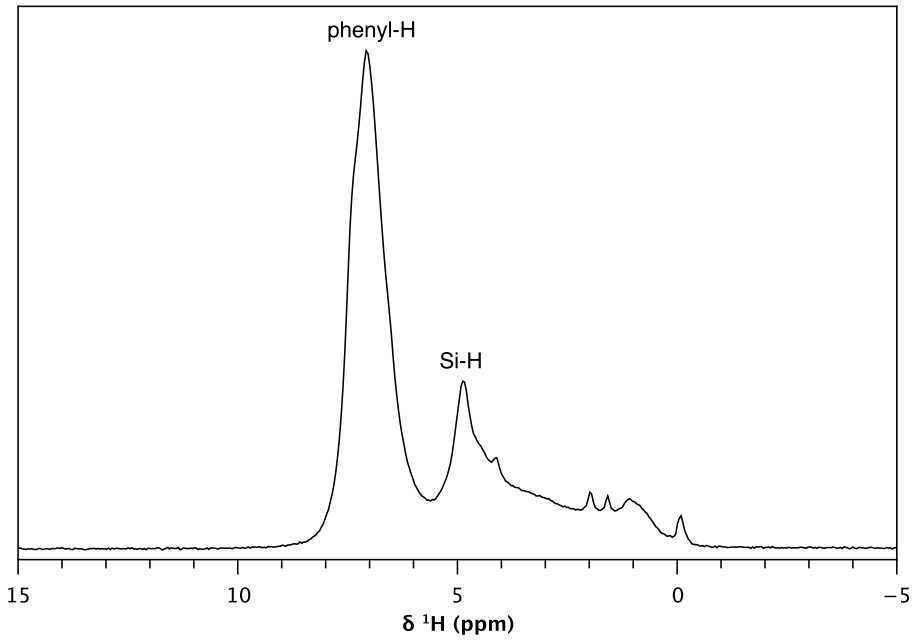

Figure 3-2. (A) ^{1}H Hahn echo spectra of **G2**. The spectra were obtained using MAS 36kHz, 10s recycle delay, 16 scans, 100 kHz (^{1}H 90˚), 20.48ms acquisition, 27.8µs echo delay.

The thermal stability of the newly grafted material was measured in an in-situ IR apparatus where the material was heated at different temperatures for 1 h time and absorption spectra were measured. In case of **G2** the absorption spectra show decent stability till 200° C (Figure 3-3.A-B) whereas at a higher temperature (300° C) peaks corresponding to the organic moieties started to disappear (Figure 3-3C) and at 400° C the organics got decomposed and the isolated SiOH grew

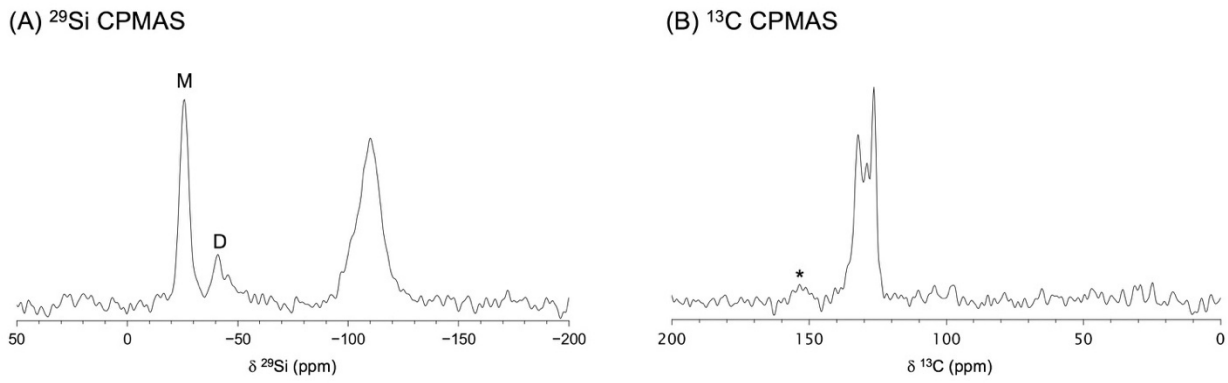

Figure 3-3. (A) ^{29}Si CPMAS and (B) ^{13}C CPMAS spectra of $PhSiH_n$@MSN acquired with B_0 = 9.4 T, ν_R = 8 kHz, $\nu_{RF}(^1H)$ = 36 kHz for the 90° and CP pulses, $\nu_{RF}(^1H)$ = 25 kHz for SPINAL-64 heteronuclear decoupling, $\nu_{RF}(^{29}Si) = \nu_{RF}(^{13}C)$ = 27 kHz for CP pulses, τ_{CP} = 5 ms (A), τ_{CP} = 4 ms (B), τ_{RD} = 7.8 s, *ns* = 3072 (A) and *ns* = 2048 (B).

back at 3747 cm^{-1}. A similar trend was also observed for **G1** (Figure 3-9). Thus, the existence absorption corresponding to silane moiety even at 200° C definitely proves that the primary silane is actually grafted and not just absorbed on the surface.

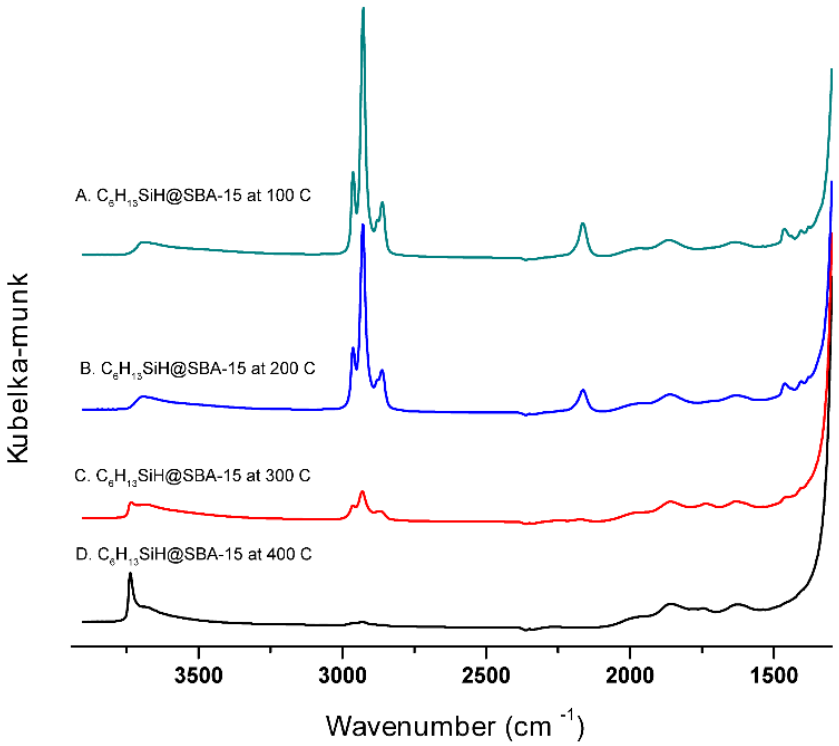

Figure 3-3. Infrared spectra of **G2** heated under vacuum at temperature (A) 100°C, (B) 200°C, (C) 300°C, (D) 400°C.

The silane grafted silica material was further modified via catalytic cross-coupling reactions with amines. Metal catalyzed homogeneous dehydrocoupling reaction between silanes and amines has been an efficient way to form Si–N bonds.[48-51] In our studies, we found that **1** is significantly effective in catalyzing dehydrogenative coupling between silanes and amines. At 5 mol % catalyst loading, the coupling between *i*PrNH$_2$ and phenylsilane gives 100% conversion in 5 minutes at room temperature (Table 3-3, Entry 1). Catalyst loading can be reduced to 1 mol % without altering the conversion (Table 3-3, Entry 2). **1** also effectively catalyzes coupling between *i*PrNH$_2$ and PhMeSiH$_2$ to provide 100 % conversion within 5 minutes.

Scheme 3-4. General dehydrocoupling reaction of silanes and amines.

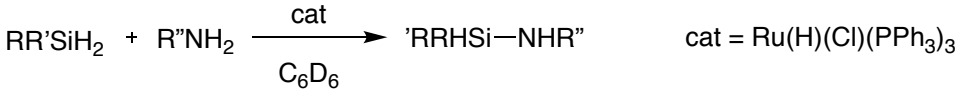

To functionalize the grafted silanes, a mixture of **G1** and *i*PrNH$_2$ in presence of **1** was stirred in methylene chloride for 6 h. The resulting material was filtered and dried under vacuum at room temperature to produce novel surface silazane grafted silica material (**G11**). The reaction was monitored via IR spectra which reveals that the Si-H absorption of **G1** disappeared and new absorption for alkyl C–H stretching (2952, 2923 and 2865 cm^{-1}) was observed (Figure 3-4C). Also, the absorption of aromatic C–H stretching corresponding to phenyl moiety remained unchanged. The amount of grafted amine was measured via elemental analysis. From elemental analysis data, the amine loading **G11** was found to be 0.58 mmol/g which is lower than Si-H loading. The difference in the loading of Si–H and amines can be attributed to different modes of coupling (Scheme 4).

Scheme 3-5. Catalytic dehydrocoupling reaction of grafted Si–H and N–H of amines.

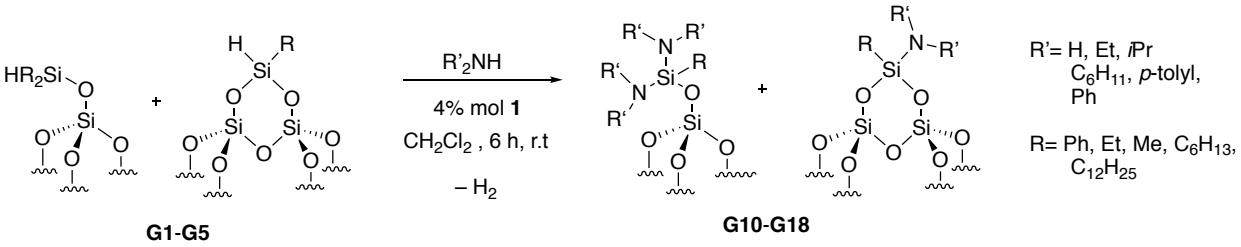

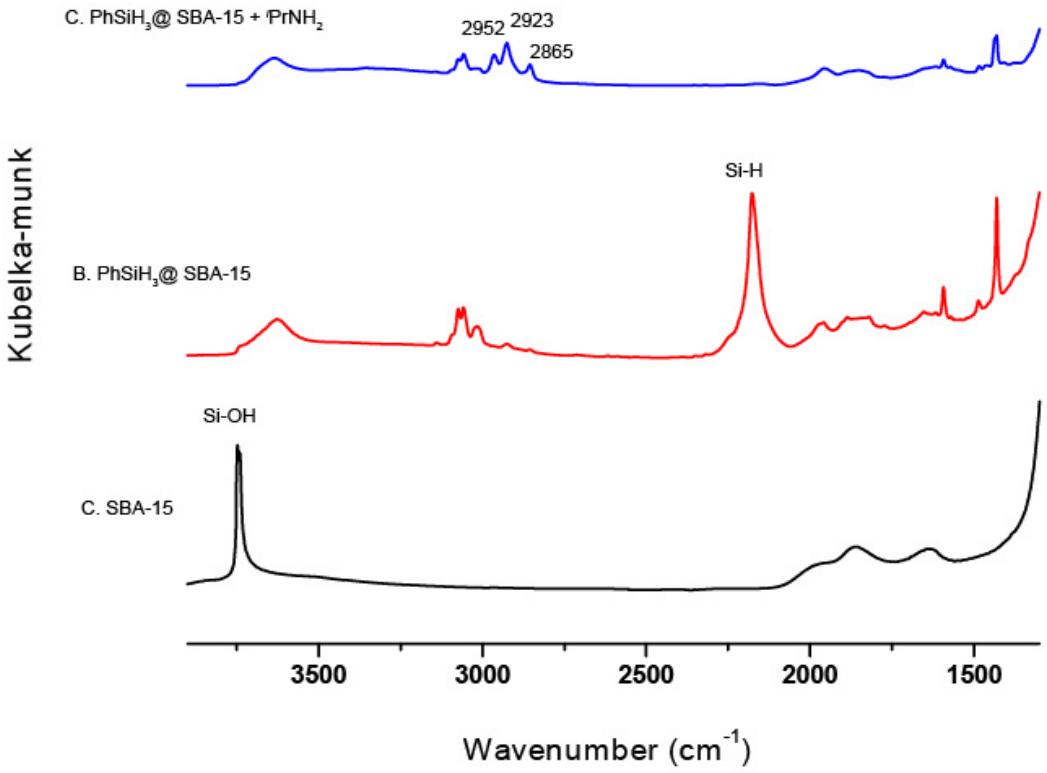

Figure 3-4. Infra-red absorption spectra of (A) treated SBA-15 (**2**), (B) **G1**, (C) **G1** + *i*PrNH$_2$ (**G10**).

The grafted Si–H bond functionalization with various combinations of silanes and amines (Table 3-5) was performed, and corresponding grafted silyl-amine (silazane) loading was measured via elemental analysis. For example, a mixture of **G4** and *i*PrNH$_2$ in presence of 4 mol % of **1** gives a silazane grafted product (**G11**) with nitrogen loading 0.58 mmol/g. Reaction works even at low catalyst loading (1 mol%) at a longer reaction time to reach full conversion. Both aromatic and aliphatic silane grafted materials showed similar reactivity towards coupling reactions with different amines. Significantly aromatic amines found to be less reactive compared to aliphatic amines. Reacting **G1** with aniline and toluidine produced silazane with N loading of

0.15 mmol/g and 0.33 mmol/g respectively.

Table 3-5. Synthesis of grafted silazane compound via catalytic dehydrocoupling reaction between different silane-amine combinations.

silane grafted	amine (10 eq) (**Product**)	cat loading (mol %)	time (h)	N loading (mmol/g)[a]
$PhSiH_3$	*i*$PrNH_2$ (**G10**)	4	6	0.58
$PhSiH_3$	*i*$PrNH_2$	1	20	–
$PhMeSiH_2$	*i*$PrNH_2$ (**G11**)	4	6	0.46
n-$C_{12}H_{25}SiH_3$	cyclohexylamine (**G12**)	4	6	0.61
$PhSiH_3$	cyclohexylamine (**G13**)	4	6	0.64
n-$C_6H_{13}SiH_3$	cyclohexylamine (**G14**)	4	6	0.57
$PhSiH_3$	Et_2NH (**G15**)	4	6	0.58
n-$C_{12}H_{25}SiH_3$	Et_2NH (**G16**)	4	6	0.54
$PhSiH_3$	toluidine (**G17**)	4	12	0.33
$PhSiH_3$	aniline (**G18**)	4	12	0.15

[a] measured from elemental analysis

In addition, a one-pot conversion from silica material (**2**) to surface silazane (**G10**) was successfully carried out (Scheme 3-6). **2** was stirred with excess phenylsilane at room temperature

Scheme 3-6. One-pot route for synthesis of surface silazane.

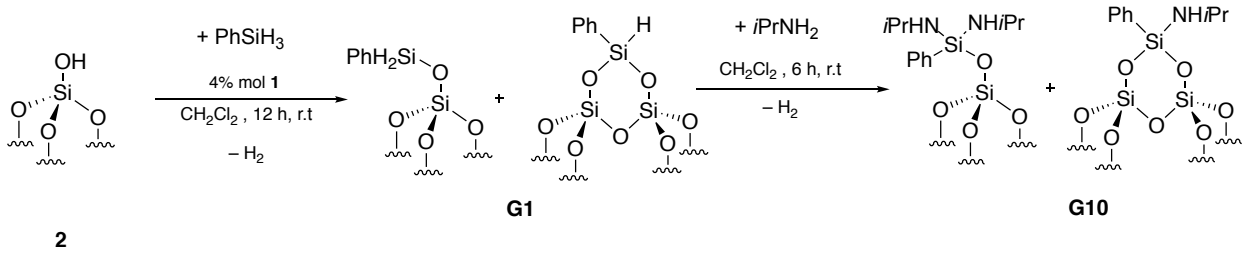

for 12 h in methylene chloride in presence of **1**. The resulting mixture was dried under vacuum to remove solvents and excess silane leaving the active catalyst on the material (**G19**). To a suspension of **G19** in methylene chloride, 10 eq of isopropyl amine was added and the mixture was stirred for 12 h. Drying under vacuum followed by vigorous washings (3 x 5 ml) with methylene chloride provided a Ru-free (measured via ICP-OES) product (**G10**).

Conclusion

Above we have described the excellent catalytic activity of **1** in dehydrogenative coupling reaction for silane-alcohol and silane-amine in solutions forming Si–O, and Si–N bonds. Further, the efficient catalyst was utilized to modify silica surface via the dehydrocoupling reaction of silanol Si-OH and Si–H bond of different silanes with hydrogen as a side product. Both aromatic and aliphatic silanes successfully produce grafted silica material. Reactions with primary and secondary silanes form unique Si–H bonds on the surface. Notably, primary silanes react more efficiently than secondary and tertiary silanes. Newly formed grafted Si–H bonds are chemically active and were successfully further modified. **1** catalytically converted Si-H bonds to Si-N bonds via dehydrocoupling reactions with different amines to produce first-ever reported silazane grafted silica material. We have also established a one-pot efficient route for conversion of silica to silazane grafted silica material using **1** as the catalyst. We believe that this process can be extended

to functionalize other metal oxides and polymeric materials, giving it greater potential in therapeutic technologies and lithographic techniques.

Experimental Procedures

General

All reactions were performed under a dry argon atmosphere using standard Schlenk techniques or under a nitrogen atmosphere in a glovebox. Benzene, methylene chloride and pentane were dried and deoxygenated using an IT PureSolv system. Benzene-d_6 was heated to reflux over Na/K alloy and vacuum transferred. Methylene chloride-d_2 was refluxed and distilled over anhydrous CaH_2 and stored under nitrogen atmosphere. Phenylsilane, *n*-hexylsilane, n-dodecylsilane, and phenylmethylsilane were synthesized by reducing corresponding trichlorosilanes with $LiAlH_4$. SBA-15 was synthesized according to the literature, calcined at 550 °C, washed with water, and then heated to 500 °C under vacuum.

^{1}H spectra were collected on Bruker Avance III 600 or AVNEO 400 MHz NMR spectrometers. Infrared spectra were recorded on a Bruker Vertex spectrometer. Infrared spectra were recorded on neat MSN samples using a Bruker Vertex 80 spectrometer with a Harrick Praying Mantis Diffuse Reflection Accessory in an ambient chamber with ZnSe windows. These samples were prepared and maintained under an inert N_2 atmosphere. Elemental analyses were performed using a PerkinElmer 2400 Series II CHN/S in the Iowa State Chemical Instrumentation Facility. Inductively coupled plasma-optical emission spectroscopy (ICP-OES) was performed on 3 samples to measure the ruthenium loading in R_3SiH@SBA-15. The samples (2.0−4.0 mg each) were digested for 24 h in aqueous HF and HCl solution (0.18% and 5% respectively) and analyzed in a PerkinElmer Optima 2100 DV ICP-OES instrument.

Solid-state NMR (SSNMR) experiments were performed on a 400 MHz (9.4 T) Varian NMR spectrometer equipped with a 5.0-mm magic angle spinning (MAS) probe. The performed experiments included one-dimensional (1D) ^{29}Si cross-polarization (CP)MAS, ^{29}Si direct polarization (DP)MAS and ^{13}C CPMAS. The experimental parameters are labeled by the following symbols: B_0 denotes the external magnetic field; ν_R denotes the MAS rate; $\nu_{RF}(X)$ denotes the RF irradiation strength at the frequency of X nuclei; τ_{CP} denotes the CP contact time; τ_{RD} denotes the recycle delay; and *ns* denotes the number of scans. The experimental parameter values are given in the corresponding caption for each figure.

Catalytic NMR scale dehydrocoupling reactions.

General. All the reactions were done under nitrogen atmosphere in a glovebox using NMR tubes as a reaction vessel. The reaction was followed by the disappearance of silane species in the reaction mixture.

Catalyst stock solution preparation: 230 mg of **1** was transferred to a 25 mol marked volumetric flask and was filled up to the mark with benzene-d_6 and the mixture was made homogeneous.

Catalytic NMR dehydrocoupling reaction: 0.9 eq of appropriate silane was transferred to an NMR tube with a syringe followed by 0.5 ml of stock solution of **1.** To this mixture, 1 eq appropriate of alcohol/amine was added and the reaction was monitored via ^{1}H NMR. Resulting products (PhSiH2O*i*Pr, PhMeSiHOMe, PhMeSiHO*i*Pr, PhMeSiHO*t*Bu, PhMeSiHOEt, *i*PrNHSiH$_2$Ph, *i*PrNHSiHMePh) are known compounds.[37, 52, 48]

General synthesis of G1 - G9

To a suspension of 2 (100 mg) in methylene chloride, appropriate silane (10 eq, 1.8 mmol) was added followed by 6.7 mg of **1** (0.007 mmol). The mixture was stirred for 6-12 h at room temperature. Resulting pale yellow suspension was filtered, washed with methylene chloride (3 x 5 ml) and dried in *vacuo* to afford the product as a white powder. Compound **G1-G9** was characterized via infra-red absorption spectroscopy.

General synthesis of G10 - G18.

To a suspension of silane grafted silica (**G1** - **G5**) (50 mg) in methylene chloride, the required amine was added followed by 3.5 mg of **1** (0.004 mmol). The mixture was stirred for 6-12 h at room temperature. The resulting white suspension was filtered, washed with methylene chloride (3 x 5 ml) and dried in *vacuo* to afford the product as a white powder. Compound G10-G18 was characterized via infra-red absorbance spectroscopy.

General one-pot synthesis of (G10 - G11) from 2

To a suspension of **2** (100 mg) in methylene chloride, required silane (10 eq, 1.8 mmol) was added followed by 6.7 mg of **1** (0.007 mmol). The mixture was stirred for 12 h at room temperature. The solvent from the resulting suspension was removed under vacuum to produce a pale-yellow solid. The solid residue was washed with pentane (3 x 5 ml), dried in *vacuo* and suspended in methylene chloride. To the suspension required amine (10 eq, 1.8 mmol) was added and stirred for 12 h at room temperature. The final suspension was filtered, washed with methylene chloride and dried in *vacuo* to provide grafted silazane product (G10 – G11). The product was characterized via infra-red spectroscopy.

References

1. Hou, Z.; Li, C.; Ma, P. a.; Cheng, Z.; Li, X.; Zhang, X.; Dai, Y.; Yang, D.; Lian, H.; Lin, J., Up-Conversion Luminescent and Porous NaYF4:Yb3+, Er^{3+}@SiO2 Nanocomposite Fibers for Anti-Cancer Drug Delivery and Cell Imaging. *Advanced Functional Materials* **2012,** *22* (13), 2713-2722.

2. Biju, V., Chemical modifications and bioconjugate reactions of nanomaterials for sensing, imaging, drug delivery and therapy. *Chemical Society Reviews* **2014,** *43* (3), 744-764.

3. Zamboulis, A.; Moitra, N.; Moreau, J. J. E.; Cattoën, X.; Wong Chi Man, M., Hybrid materials: versatile matrices for supporting homogeneous catalysts. *Journal of Materials Chemistry* **2010,** *20* (42), 9322-9338.

4. Léonard, A.; Dandoy, P.; Danloy, E.; Leroux, G.; Meunier, C. F.; Rooke, J. C.; Su, B.-L., Whole-cell based hybrid materials for green energy production, environmental remediation and smart cell-therapy. *Chemical Society Reviews* **2011,** *40* (2), 860-885.

5. Wight, A. P.; Davis, M. E., Design and Preparation of Organic−Inorganic Hybrid Catalysts. *Chemical Reviews* **2002,** *102* (10), 3589-3614.

6. Yue, C. J.; Liu, Y.; He, R., Olefins isomerization by hydride-complexes of ruthenium. *Journal of Molecular Catalysis A: Chemical* **2006,** *259* (1), 17-23.

7. Jiang, H.; Xu, F.-J., Biomolecule-functionalized polymer brushes. *Chemical Society Reviews* **2013,** *42* (8), 3394-3426.

8. Hui, C. M.; Pietrasik, J.; Schmitt, M.; Mahoney, C.; Choi, J.; Bockstaller, M. R.; Matyjaszewski, K., Surface-Initiated Polymerization as an Enabling Tool for Multifunctional (Nano-)Engineered Hybrid Materials. *Chemistry of Materials* **2014,** *26* (1), 745-762.

9. Chen, Y.; Chen, H.; Shi, J., In Vivo Bio-Safety Evaluations and Diagnostic/Therapeutic Applications of Chemically Designed Mesoporous Silica Nanoparticles. *Advanced Materials* **2013,** *25* (23), 3144-3176.

10. Cotí, K. K.; Belowich, M. E.; Liong, M.; Ambrogio, M. W.; Lau, Y. A.; Khatib, H. A.; Zink, J. I.; Khashab, N. M.; Stoddart, J. F., Mechanised nanoparticles for drug delivery. *Nanoscale* **2009,** *1* (1), 16-39.

11. Ambrogio, M. W.; Thomas, C. R.; Zhao, Y.-L.; Zink, J. I.; Stoddart, J. F., Mechanized Silica Nanoparticles: A New Frontier in Theranostic Nanomedicine. *Accounts of Chemical Research* **2011,** *44* (10), 903-913.

12. Ariga, K.; Ji, Q.; Mori, T.; Naito, M.; Yamauchi, Y.; Abe, H.; Hill, J. P., Enzyme nanoarchitectonics: organization and device application. *Chemical Society Reviews* **2013,** *42* (15), 6322-6345.

13. Tarn, D.; Ashley, C. E.; Xue, M.; Carnes, E. C.; Zink, J. I.; Brinker, C. J., Mesoporous Silica Nanoparticle Nanocarriers: Biofunctionality and Biocompatibility. *Accounts of Chemical Research* **2013,** *46* (3), 792-801.

14. Guo, Y.; Mishra, M. K.; Wang, F.; Jankolovits, J.; Kusoglu, A.; Weber, A. Z.; Van Dyk, A.; Beshah, K.; Bohling, J. C.; Roper Iii, J. A.; Radke, C. J.; Katz, A., Hydrophobic Inorganic Oxide Pigments via Polymethylhydrosiloxane Grafting: Dispersion in Aqueous Solution at Extraordinarily High Solids Concentrations. *Langmuir* **2018,** *34* (39), 11738-11748.

15. Der Voort, P. V.; Vansant, E. F., Silylation of the Silica Surface A Review. *Journal of Liquid Chromatography & Related Technologies* **1996,** *19* (17-18), 2723-2752.

16. Carlos, L. D.; Ferreira, R. A. S.; Bermudez, V. d. Z.; Ribeiro, S. J. L., Lanthanide-Containing Light-Emitting Organic–Inorganic Hybrids: A Bet on the Future. *Advanced Materials* **2009,** *21* (5), 509-534.

17. Brun, N.; Julián-López, B.; Hesemann, P.; Laurent, G.; Deleuze, H.; Sanchez, C.; Achard, M.-F.; Backov, R., Eu3+@Organo-Si(HIPE) Macro-Mesocellular Hybrid Foams Generation: Syntheses, Characterizations, and Photonic Properties. *Chemistry of Materials* **2008,** *20* (22), 7117-7129.

18. Hoffmann, F.; Cornelius, M.; Morell, J.; Fröba, M., Silica-Based Mesoporous Organic–Inorganic Hybrid Materials. *Angewandte Chemie International Edition* **2006,** *45* (20), 3216-3251.

19. Hair, M. L.; Hertl, W., Reactions of chlorosilanes with silica surfaces. *The Journal of Physical Chemistry* **1969,** *73* (7), 2372-2378.

20. Goodwin, J. W.; Harbron, R. S.; Reynolds, P. A., Functionalization of colloidal silica and silica surfaces via silylation reactions. *Colloid and Polymer Science* **1990,** *268* (8), 766-777.

21. Anwander, R.; Nagl, I.; Widenmeyer, M.; Engelhardt, G.; Groeger, O.; Palm, C.; Röser, T., Surface Characterization and Functionalization of MCM-41 Silicas via Silazane Silylation. *The Journal of Physical Chemistry B* **2000,** *104* (15), 3532-3544.

22. Reiner, A., SOMC@PMS. Surface Organometallic Chemistry at Periodic Mesoporous Silica. *Chemistry of Materials* **2001,** *13*, 4419-4438.

23. Liberman, A.; Mendez, N.; Trogler, W. C.; Kummel, A. C., Synthesis and surface functionalization of silica nanoparticles for nanomedicine. *Surface science reports* **2014,** *69* (2-3), 132-158.

24. Jiang, H.; Zheng, Z.; Song, W.; Li, Z.; Wang, X., Alkoxysilane Functionalized Polyurethane/Polysiloxane Copolymers: Synthesis and the Effect of End-Capping Agent. *Polymer Bulletin* **2007,** *59* (1), 53-63.

25. Flagg, D. H.; McCarthy, T. J., Rapid and Clean Covalent Attachment of Methylsiloxane Polymers and Oligomers to Silica Using B(C6F5)3 Catalysis. *Langmuir* **2017,** *33* (33), 8129-8139.

26. Li, Y.-H.; Buriak, J. M., Dehydrogenative Silane Coupling on Silicon Surfaces via Early Transition Metal Catalysis. *Inorganic Chemistry* **2006,** *45* (3), 1096-1102.

27. Yang, Z.; Wahl, M. H.; Veinot, J. G. C., Size-independent organosilane functionalization of silicon nanocrystals using Wilkinson's catalyst. *Canadian Journal of Chemistry* **2014,** *92* (10), 951-957.

28. Heeribout, L.; d'Espinose de la Caillerie, J. B.; Legrand, A. P.; Mignani, G., A New Straightforward Approach to Generate Si–H Groups on Silica. *Journal of Colloid and Interface Science* **1999,** *215* (2), 296-299.

29. Plumeré, N.; Speiser, B.; Mayer, H. A.; Joosten, D.; Wesemann, L., High-Temperature Chlorination-Reduction Sequence for the Preparation of Silicon Hydride Modified Silica Surfaces. *Chemistry - A European Journal* **2009,** *15* (4), 936-946.

30. Moitra, N.; Ichii, S.; Kamei, T.; Kanamori, K.; Zhu, Y.; Takeda, K.; Nakanishi, K.; Shimada, T., Surface Functionalization of Silica by Si–H Activation of Hydrosilanes. *Journal of the American Chemical Society* **2014,** *136* (33), 11570-11573.

31. Blackwell, J. M.; Foster, K. L.; Beck, V. H.; Piers, W. E., B(C6F5)3-Catalyzed Silation of Alcohols: A Mild, General Method for Synthesis of Silyl Ethers. *The Journal of Organic Chemistry* **1999,** *64* (13), 4887-4892.

32. Hog, D. T.; Oestreich, M., B(C6F5)3-Catalyzed Reduction of Ketones and Imines Using Silicon-Stereogenic Silanes: Stereoinduction by Single-Point Binding. *European Journal of Organic Chemistry* **2009,** *2009* (29), 5047-5056.

33. Bedard, T. C.; Corey, J. Y., Conversion of hydrosilanes to alkoxysilanes catalyzed by Cp2TiCl2/nBuLi. *Journal of Organometallic Chemistry* **1992,** *428* (3), 315-333.

34. Xin, S.; Harrod, J. F., Reactions of silanes with allylic alcohols catalyzed by titanocene derivatives: an approach to catalytic cross dehydrocoupling/co-intramolecular hydrosilation. *Journal of Organometallic Chemistry* **1995,** *499* (1), 181-191.

35. Peterson, E.; Khalimon, A. Y.; Simionescu, R.; Kuzmina, L. G.; Howard, J. A. K.; Nikonov, G. I., Diversity of Catalysis by an Imido-Hydrido Complex of Molybdenum. Mechanism of Carbonyl Hydrosilylation and Silane Alcoholysis. *Journal of the American Chemical Society* **2009,** *131* (3), 908-909.

36. Gregg, B. T.; Cutler, A. R., Manganese Carbonyl Bromide-Catalyzed Alcoholysis of the Monohydrosilane HSiMe2Ph. *Organometallics* **1994,** *13* (3), 1039-1043.

37. Mukherjee, D.; Thompson, R. R.; Ellern, A.; Sadow, A. D., Coordinatively Saturated Tris(oxazolinyl)borato Zinc Hydride-Catalyzed Cross Dehydrocoupling of Silanes and Alcohols. *ACS Catalysis* **2011,** *1* (7), 698-702.

38. Chang, S.; Scharrer, E.; Brookhart, M., Catalytic silane alcoholysis based on the C5H5(CO)(PPh3)Fe+ moiety. NMR spectroscopic identification of key intermediates. *Journal of Molecular Catalysis A: Chemical* **1998,** *130* (1), 107-119.

39. Corbin, R. A.; Ison, E. A.; Abu-Omar, M. M., Catalysis by cationic oxorhenium(v): hydrolysis and alcoholysis of organic silanes. *Dalton Transactions* **2009,** (15), 2850-2855.

40. Schubert, U.; Lorenz, C., Conversion of Hydrosilanes to Silanols and Silyl Esters Catalyzed by [Ph3PCuH]6. *Inorganic Chemistry* **1997,** *36* (6), 1258-1259.

41. Schmidt, D. R.; O'Malle, S. J.; Leighton, J. L., Catalytic Asymmetric Silane Alcoholysis: Practical Access to Chiral Silanes. *Journal of the American Chemical Society* **2003,** *125* (5), 1190-1191.

42. Corriu, R. J. P.; Moreau, J. J. E., Asymmetric synthesis at silicon: II. Alcoholysis of prochiral organosilicon compounds catalysed by rhodium complexes. *Journal of Organometallic Chemistry* **1976,** *120* (3), 337-346.

43. Chung, M.-K.; Ferguson, G.; Robertson, V.; Schlaf, M., Nature of the active silane alcoholysis catalyst in the RuwClx(CO)y(PMe3)z (w, x, y, z = 1 or 2) system; Ru2(μ-Cl)2Cl2(CO)4(PMe3)2 as a new catalyst for silane alcoholysis in a polar solvent. *Canadian Journal of Chemistry* **2001,** *79* (5-6), 949-957.

44. Oehmichen, U.; Singer, H., Die alkoholyse des triethylsilans katalysiert von [(CH3)3P]2Ru(CO)2Cl2. *Journal of Organometallic Chemistry* **1983,** *243* (2), 199-204.

45. Ito, H.; Takagi, K.; Miyahara, T.; Sawamura, M., Gold(I)−Phosphine Catalyst for the Highly Chemoselective Dehydrogenative Silylation of Alcohols. *Organic Letters* **2005,** *7* (14), 3001-3004.

46. Caseri, W.; Pregosin, P. S., Hydrosilylation chemistry and catalysis with cis-PtCl2(PhCH:CH2)2. *Organometallics* **1988,** *7* (6), 1373-1380.

47. Eedugurala, N.; Wang, Z.; Chaudhary, U.; Nelson, N.; Kandel, K.; Kobayashi, T.; Slowing, I. I.; Pruski, M.; Sadow, A. D., Mesoporous Silica-Supported Amidozirconium-Catalyzed Carbonyl Hydroboration. *ACS Catalysis* **2015,** *5* (12), 7399-7414.

48. Dunne, J. F.; Neal, S. R.; Engelkemier, J.; Ellern, A.; Sadow, A. D., Tris(oxazolinyl)boratomagnesium-Catalyzed Cross-Dehydrocoupling of Organosilanes with Amines, Hydrazine, and Ammonia. *Journal of the American Chemical Society* **2011,** *133* (42), 16782-16785.

49. Cibuzar, M. P.; Waterman, R., Si–N Heterodehydrocoupling with a Lanthanide Compound. *Organometallics* **2018,** *37* (23), 4395-4401.

50. Forosenko, N. V.; Basalov, I. V.; Cherkasov, A. V.; Fukin, G. K.; Shubina, E. S.; Trifonov, A. A., Amido Ca(ii) complexes supported by Schiff base ligands for catalytic cross-dehydrogenative coupling of amines with silanes. *Dalton Transactions* **2018,** *47* (36), 12570-12581.

51. Morris, L. J.; Whittell, G. R.; Eloi, J.-C.; Mahon, M. F.; Marken, F.; Manners, I.; Hill, M. S., Ferrocene-Containing Polycarbosilazanes via the Alkaline-Earth-Catalyzed Dehydrocoupling of Silanes and Amines. *Organometallics* **2019,** *38* (19), 3629-3648.

52. Obradors, C.; Martinez, R. M.; Shenvi, R. A., Ph(i-PrO)SiH2: An Exceptional Reductant for Metal-Catalyzed Hydrogen Atom Transfers. *Journal of the American Chemical Society* **2016,** *138* (14), 4962-4971.

53. Luo, X. L.; Crabtree, R. H., Homogeneous catalysis of silane alcoholysis via nucleophilic attack by the alcohol on an Ir(.eta.2-HSiR3) intermediate catalyzed by [IrH2S2(PPh3)2]SbF6 (S = solvent). *Journal of the American Chemical Society* **1989,** *111* (7), 2527-2535.

54. Li, Y.; Kawakami, Y., Efficient synthesis of poly (silyl ether) s by pd/c and rhcl (pph3) 3-catalyzed cross-dehydrocoupling polymerization of bis (hydrosilane) s with diols. *Macromolecules* **1999,** *32* (20), 6871-6873.

55. Seino, M.; Imae, I.; Kawakami, Y., Catalytic Cross-Dehydrocoupling Polymerization of Phenylsilane with Water. A New Approach to Poly(phenylsilsesquioxane). *Polymer Journal* **2003,** *35* (2), 197-202.

Additional information

Table 3-6. Comparison of reported catalytic dehydrocoupling reactions.

entry	catalysts (cat loading %)	substrate	condition	product	yield (%)
1	Cp_2TiCl_2/*n*BuLi (5 %)[32]	$PhMeSiH_2$ + EtOH	r.t, 10 min	$MePhSi(OEt)_2$	95
2	$[Ir(H)_2(PPh_3)(THF)_2]SbF_6$ (1 %)[53]	Et_3SiH + MeOH	r.t, 1 h	Et_3SiOMe	95
3	$RhCl(PPh_3)_3$ (1 %)[54]	Et_3SiH + glycol	r.t, 30 min	Et_3SiO-$(CH_2)_n$-$OSiEt_3$	100
4	$PdCl_2.2H_2O$ (5 %)[55]	Et_3SiH + MeOH	60 °C, 10 min	Et_3SiOMe	100
5	$Ru_2(\mu$-$Cl)_2Cl_2(CO)_4(PMe_3)_2$[43]	Et_3SiH + *i*PrOH	r.t, 10 min	Et_3SiO*i*Pr	90
6	To^MZnH (10 %)[36]	$PhMeSiH_2$ + MeOH	45 °C, 10 h	PhMeSiHOMe	100
7	AuCl(Xanthphos) (1 %)[44]	Et_3SiH + $HOCH_2CH_2Ph$	r.t, 2 h	$Et_3SiOCH_2CH_2Ph$	100
8	$Ru_2(\mu$-$Cl)_2Cl_2(CO)_4(PPh_3)_2$ (1 %)[42]	$PhMeSiH_2$ + MeOH	r.t, 30 min	$PhMeSi(OMe)_2$	100
9	$RuHCl(PPh_3)_3$ (1 %)	$PhMeSiH_2$ + MeOH	r.t, 5 min	PhMeSiHOMe	100

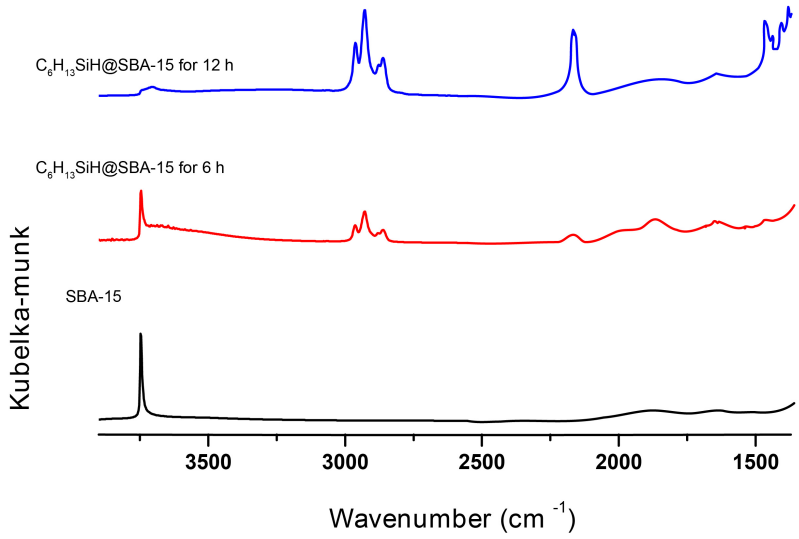

Figure 3-5. Infrared spectra of **G1** at different reaction time (A) free SBA-15, (B) reaction with phenylsilane for 6h, (C) reaction with phenylsilane after 12 h.

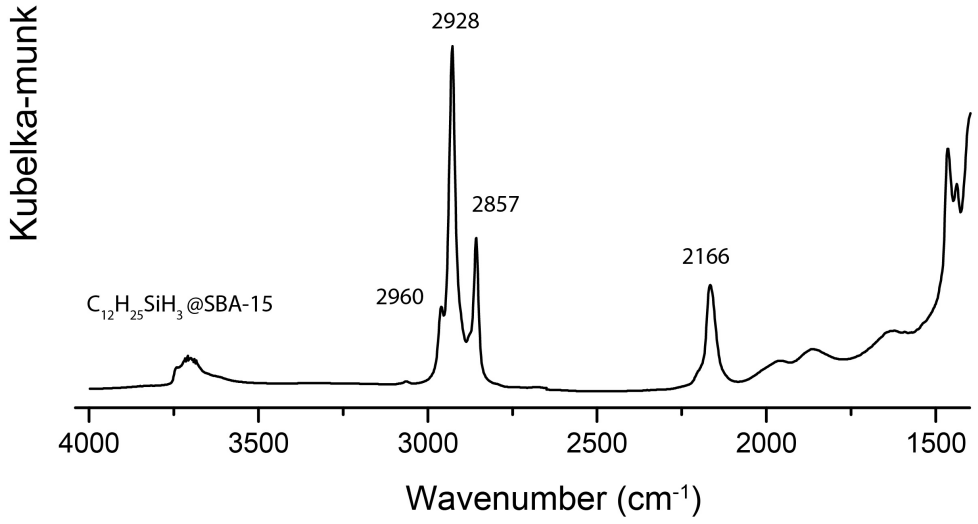

Figure 3-6. Infrared absorption spectra of **G3.**

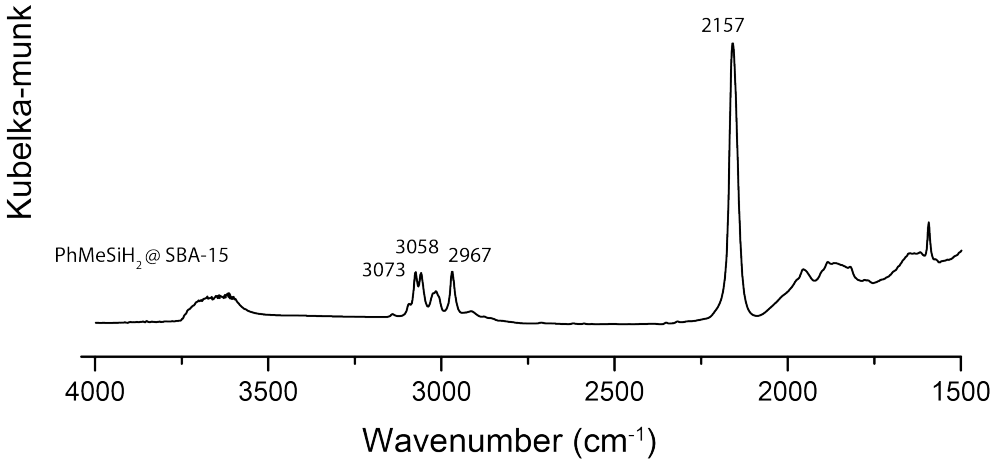

Figure 3-7. Infrared absorption spectra of **G4.**

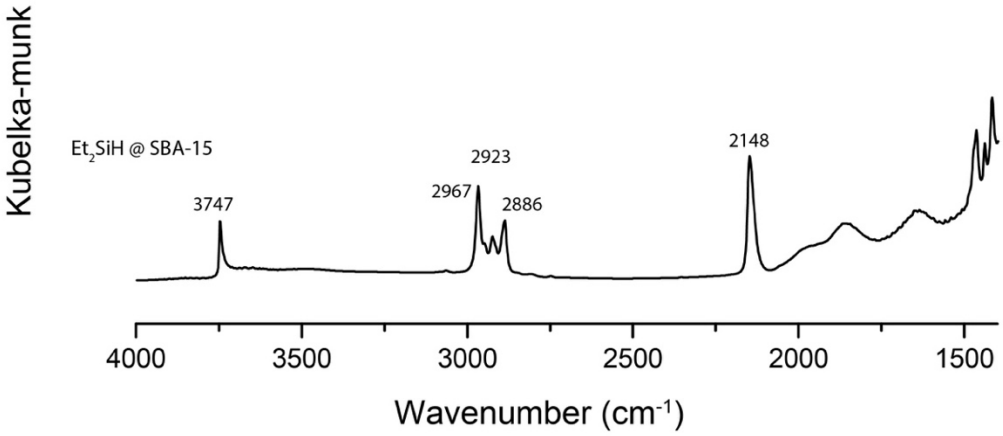

Figure 3-8. Infrared absorption spectra of **G5.**

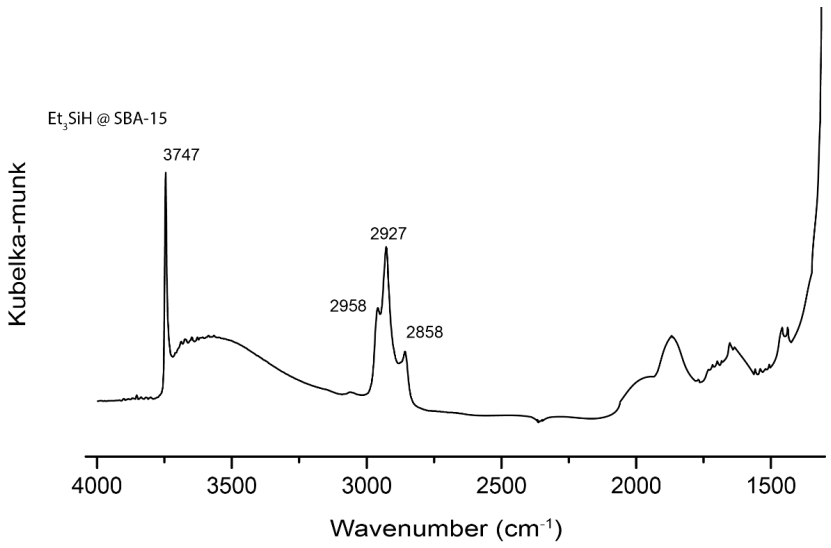

Figure 3-9. Infrared absorption spectra of **G6.**

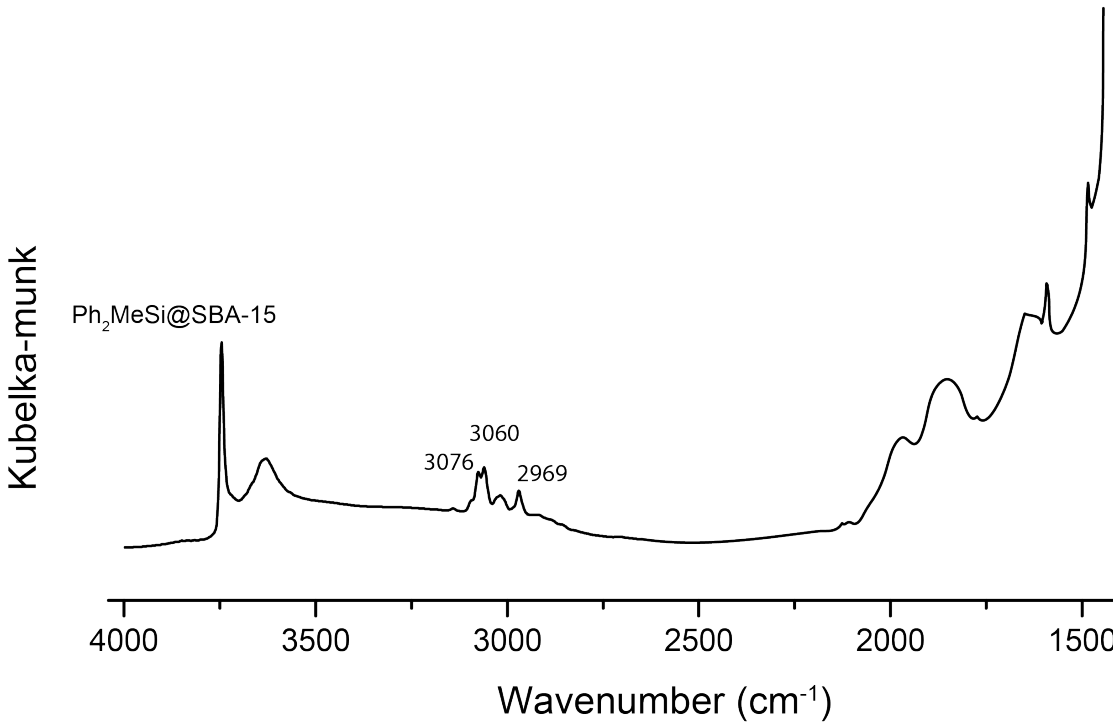

Figure 3-10. Infrared absorption spectra of **G7.**

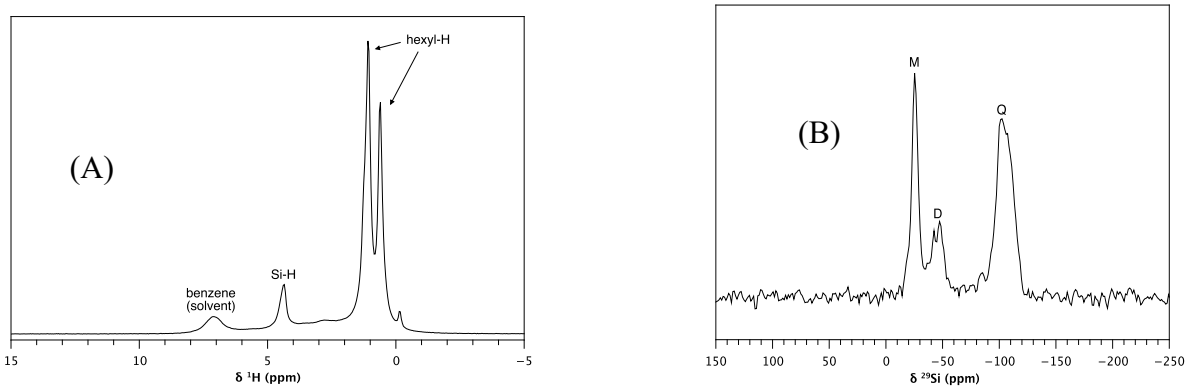

Figure 3-11. (A) ^{1}H Hahn echo spectra of **G2**. The spectra were obtained using MAS 36kHz, 10s recycle delay, 16 scans, 100kHz (^{1}H 90˚), 20.48ms acquisition, 27.8µs echo delay and (B) ^{29}Si[6] CPMAS spectra of G2. The spectra is obtained using MAS 10kHz, 83kHz (^{1}H CP) and 63kHz (^{29}Si CP), 4ms contact time, 1.3s recycle delay, 83kHz SPINAL-64 ^{1}H decoupling.

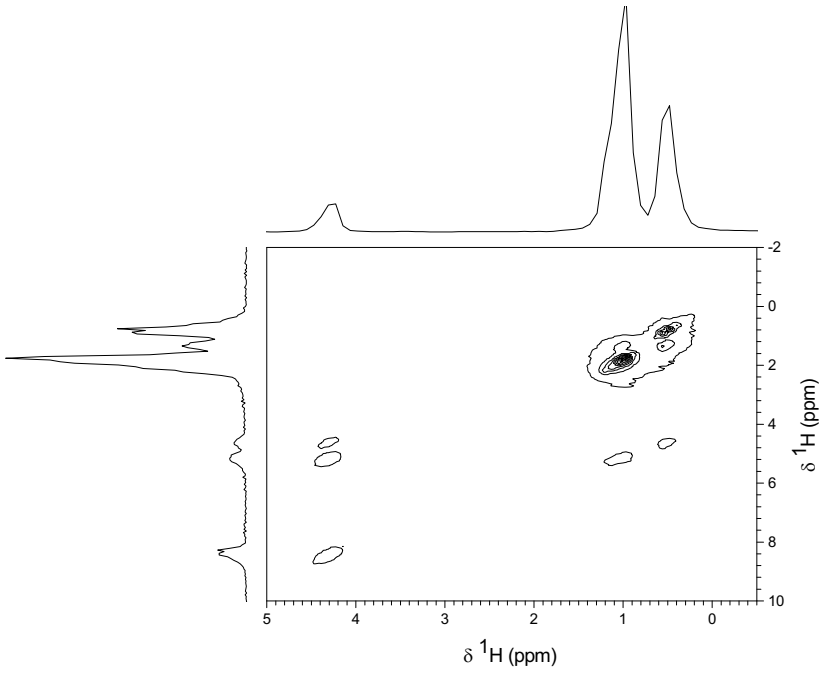

Figure 3-12. ^{1}H DQSQ correlation spectra of **G2**. The spectra are obtained using MAS 36kHz, 100kHz (^{1}H 90˚), 4 scans, 6s recycle delay, 27.8µs dwell time and 512 point in indirect dimension

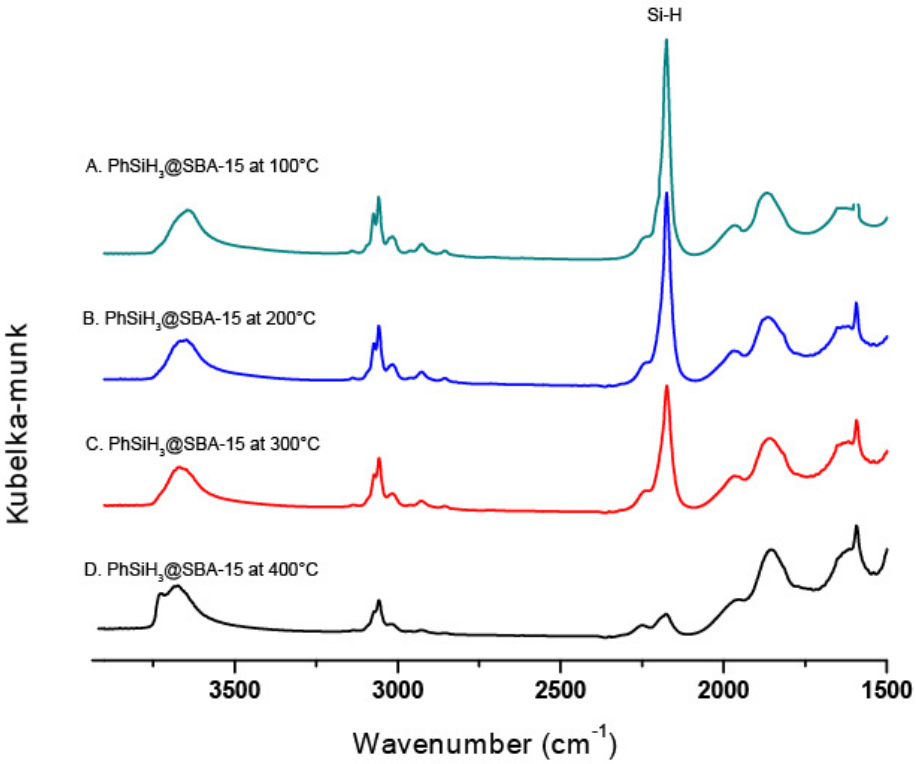

Figure 3-13. Infrared spectra of **G1** heated under vacuum at temperature (A) 100°C, (B) 200°C, (C) 300°C, (D) 400°C.

Table 3-7. $RuHCl(PPh_3)_3$ catalyzed cross-dehydrocoupling of hydrosilanes and amines.

Entry	substrates		cat (% mol)	time(min)	Product
	amines[b]	**silanes**			
1	*i*PrNH$_2$	PhSiH$_3$	5	< 5	*i*PrNHSiH$_2$Ph
2	*i*PrNH$_2$	PhSiH$_3$	1	< 5	*i*PrNHSiH$_2$Ph
3	*i*PrNH$_2$	PhMeSiH$_2$	1	<5	*i*PrNHSiHMePh
4	*i*PrNH$_2$	PhMeSiH$_2$	0.25	20	*i*PrNHSiHMePh

[a] reaction was monitored via ^{1}H NMR spectroscopy, [b] 0.9 eq of amine was used.

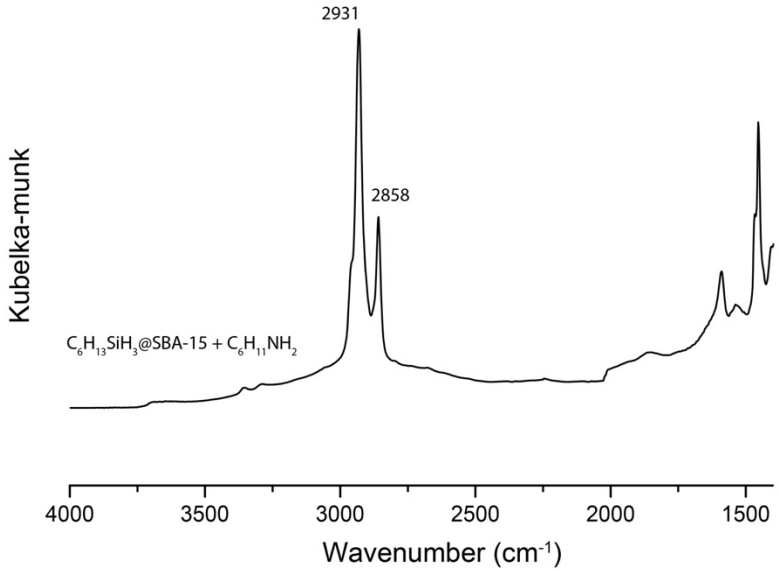

Figure 3-14. Infrared absorption spectra of **G11.**

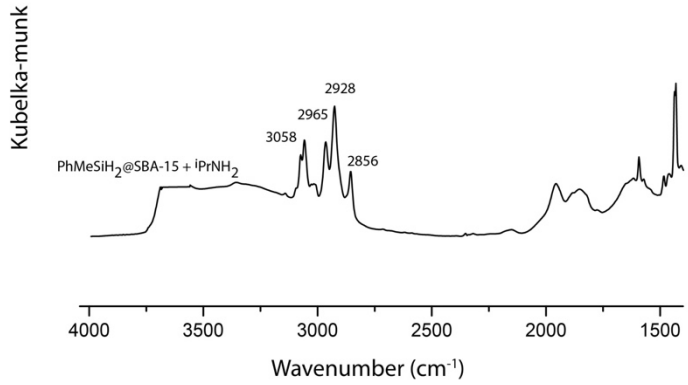

Figure 3-15. Infrared absorption spectra of **G12.**

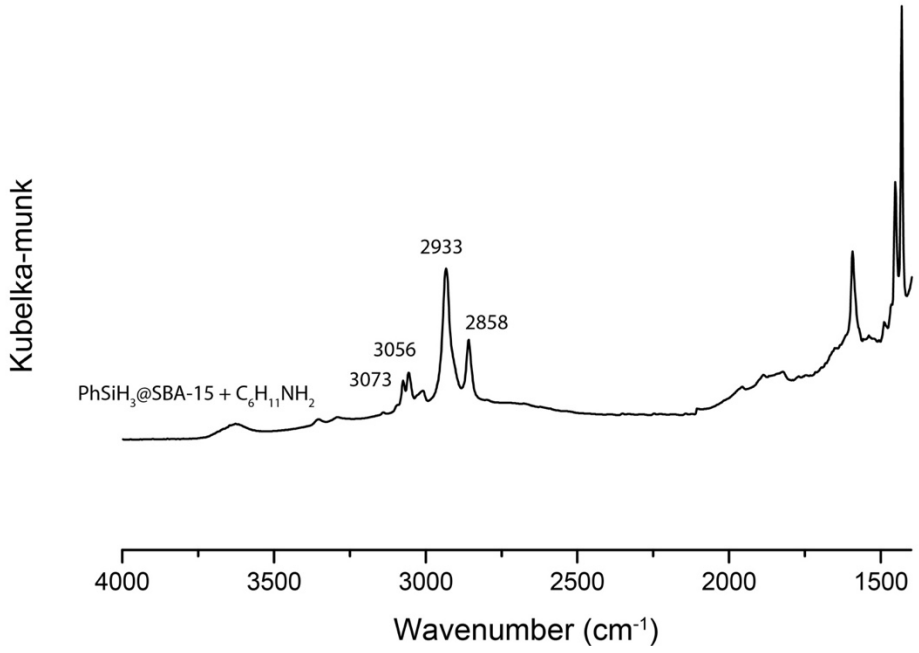

Figure 3-16. Infrared absorption spectra of **G13.**

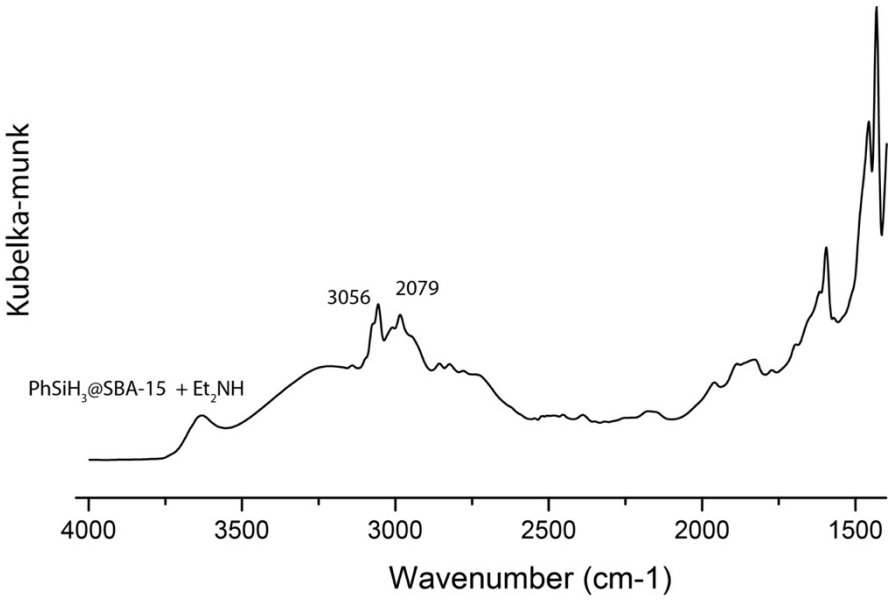

Figure 3-17. Infrared absorption spectra of **G15.**

CHAPTER 4. SYNTHESIS OF A NEW TRIS(OXAZOLINYL)BORATO RUTHENIUM COMPOUND AND ITS APPLICATION IN CATALYTIC CYCLOISOMERIZATION OF 1,6-DIENES

Abhranil Biswas, Jacob Brunton, Aaron Sadow*

Abstract

A new tris(oxazolinyl)borato (To^M) ruthenium compound has been synthesized from To^MTl and $Ru(NCPh)_4Cl_2$. Compound $To^MRu(NCPh)_2Cl$ (**4**) shows a C_s symmetric geometry around the ruthenium center concluded from NMR spectral data. Further, **4** demonstrates excellent catalytic activity for cycloisomerization of 1,6-dienes to produce cyclopentane derivatives upon heating in an appropriate solvent. Significantly, an internal alkene (**5**) was observed as side product resulting from an olefinic isomerization in aprotic solvent CH_2Cl_2 where only cyclization was observed in protic solvent *i*PrOH. Reaction conditions were further optimized using diethyl diallylmalonate (**6**) to obtain *exo*-methylenecyclopentane (**6a**) products in high yield. The study was further extended to successfully cyclize 1,6-dienes with various functional groups (**7**-**17**) with high yield under optimized reaction conditions. In addition, at higher catalyst loading the reaction shows less selectivity towards *exo*-methylene isomer in *i*PrOH whereas in CH_2Cl_2 the selectivity remains unaffected. On the basis of previously reported studies, a ruthenium hydride intermediate can be proposed. Also, the significant difference in product selectivity in solvents CH_2Cl_2 and *i*PrOH concludes that the pathways might have different intermediates and a detailed study is required.

Introduction

Dienes,[1-4] diynes[5-7] and enynes[8-10] are very powerful synthetic precursors for the construction of homonuclear and heteronuclear cyclic compounds,[11, 12] which are important building blocks for

the synthesis of various natural products, pharmaceutical compounds, and functional materials. [13-16] Metal-catalyzed activation of an alkene C–H bond followed by intra-molecular hydrovinylation (i.e., cycloisomerization) provides an effective, atom economical[17] route for the synthesis of cyclic compounds.[18, 19] In seminal work for example, Molander and co-workers reported organoyttrium-catalyzed selective reductive cyclization/silylation of 1,5- and 1,6-dienes to produce substituted carbocycles.[2, 20] There are a few challenges, however, including isomerization of either olefin in the diene without cyclization, terminal vs internal vinylic C–H bond activation to give internal or exocyclic alkenes, access to larger-than-five membered rings, stereoselective cyclization including enantioselectivity and/or diastereoselectivity.[21] Early reported catalytic systems generally lacked the requisite isomeric selectivity and the general substrate scope.[22] Notably, control over selectivity is more easily achieved in α,ω-enyne cycloisomerization compared to reactions of α,ω-dienes because of the reactivity difference between terminal alkenes and alkynes.[23]

Transition metal-catalyzed cycloisomerization of 1,6-dienes can provide valuable exo-methylenecyclopentane, and significant efforts have been devoted to identification of selective and versatile catalyst systems for this transformation. In one of the earliest examples Bogdanovic, Wilke and co-workers reported a nickel-phosphine catalyzed cycloisomerization of diallylether,

Scheme 4-1. Products from olefin isomerization and cycloisomerization of 1,6-diene

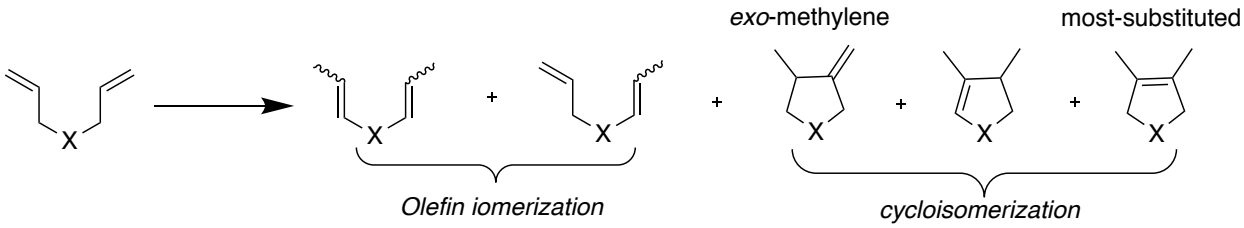

along with olefin isomerization as the major product.[24, 25] High selectivity towards the single *exo*-methylenecyclopentane isomer was achieved via $[Rh(cod)Cl]_2$ and nickel-phosphine catalyzed

reactions.[21, 26-28] Palladium is also known to catalyze cycloisomerization, but predominantly furnish the more substituted olefin.[21] Dixneuf and co-workers used ruthenium allenylidine based complexes as catalyst for selective *exo*-methylenecyclopentane products from 1,6-dienes.[29] Also, Grubbs catalyst and its derivatives have been utilized for selective cycloisomerization in presence of an external olefin producing *exo*-methylene isomer as the major product.[30] $[RuCl_2(cod)]_n$, the first non-metathesis ruthenium catalyst for diene cycloisomerization, reported by Itoh and co-workers, converts diallylmalonate in *i*PrOH at 90 °C.[31] Focused microwave heating improves the overall yield of cycloisomerization product as well as the selectivity towards *exo*-methylenecyclopentane isomer.[32] Although several reports have demonstrated effective ruthenium-based catalysis for cycloisomerization (of dienes and allenens),[33] few of the catalytically active ruthenium complexes contain ancillary, non-labile ligands (other than cod and Cp), limiting the possibility of ligand modification to improve catalytic activity, regioselectivity, diastereoselectivity, and enantioselectivity, as well as access new rings and heterocycles. As a first step to access such improved conversions, we targeted new tris(4,4-dimethyl-2-oxazolinyl)phenylborato (To^M) ruthenium compounds as possible catalysts for 1,6-diene cycloisomerization. These compounds could provide a platform for the preparation of C_3 and C_1-symmetric optically active catalysts, as well as systematically modifying the steric properties of the metal center. Here, we describe the synthesis and catalytic performance of these new ruthenium compounds.

Results and Discussion

The reaction of equimolar $Ru(NCMe)_4Cl_2$[37] (**1**) and To^MTl[39] (**2**) in CH_2Cl_2 at 60 °C for 12 h gives a new species, as identified by ^1H and ^{11}B NMR spectroscopy and tentatively assigned as $To^MRuCl(NCMe)_2$[38] (**3**). Unfortunately, both the reactants were present even after heating for 48

h. The reaction of **2** and two equiv. of **1** gives full conversion of **2** to product, however, residual **1** remains in the mixture. Even though **3** can be synthesized in high yield, its purification from the mixture of **1** and **3** by crystallization, solvent extraction, or chromatography was not successful.

Equation 4-1. Synthesis of [To^{M}Ru(NCPh)$_2$Cl].

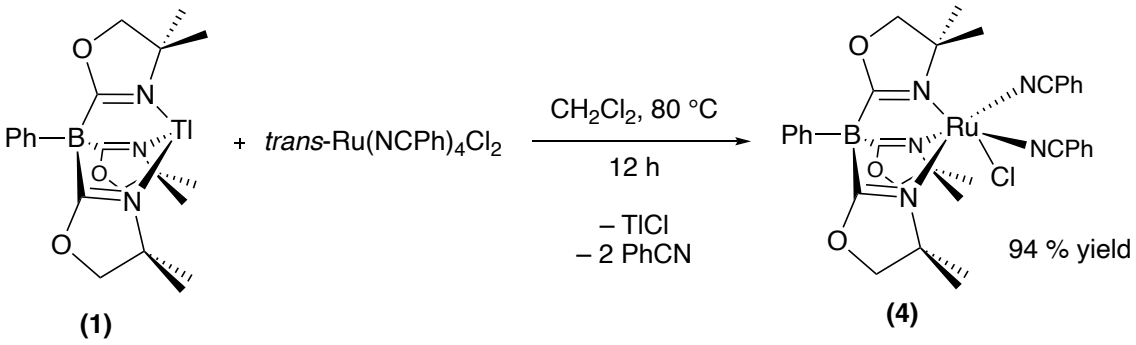

(1) (4)

Instead, we attempted to prepare derivatives. We noticed that Ru(NCMe)$_4$Cl$_2$ is a mixture of cis and trans isomers, and we speculated that the cis isomer was less reactive toward **1**. Stereo chemically pure *trans*-Ru(NCPh)$_4$Cl$_2$ is accessible and was allowed to react with **1** at 80 °C in methylene chloride over 12 h, from which To^{M}RuCl(NCPh)$_2$ (**4**) and TlCl (white solid) were formed. In methylene chloride-d_2, a sharp resonance in ^{11}B NMR was observed at –19.32 ppm and was assigned to **4**. In ^{1}H NMR, resonances due to two phenyl groups from benzonitriles (coordinated) and one phenyl group on To^{M} ligand appears from 7.09 – 7.81 (multiplet, 15 H) ppm. Further analysis of ^{1}H NMR spectra of **4** shows a C_s-symmetric geometry around the metal center. As a result of the mirror plane that includes Cl, ruthenium center, trans-oxazoline, the –CMe$_2$– and –CH$_2$– groups on that ring are equivalent and appear as singlet resonances (1.50 and 3.96 respectively, labeled as *trans* in the Newman projection in Figure 4-1). Although the other two oxazoline rings are related by the mirror plane, the –CH$_2$– within each ring are *endo* or *exo* with respect to the chloride and were observed as two coupled doublets (3.83 and 4.08 ppm, $^{2}J_{HH}$ = 11.76 Hz). The methyl substituents in the CMe$_2$ groups of these oxazolines are also inequivalent

(but not coupled), resulting in two singlet resonances (1.39 and 1.61 ppm, for *endo* and *exo* although unable to determine which one is which)

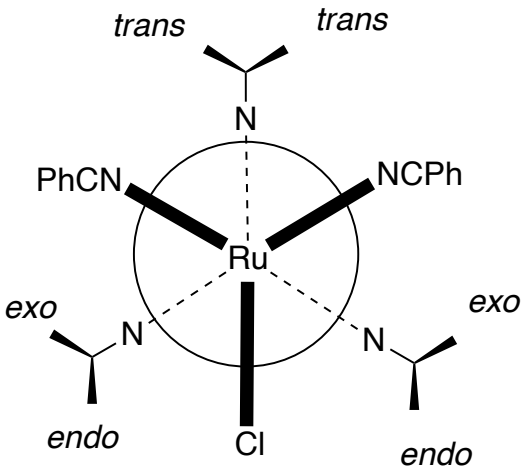

Figure 4-1. Newman projection illustrating C_s-symmetry of [Ru(κ^3–To^M)(NCPh)$_2$Cl]. The groups attached to N represent CH_2 and CMe_2 substituents on the oxazoline.

The catalytic activity of various ruthenium complexes along with solvent effect was measured with respect to the cycloisomerization of **6** to **6′** (with three probable regio-isomers **6′a**, **6′b**, **6′c**) under inert atmosphere (Ar and N_2). As reported by Yamamoto et al, [$RuCl_2$(cod)]n catalyzes cycloisomerization of **6** in protic solvent (*i*PrOH) at 90 °C (Table 1, entry 3) with high yield of **6′**, whereas after heating at 90 °C in an aprotic solvent (CH_2Cl_2) for 48 h only starting material was recovered (Table 1, entry 2). Significantly, **4** catalyzes cycloisomerization of **6** in CH_2Cl_2 to produce **6′** at a moderate yield along with an internal alkene (**5**) as side product resulting from olefin isomerization. For comparison, ruthenium complexes such as Ru(cod)$(NCMe)_2Cl_2$, $[Ru(CO)_2Cl_2]_n$ and $[Ru(p\text{-cymene})Cl_2]_2$ show low conversion of **6** to **6′** in CH_2Cl_2 (Table 4-1, Entry 4-6) whereas in presence of $RuClH(PPh_3)_3$ and **1** only olefin isomerization was observed (Table 1, entry 7, 9). Further, in a protic solvent (*i*PrOH) compound **4** catalyzes cycloisomerization of **6** to produce **6′** exclusively at high yield (Table 1, entry 12). Also, reduced catalytic activity was

observed in the presence of air as the yield for cycloisomerization was found to be 42 % in 2-propanol and <5 % in methylene chloride. The above observation is in accordance with the previously reported work by Yamamoto.

Table 4-1. Cycloisomerization of **6** under various conditions.[a]

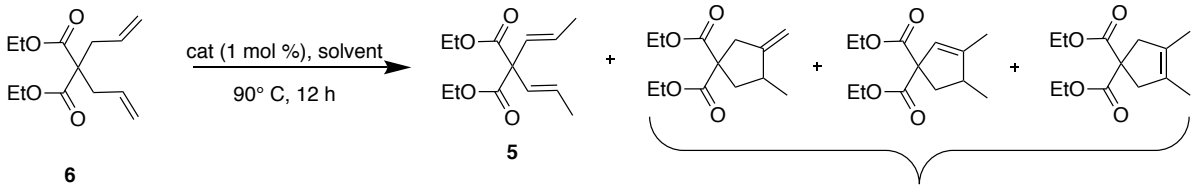

entry	catalyst	solvent	conversion (%)	selectivity (%)	
				5	**6′**
1	**4**	CH_2Cl_2	70	10	90
2	**4**[b]	CH_2Cl_2	<5	50	50
3	$[RuCl_2(cod)]_n$	CH_2Cl_2	0	-	-
4	$[RuCl_2(cod)]_n$[c]	*i*PrOH	90	-	100
5	$Ru(cod)(NCMe)_2Cl_2$	CH_2Cl_2	10	0	10
6	$[Ru(CO)_2Cl_2]_n$	CH_2Cl_2	<5	0	5
7	$[Ru(p\text{-cymene})Cl_2]_2$	CH_2Cl_2	10	trace	10
8	$RuClH(PPh_3)_3$	CH_2Cl_2	38	45	0
9	$RuClH(PPh_3)_3$	*i*PrOH	100	100	0
10	$RuCl_2(NCMe)_4$	CH_2Cl_2	60	60	0
11	$RuCl_2(NCPh)_4$	CH_2Cl_2	0	-	-

12	**4**	*i*PrOH	96	trace	>99
13	**4** [b]	*i*PrOH	42	trace	>99

[a] reactions were carried out under N_2 atmosphere, all isolated yields are reported, [b] reaction was carried out in the air, [c] reaction in 24 h (from literature report)[31]

Catalytic cycloisomerization of **6** using **4** as catalyst was further explored with respect to the relative yields of the individual cyclic isomers (**a**, **b** and **c**) as well as overall cycloisomerization yield. In presence of 1 mol % of **4**, **6′** was obtained from **6** in 63% yield in CH_2Cl_2 with high selectivity towards **6′a** (*exo*-methylene isomer) upon heating at 90 °C for 12 h. Isolated products were identified via ^{1}H NMR in $CDCl_3$, as **6′a** showed two sharp olefinic peaks at 4.79 and 4.90 ppm (accounting for one H each) assigned to *exo*-methylene =C*H*$_2$. In contrast, endo-methylene product **6′b** showed a sharp singlet at 5.42 ppm resulting from the only olefinic proton. In addition, most substituted product **6′c** shows no olefinic peak as expected and a sharp singlet at 1.24 ppm corresponding to –C*H*$_3$ on cyclopentene ring was observed. With increased catalyst loading (5 mol%) the selectivity does not change however overall yield of **6′** got lowered to 60%. Further, with longer reaction time selectivity as well as the yield of cycloisomerization remains the same. In a protic solvent (*i*PrOH) the product **6′** was obtained in 95% yield upon heating at 90 °C for 12 h with decent selectivity towards **6′a** (96%). Both higher catalyst loading (5 mol %) and longer reaction time (24 h) resulted in olefinic bond isomerization of *exo*-methylene isomer to obtain less selectivity (Table 2, entry 5-6). On the basis of the above result, cycloisomerization in *i*PrOH in presence of 1 mol % of **4** proved to be the best choice for further studies.

Table 4-2. Selectivity in cycloisomerization of **6** under various conditions.

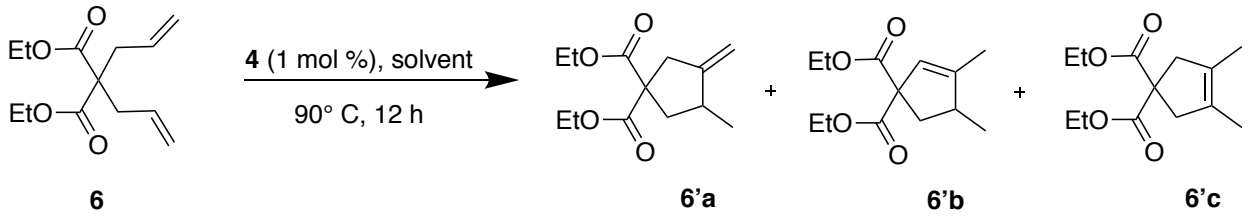

6 **6'a** **6'b** **6'c**

entry	solvent	cat loading (mol %)	yield[a] (%)	selectivity (%) (**6′a / 6′b / 6′c**)
1	CH_2Cl_2	1	63	>99 / - / -
2	CH_2Cl_2	5	60	>99 / - / -
3	CH_2Cl_2	1	62	>99 / - / -
4	*i*PrOH	1	95	96 / 4 / -
5	*i*PrOH	5	97	68 / 15 / 17
6	*i*PrOH	0.1	70	>99 / - / -
7	*i*PrOH	1	96	52 / 18 / 30

[a] isolated yield reported

As mentioned above functional group tolerance in catalytic cycloisomerization of 1,6-dienes is of particular interest as these cyclic products are of synthetic significance. Here we investigate functional group compatibility of current protocol for 1,6-heptadiens with various functional groups at the 4-position. Compounds **7**-**21** were subjected to cycloisomerization under the optimized reaction conditions (Table 2, entry 4). Cycloisomerization products were obtained for compounds **7**-**17** in very high yield (Table 3). As observed with **6**, compounds with groups like sulfone (**7**), a dinitrile (**9**), a cyclic ester (**14**) and acyclic ester (**16**) gave very high selectivity towards *exo*-methylenecyclopentane products (**7′a, 9′a, 14′a** and **16′a**). In contrast, dienes like **8** and **15** with functional groups ketone and ester produced internal alkenes **8′b** and **15′b** in high

selectivity. Also, compounds **11** and **12** with functional groups amide and ketone respectively produced the most substitute olefinic isomers (**11′c** and **12′c**) with a yield of 98% and 95%. In addition, a diallyl fluorene (**13**) having no coordinating group underwent cycloisomerization to furnish **13′a** in excellent yield. These results are in marked contrast to the palladium-catalyzed silylative cyclization, in which only dienes possessing at least one homoallylic ester, ketone or ether group underwent cyclization. The current protocol was further tested to heterocycle formations. 1,6-dienes with heteroatoms like N, O, S and Si at the 4-position (compounds **17**-**21**) were subjected to cycloisomerization and only *N,N*-diallylacetoamide **17** was converted to an N,N pyrrolidine derivative **17′b** in 98% yield as a mixture two different rotamers in a ratio of 3:2 . The diallyl ether **20** and diallyl sulfane **21** however, gave no cyclization product using the **4** as the catalyst, indicative of the substituents at the 4-position being essential for the cyclization (Table 3). The successful cyclization of the diallyl compounds with secondary or tertiary centers on the tether connecting two alkene termini could be assigned to the Thorpe-Ingold effect. Also, failure to cyclize sulfane **21** could be resulting from the strong coordination by the sulfur atom and deactivating the ruthenium catalyst. Surprisingly, diene **18** failed to cyclize whereas it has a tertiary center at the 4-position (Table 3). The failure might be ascribed to the elongation of the tether by the two Si–C single bonds. In addition, a tetraallyl ammonium salt under optimized cycloisomerization condition produced an olefinic isomerized product instead of cyclization.

Table 4-3. **4** catalyzed cycloisomerization of 1,6-heptadienes[a].

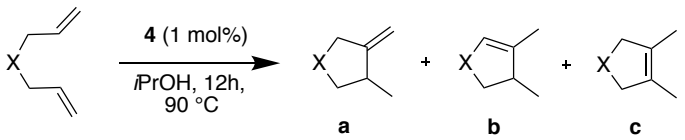

	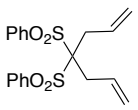	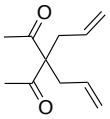	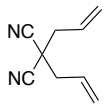	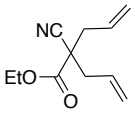	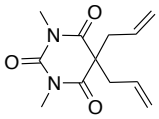
	7	**8**	**9**	**10**	**11**
overall yield (a+b+c) :	97%	91%	95%	92%	98%
a/b/c :	>99 / - / -	- / 80 / 20	97 / 3 / -	55 / 45 / -	- / - / >99
dr:	-	-	-	3:1	-
	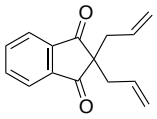	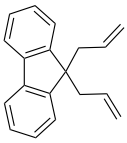	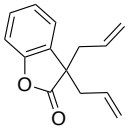	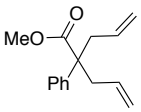	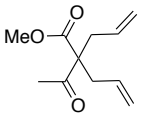
	12	**13**	**14**	**15**	**16**
overall yield (a+b+c) :	95%	95%	91%	97%	95%
a/b/c :	- / 26 / 74	85 / 7 / 8	>99 / - / -	37 / 63 / -	91 / 9 / -
dr:	-	-	2.1:1	1.9:1	1.2:1
	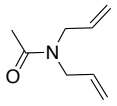	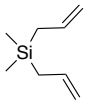	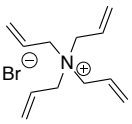	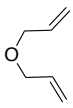	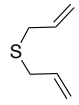
	17	**18**	**19**	**20**	**21**
overall yield (a+b+c) :	98%	-	-	-	-
a/b/c :	- / >99 / -				
dr:	-				

[a] reactions were carried out under N_2 atmosphere, all isolated yields are reported.

Controlling the stereoselectivity in diene-cyclization is significant because of its application in organic synthesis. Even though early transition metal like Ti was reported to have high diastereoselectivity in cycloisomerization, diastereocontrolled diene-cycloisomerization using late-transition-metal catalyst has been rarely achieved[33, 34]. Here we examine distereocontrol of **4** as a cycloisomerization catalyst, with respect to dienes possessing a pro-chiral center at 4-position. Compounds **14** and **16** in presence of **4** produces *exo*-methylenecyclopentane products

14′a and **16′a** in high yield with diastereoselectivities 2.1:1 and 1.2:1 respectively. Further, catalysis on compounds **10** and **15** showed low selectivity towards *exo*-methylene isomer producing **10a** (55 % selectivity) and **15a** (35% selectivity) with diastereo-selectivity of 3:1 and 1.9:1 respectively. In contrast, the internal olefinic product **10b** shows diastereo-selectivity of 1:1 whereas for **15b** only one diastereomer was obtained (Table 3). The configuration of these isomers was not established.

Conclusions

In summary, this work presents the synthesis of a new tris(oxazolinyl)borato ruthenium compound. The C_s symmetric molecule was shown to catalyze cycloisomerization of 1,6-dienes with moderate selectivity. A significant difference in product selectivity in deferent solvents refers to different mechanisms. Formation of *exo*-methylenecyclopentane has been proposed to follow two

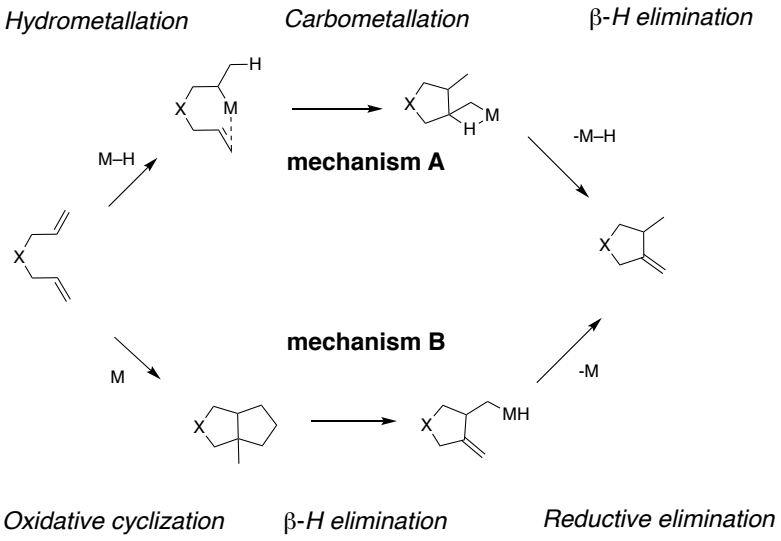

Figure 4-2. General mechanisms of cycloisomerization leading to *exo*-methylenecyclopentane.

principle mechanisms (Figure 4-1). One of the pathways involves a metal-hydride moiety (mechanism A), whereas the other takes place via a metallacycle intermediate (mechanism B). Yamamoto previously postulated that $[RuCl_2(cod)]_n$ in protic solvent *i*PrOH forms a catalytically active ruthenium hydride intermediate. A similar ruthenium hydride species can be proposed for **4** to form To^{M}RuH that resulted in the isomerization of *exo*-methylene isomers and provided low selectivity. Although ruthenium species are well known for olefin isomerization, a detailed study is needed to identify active catalysts as well as a plausible mechanistic pathway. Further, catalysis in CH_2Cl_2 produces *exo*-methylene isomer with high selectivity and a further olefin isomerization was not observed. The change in reactivity in CH_2Cl_2 might result from a significantly different mechanism and a further in-depth investigation is needed. In addition, reactivity of tris(oxazolinyl)borato ruthenium compound can be further extended to various existing chiral ligand systems and it would be interesting to see how the selectivity changes in the presence of these ligands.

Experimental Procedures

General

All manipulations were performed using either Schlenk techniques, or in a glovebox under an inert atmosphere of nitrogen unless otherwise indicated. Dry, oxygen-free solvents were used throughout. Methylene chloride, pentane, and tetrahydrofuran were dried and deoxygenated using an IT PureSolv system. *i*PrOH was dried over activated Mg, distilled and stored under N_2. Dichlorophenylborane was purchased from Aldrich and distilled prior to use. 4,4-dimethyl-2-oxazoline, dienes (**6**, **20** and **21)** were purchased from Acros and used as received. $RuHCl(PPh_3)$[36], $Ru(NCMe)_4Cl_2$[37], *trans*-$Ru(NCPh)_4Cl_2$[38], To^{M}Tl[39], dienes **7**-**19**[40-52] were synthesized following literature procedures. Dienes **6**, **20** and **21** were purchased from Alfa Aesar, dried over molecular

sieves (4 Å) and stored under N_2 atmosphere. Products **6′a**, **7′a**, **9′a**, **10′a, 10′b**, **13′a**, **14′a**, **15′a**, **16′a**, **16′b** and **17′b** are known compounds. [31, 52-54]

^{1}H, $^{13}C\{^{1}H\}$, ^{11}B, and ^{15}N spectra were collected on Bruker Avance III 600. NMR signals (^{1}H, ^{13}C, and ^{15}N) were assigned based on COSY, HMQC, and HMBC experiments. ^{15}N chemical shifts were determined by $^{1}H–^{15}N$ HMBC experiments. ^{15}N chemical shifts were initially referenced to NH_3 and recalibrated to the CH_3NO_2 chemical shift scale by adding −381.9 ppm. Infrared spectra were recorded on a Bruker Vertex spectrometer.

Synthesis of To^{M}Ru(NCPh)$_2$Cl (**4**). In the glovebox **1** (0.200 g, 0.341 mmol) and *trans*-$Ru(NCPh)_4Cl_2$ (0.200 g, 0.341 mmol) were combined in a 100 mL Schlenk flask containing a magnetic stirring bar. Methylene chloride (50 mL) was added to the flask, and the solution was allowed to stir 12 h at 80 °C. The cloudy yellow solution was filtered, and the solvent was removed from the filtrate under vacuum. The resulting yellow solid was washed with 1:1 CH_2Cl_2/pentane mixture to produce **4** (94 % yield) with trace amount of benzonitrile remining. ^{1}H NMR (methylene chloride-d_2, 600 MHz): δ 1.40 (s, 6 H, CNC*Me*$_2$CH$_2$O *trans* to Cl), 1.51 (s, 6 H, CNC*Me*$_2$CH$_2$O *cis* to Cl), 1.60 (s, 6 H, CNC*Me*$_2$CH$_2$O *cis* to Cl), 3.82 (d, $^{2}J_{HH}$ = 7.9 Hz, 2 H, CNCMe$_2$C*H*$_2$O *cis* to Cl), 3.97 (s, 2 H, CNCMe$_2$C*H*$_2$O *trans* to Cl), 4.09 (d, $^{2}J_{HH}$ = 7.9 Hz, 2 H, CNCMe$_2$C*H*$_2$O *cis* to Cl), 7.50 (m, 6 H, C$_6$*H*$_5$CN), 7.69 (m, 4 H, C$_6$*H*$_5$CN), 7.68-7.61 (m, 3 H, C$_6$*H*$_5$B), 7.81 (d, $^{2}J_{HH}$ = 7.4, 2 H, *o*-C$_6$*H*$_5$B), $^{13}C\{^{1}H\}$ NMR (methylene chloride-d_2, 150 MHz): δ 25.61 (CNC*Me*$_2$CH$_2$O *trans* to Cl), 26.37 (CNC*Me*$_2$CH$_2$O *cis* to Cl), 27.56 (CNC*Me*$_2$CH$_2$O *cis* to Cl), 70.22 (CN*C*Me$_2$CH$_2$O *trans* to Cl), 70.80 (CN*C*Me$_2$CH$_2$O *cis* to Cl), 79.99 (CNCMe$_2$*C*H$_2$O *trans* to Cl), 80.77 (CNCMe$_2$*C*H$_2$O *cis* to Cl), 113.62 (N*C*Ph), 129.21 (NC*C*$_6$H$_5$), 129.11 (NC*C*$_6$H$_5$), 132.13 (NC*C*$_6$H$_5$), 132.17 (*C*$_6$H$_5$B), 132.22 (NC*C*$_6$H$_5$), 132.75 (*C*$_6$H$_5$B), 135.30 (*C*$_6$H$_5$B). $^{15}N\{^{1}H\}$

NMR (methylene chloride-d_2, 61 MHz): δ −200.5 ($CNCMe_2CH_2O$ *trans* to Cl), –187.3 ($CNCMe_2CH_2O$ *cis* to Cl). ^{11}B NMR (methylene chloride-d_2, 192 MHz): δ −19.3. IR (KBr, cm^{-1}): ν 3045, 2967, 2931, 2877, 2230, 2210, 1606, 1586, 1487, 1463, 1445. ESI-HRMS (*m/z*): $[M]^+$ calcd for $C_{35}H_{39}BClN_5O_3Ru$, 725.1878, found, 725.1899.

General procedure for catalytic cycloisomerization. In a glovebox 10 mmol of appropriate 1,6-diene was dissolved in 5 ml of dry *i*PrOH and the mixture was transferred to a storage tube. To the mixture 72.5 mg of **4** (0.1 mmol) was added and the resulting solution was heated at 90 °C for 12 h. The yellow colored solution was passed through a celite plug, concentrated under vacuum and was purified by column chromatography.

(6′). yield 95 % (2.28 g, 9.5 mmol), ethylacetate : hexane = 30 : 70 (R_f = 0.28)

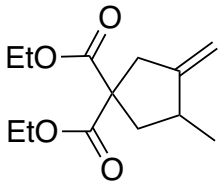

6′a: ^1H NMR ($CDCl_3$, 600 MHz): δ 1.10 (d, $^3J_{HH}$ = 6.4 Hz, 3 H, CH*Me*), 1.24 (m, 6 H, CH_2CH_3), 1.74 (m, 1 H, CH_2CHMe), 2.56 (m, 2 H, CH_2CHMe, $CHMe$), 2.93 (m, 1 H, CH_2CCH_2), 3.03 (m, 1 H, CH_2CCH_2), 4.18 (m, 2 H, CH_2CH_3), 4.79 (br, 1 H, CCH_2), 4.90 (br, 1 H, CCH_2). $^{13}C\{^1H\}$ NMR ($CDCl_3$, 150 MHz): δ 14.03, 17.99, 37.29, 40.51, 42.13, 58.23, 61.42, 61.43, 105.39, 153.45, 171.89, 172.01.

(7′). yield 97 % (3.65 g, 9.7 mmol), ethylacetate : hexane = 40 : 60 (R_f = 0.34)

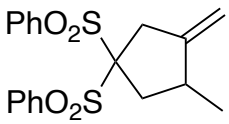

7′a: ^1H NMR ($CDCl_3$, 600 MHz): δ 1.08 (d, $^3J_{HH}$ = 5.9 Hz, 3 H, CH*Me*), 2.22 (m, 1 H, $CHMe$), 2.75 (m, 2 H, CH_2CHMe), 3.27 (br, 1 H, CH_2CCH_2), 4.72 (s, 1 H, CCH_2), 4.77 (s, 1 H, CCH_2), 7.57-8.08 (m, 10 H, *Ph*SO_2). $^{13}C\{^1H\}$ NMR ($CDCl_3$, 150 MHz): δ 17.35, 37.69, 38.46, 39.37, 91.07, 106.42, 128.72, 128.77, 131.25, 131.30, 134.56, 134.67, 136.06, 136.92, 150.39.

(8′). yield 95 % (1.64 g, 9.1 mmol), ethylacetate : hexane = 25 : 75 (R_f = 0.33)

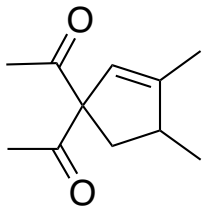

8′b: ^{1}H NMR ($CDCl_3$, 600 MHz): δ 1.04 (d, $^3J_{HH}$ = 6.8 Hz, 3 H, CH*Me*), 1.74 (s, 3 H, CHC*Me*), 1.82 (m, 1 H, CH_2CHMe), 2.10 (s, 3 H, COCH_3), 2.13 (s, 3 H, COCH_3), 2.67 (m, 2 H, CH_2C*H*Me), 5.56 (s, 1 H, C*H*CMe). $^{13}C\{^1H\}$ NMR ($CDCl_3$, 150 MHz): δ 13.61, 14.95, 26.89, 27.09, 38.58, 41.90, 79.38, 128.80, 151.81, 206.72, 207.28. ESI-HRMS (*m/z*): $[M+H]^+$ calcd for $C_{11}H_{16}O_2$, 181.1229, found 181.1219.

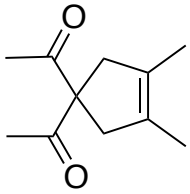

8′c: ^{1}H NMR ($CDCl_3$, 600 MHz): δ 1.59 (s, 6 H, C*Me*), 2.12 (s, 6 H, CO*Me*), 2.81 (s, 4 H, CH_2CMe). $^{13}C\{^1H\}$ NMR ($CDCl_3$, 150 MHz): δ 14.29, 26.66, 43.01, 71.64, 122.04, 207.40. ESI-HRMS (*m/z*): $[M+H]^+$ calcd for $C_{11}H_{16}O_2$, 181.1229, found 181.1219.

(9′). yield 95 % (1.38 g, 9.5 mmol), ethylacetate : hexane = 40 : 60 (R_f = 0.41)

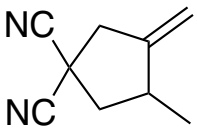

9′a: ^{1}H NMR ($CDCl_3$, 600 MHz): δ 1.24 (d, $^3J_{HH}$ = 6.7 Hz, 3 H, CH*Me*), 1.99 (m, 1 H, CH_2CHMe), 2.75 (m, 1 H, CH_2CHMe), 2.84 (m, 1 H, C*H*Me), 3.10 (d, $^2J_{HH}$ = 10 Hz, 1 H, CH_2CCH$_2$), 3.05 (d, $^3J_{HH}$ = 11 Hz, 1 H, CH_2CCH$_2$), 5.06 (s, 1 H, CCH_2), 5.14 (s, 1 H, CCH_2). $^{13}C\{^1H\}$ NMR ($CDCl_3$, 150 MHz): δ 17.96, 31.88, 36.58, 44.75, 45.70, 109.92, 116.02, 116.20, 147.51.

(10′). yield 95 % (1.78 g, 9.2 mmol), ethylacetate : hexane = 30 : 70 (R_f = 0.30)

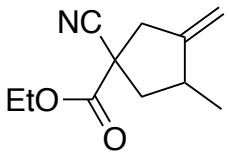

10′a: ^{1}H NMR ($CDCl_3$, 600 MHz): Diastereomer **A**. δ 1.18 (d, $^3J_{HH}$ = 6.6 Hz, 3 H, CH*Me*), 1.33 (m, 3 H, CH_2CH_3), 1.87 (m, 1 H, CH_2CHMe), 2.51 (m, 1 H, CH_2CHMe), 2.84 (m, 1 H, CHMe), 2.97 (m, 1 H, CH_2CCH_2), 3.13 (m, 1 H, CH_2CCH_2), 4.26 (m, 2 H, CH_2CH_3), 4.94 (br, 2 H, CCH_2). Diastereomer **B**. δ 1.18 (d, $^3J_{HH}$ = 6.6 Hz, 3 H, $CHMe_2$), 1.33 (m, 3 H, CH_2CH_3), 1.87 (m, 1 H, CH_2CHMe), 2.51 (m, 1 H, CH_2CHMe), 3.07 (m, 1 H, CHMe), 3.13 (m, 1 H, CH_2CCH_2), 4.26 (m, 2 H, CH_2CH_3), 4.91 (br, 2 H, CCH_2).

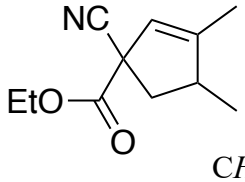

10′b: ^{1}H NMR ($CDCl_3$, 600 MHz): δ 1.18 (d, $^3J_{HH}$ = 6.6 Hz, 3 H, CH*Me*), 1.33 (m, 3 H, CH_2CH_3), 1.87 (m, 1 H, CH_2CHMe), 2.51 (m, 1 H, CH_2CHMe), 2.84 (m, 1 H, CHMe), 3.03 (s, 1 H, CHC*Me*), 4.26 (m, 2 H, CH_2CH_3), 5.08 (s, 1 H, CHCMe). ESI-HRMS (*m/z*): $[M+H]^+$ calcd for $C_{11}H_{15}NO_2$, 194.1176, found 194.1172.

(11′). yield 95 % (2.32 g, 9.8 mmol), ethylacetate: hexane = 40 : 60 (R_f = 0.46)

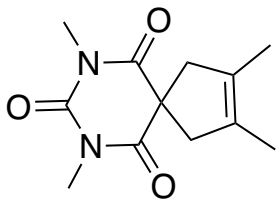

11′c: ^{1}H NMR ($CDCl_3$, 600 MHz): δ 1.64 (s, 6 H, CH_2CMe), 2.92 (s, 4 H, CH_2CMe), 3.31 (s, 6 H, CON*Me*). $^{13}C\{^1H\}$ NMR ($CDCl_3$, 150 MHz): δ 13.20, 28.96, 50.03, 53.32, 127.85, 151.52, 172.83. ESI-HRMS (*m/z*): $[M+H]^+$ calcd for $C_{15}H_{18}O_2$, 231.1385, found 231.1385.

(12′). yield 95 % (2.15 g, 9.5 mmol), ethylacetate : hexane = 25 : 75 (R_f = 0.28)

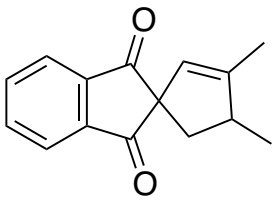

12′b: ^{1}H NMR ($CDCl_3$, 600 MHz): δ 1.19 (d, $^3J_{HH}$ = 7 Hz, 3 H, CH*Me*), 1.78 (s 3 H, CHC*Me*) 1.81 (m, 1 H, CH_2CHMe), 2.45 (m, 1 H, CH_2CHMe), 2.98 (m, 1 H, C*H*Me), 4.95 (s, 1 H, C*H*CMe), 7.83 (m, 2 H, *m*-C_6H_4-), 7.97 (m, 2 H, *o*-C_6H_4-). ^{13}C{^{1}H} NMR ($CDCl_3$, 150 MHz). ESI-HRMS (*m/z*): $[M]^+$ calcd for $C_{15}H_{14}O_2$, 226.0921, found 226.0908.

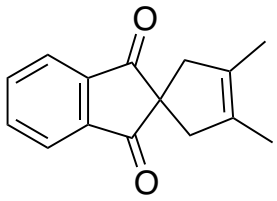

12′c: ^{1}H NMR ($CDCl_3$, 600 MHz): δ 1.65 (s, 6 H, CH_2C*Me*), 2.66 (s, 4 H, CH_2CMe), 7.83 (m, 2 H, *m*-C_6H_4-), 7.97 (m, 2 H, *o*-C_6H_4-). ESI-HRMS (*m/z*): $[M]^+$ calcd for $C_{15}H_{14}O_2$, 226.0921, found 226.0908.

(13′). yield 95 % (2.34 g, 9.5 mmol), ethylacetate : hexane = 10 : 90 (R_f = 0.27)

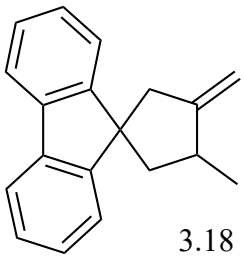

13′a. ^{1}H NMR ($CDCl_3$, 400 MHz): δ 1.32 (d, $^3J_{HH}$ = 4 Hz, 3 H, CH*Me*), δ 1.99 (m, 1 H, CH_2CHMe), δ 2.17 (m, 1 H, CH_2CHMe), δ 2.71 (d, $^2J_{HH}$ = 10.8 Hz, 1 H, CH_2CCH$_2$), δ 3.05 (d, $^2J_{HH}$ = 11 Hz, 1 H, CH_2CCH$_2$), δ 3.18 (m, 1 H, C*H*Me), δ 5.08 (d, $^2J_{HH}$ = 7.5 Hz, 2 H, CCH_2), δ 7.27-7.73 (m, 8 H). ^{13}C{^{1}H} NMR ($CDCl_3$, 150 MHz): δ 19.71, 38.45, 45.15, 50.24, 55.41, 105.83, 119.61, 119.69, 122.67, 123.18, 126.93, 127.09, 127.32, 127.43, 139.33, 139.83, 150.28, 153.47, 157.09.

(14′). yield 95 % (1.95 g, 9.1 mmol), ethylacetate: hexane = 25 : 75 (R_f = 0.45)

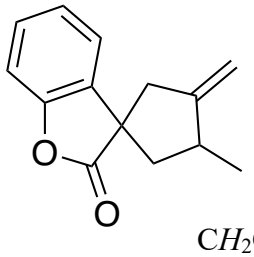

14′a. ^{1}H NMR ($CDCl_3$, 600 MHz): Diastereomer **A.** δ 1.22 (d, $^3J_{HH}$ = 6.7 Hz, 3 H, CH*Me*), δ 1.69 (m, 1 H, C*H*$_2$CHMe), δ 2.46 (m, 1 H, C*H*$_2$CHMe), δ 2.71 (d, $^2J_{HH}$ = 10 Hz, 1 H, C*H*$_2$CCH$_2$), δ 3.02 – 3.13 (br, 2 H, C*H*Me, C*H*$_2$CCH), δ 4.95 (s, 1 H, CC*H*$_2$), δ 5.00 (s, 1 H, CC*H*$_2$), δ 7.08-7.30 (m, 4 H, C$_6$*H*$_4$). ^{13}C{^{1}H} NMR ($CDCl_3$, 150 MHz): δ 17.52, 37.23, 44.84, 46.86, 49.62, 105.87, 110.50, 122.71, 124.43, 128.55, 132.36, 152.43, 153.65, 180.91. Diastereomer **B**. δ 1.27 (d, $^3J_{HH}$ = 6.6 Hz, 3 H, CH*Me*$_2$), δ 2.03 (m, 1 H, C*H*$_2$CHMe), δ 2.17 (m, 1 H, C*H*$_2$CHMe), δ 2.63 (d, $^2J_{HH}$ = 10 Hz, 1 H, C*H*$_2$CCH$_2$), δ 3.02 – 3.13 (br, 2 H, C*H*Me, C*H*$_2$CCH), δ 5.03 (s, 1 H, CC*H*$_2$), δ 5.06 (s, 1 H, CC*H*$_2$), δ 7.08-7.30 (m, 4 H, C$_6$*H*$_4$). ^{13}C{^{1}H} NMR ($CDCl_3$, 150 MHz): δ 19.12, 37.66, 44.58, 47.63, 50.63, 107.27, 110.63, 122.97, 124.36, 128.53, 133.57, 152.05, 153.28, 180.02.

(15′). yield 95 % (2.23 g, 9.7 mmol), ethylacetate: hexane = 25 : 75 (R_f = 0.3)

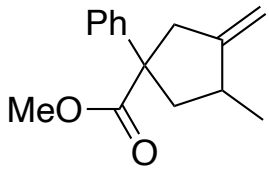

15′a: ^{1}H NMR ($CDCl_3$, 600 MHz): Diastereomer **A**. δ 1.13 (d, $^3J_{HH}$ = 6.6 Hz, 3 H, CH*Me*), 1.51 (m, 1 H, C*H*$_2$CHMe), 2.35 (m, 1 H, C*H*$_2$CHMe), 2.70 (m, 1 H, C*H*$_2$CCH$_2$), 2.76 (m, 1 H, C*H*Me), 3.29 (m, 1 H, C*H*$_2$CCH$_2$), 3.61 (s, 3 H, CO*Me*), 4.84 (s, 1 H, CC*H*$_2$), 4.96 (s, 1 H, CC*H*$_2$). 7.19-7.34 (m, 5 H, C$_6$*H*$_5$C), Diastereomer **B**. δ 1.10 (d, $^3J_{HH}$ = 6.6 Hz, 3 H, CH*Me*), 2.16 (m, 1 H, C*H*$_2$CHMe), 2.43 (m, 1 H, C*H*$_2$CHMe), 2.73 (m, 1 H, C*H*Me), 3.54 (m, 1 H, C*H*$_2$CCH$_2$),), 3.62 (s, 3 H, COC*H*$_3$), 4.82 (s, 1 H, CC*H*$_2$), 5.00 (s, 1 H, CC*H*$_2$). 7.19-7.34 (m, 5 H, C$_6$*H*$_5$C),

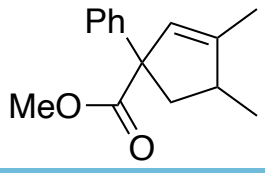

15′b: ^{1}H NMR ($CDCl_3$, 600 MHz): Diastereomer **A**. δ 0.98 (d, $^3J_{HH}$ = 7.2 Hz, 3 H, CH*Me*), 1.64 (s, 3 H, CHC*Me*), 2.48 (m, 1 H, C*H*$_2$CHMe),

2.84 (m, 1 H, C*H*Me), 2.57 (m, 1 H, C*H*Me), 3.22 (m, 1 H, CH_2CHMe), 3.65 (s, 3 H, CO*Me*) 5.66 (s, 1 H, C*H*CMe), 7.19-7.34 (m, 5 H, C_6H_5C). Diastereomer **B**. δ 1.06 (d, $^3J_{HH}$ = 7.2 Hz, 3 H, CH*Me*), 1.78 (s, 1 H, CHC*Me*), 2.48 (m, 1 H, CH_2CHMe), 2.84 (m, 1 H, C*H*Me), 2.57 (m, 1 H, C*H*Me), 3.22 (m, 1 H, CH_2CHMe), 3.63 (s, 3 H, CO*Me*), 5.69 (s, 1 H, C*H*CMe), 7.19-7.34 (m, 5 H, C_6H_5C). ESI-HRMS (*m/z*): $[M]^+$ calcd for $C_{15}H_{19}O_2$, 231.1385, found 231.1380.

(16′). yield 95 % (1.86 g, 9.5 mmol), ethylacetate : hexane = 20 : 80 (R_f = 0.30)

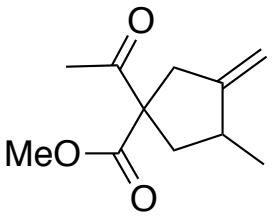

16′a: ^{1}H NMR ($CDCl_3$, 400 MHz): Diastereomer **A**. δ 1.12 (d, $^3J_{HH}$ = 6.4 Hz, 3 H, CH*Me*), 1.64 (m, 1 H, CH_2CHMe), 2.17 (s, 3 H, COO*Me*), 2.52 (m, 3 H, CH_2CHMe, C*H*Me, CH_2CCH$_2$), 2.92 (m, 1 H, CH_2CCH$_2$), 3.75 (s, 3 H, CO*Me*), 4.92 (br, 2 H, CCH_2); ^{13}C{^{1}H} NMR ($CDCl_3$, 150 MHz): δ 17.75, 26.55, 27.44, 38.95, 41.14, 52.76, 64.95, 105.57, 153.21, 173.31, 203.61. Diastereomer **B**. δ 1.10 (d, $^3J_{HH}$ = 6.4 Hz, 3 H, CH*Me*), 1.77 (m, 1 H, CH_2CHMe), 2.20 (s, 3 H, COO*Me*), 2.80 (m, 3 H, CH_2CHMe, C*H*Me, CH_2CCH$_2$), 2.92 (m, 1 H, CH_2CCH$_2$), 3.78 (s, 3 H, CO*Me*), 4.80 (m, 2 H, CCH_2); ^{13}C{^{1}H} NMR ($CDCl_3$, 150 MHz): δ 17.91, 26.02, 37.09, 39.07, 40.75, 52.68, 64.24, 105.51, 153.17, 173.9, 203.61.

(17′). yield 95 % (1.36 g, 9.8 mmol), ethylacetate : hexane = 25 : 75 (R_f = 0.26)

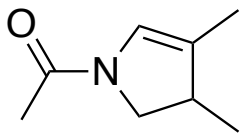

17′b: ^{1}H NMR ($CDCl_3$, 400 MHz): Rotamer **A**. δ 1.11 (d, $^3J_{HH}$ = 7 Hz, 3 H, CH*Me*), 1.73 (s, 3 H, CHC*Me*), 2.10 (s, 3 H, CH_3CON), 2.86 (m, 1 H, C*H*Me), 3.42 (m, 1 H, CH_2CHMe), 4.05 (m, 1 H, CH_2CHMe), δ 6.12 (s, C*H*CMe); ^{13}C{^{1}H} NMR ($CDCl_3$, 150 MHz): δ 11.73, 18.77, 21.56, 38.87, 53.05, 123.66, 126.91,

165.43. Rotamer **B**. δ 1.15 (d, $^{3}J_{HH}$ = 7 Hz, 3 H, CH*Me*), 1.71 (s, 3 H, CHC*Me*), 2.03 (s, 3 H, CH_3CON), 2.97 (m, 1 H, C*H*Me), 3.34 (m, 1 H, CH_2CHMe), 4.05 (m, 1 H, CH_2CHMe), δ 6.67 (s, C*H*CMe); ^{13}C{^{1}H} NMR ($CDCl_3$, 150 MHz): δ 10.90, 17.31, 21.86, 40.62, 54.73, 122.07, 125.86, 165.02.

Additional Information

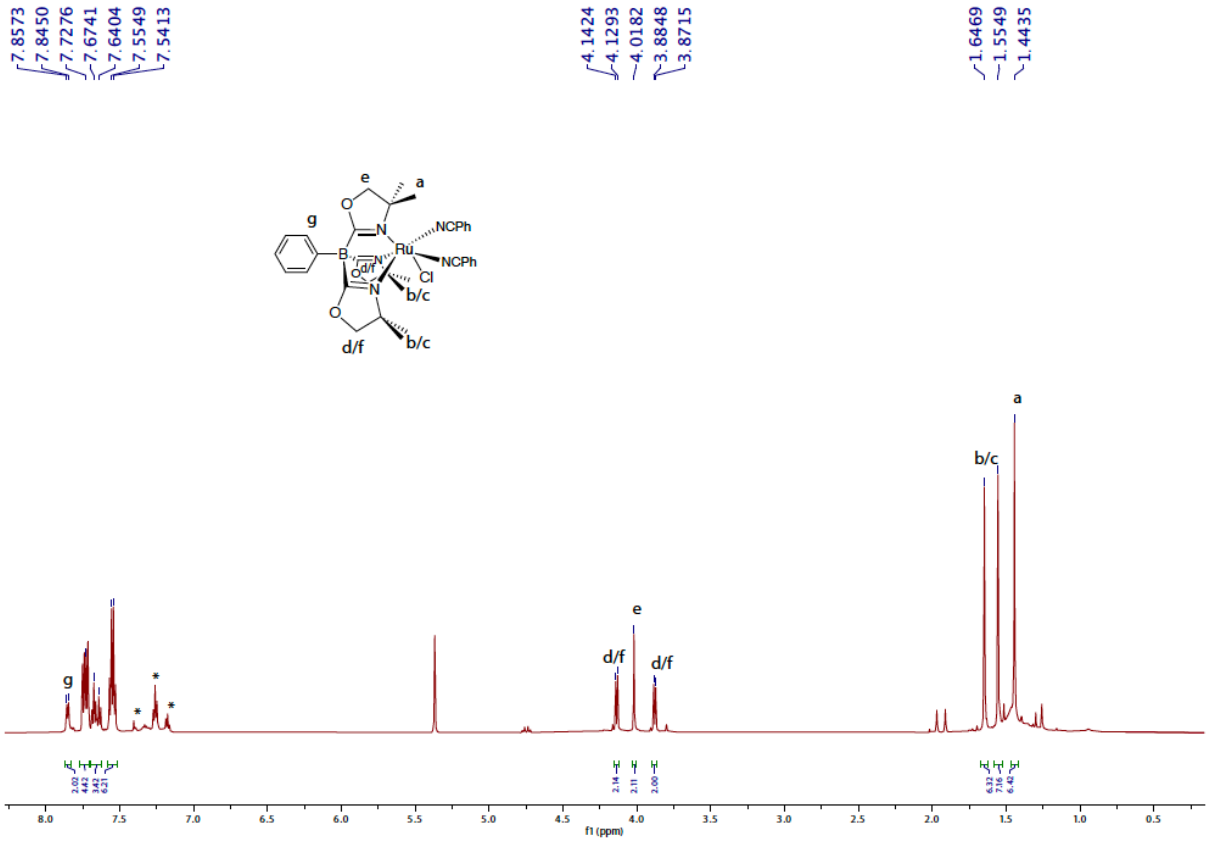

Figure 4-3. ^{1}H NMR spectrum of To^{M}RuCl(NCPh)$_2$ (4) in methylene chloride-d_2.

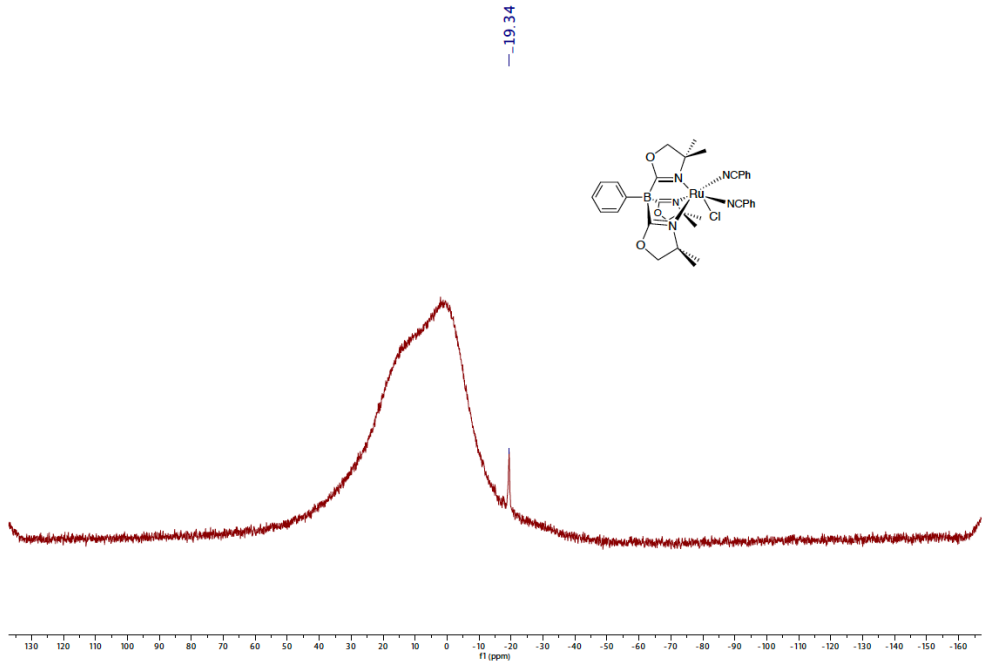

Figure 4-4. ^{11}B NMR spectrum To^{M}RuCl(NCPh)$_2$ (**4**) in methylene chloride-d_2.

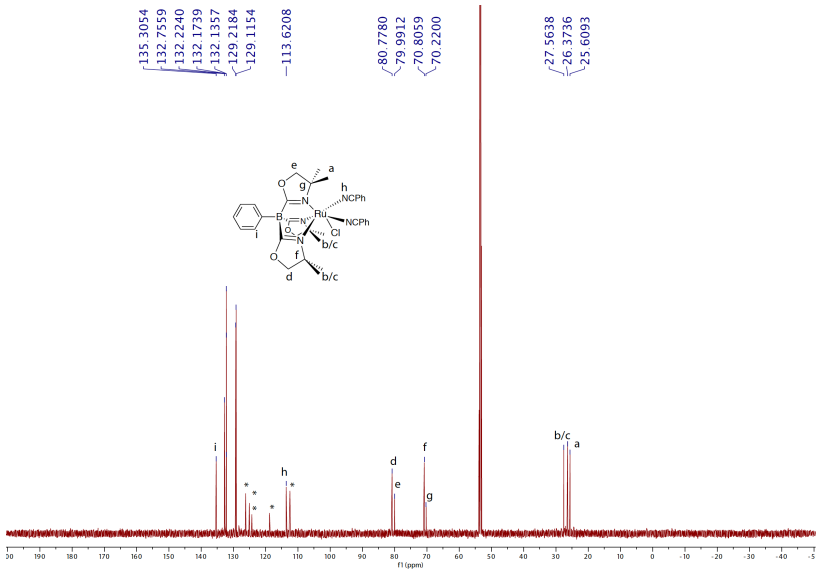

Figure 4-5. ^{13}C{^{1}H} NMR spectrum To^{M}RuCl(NCPh)$_2$ (**4**) in methylene chloride-d_2.

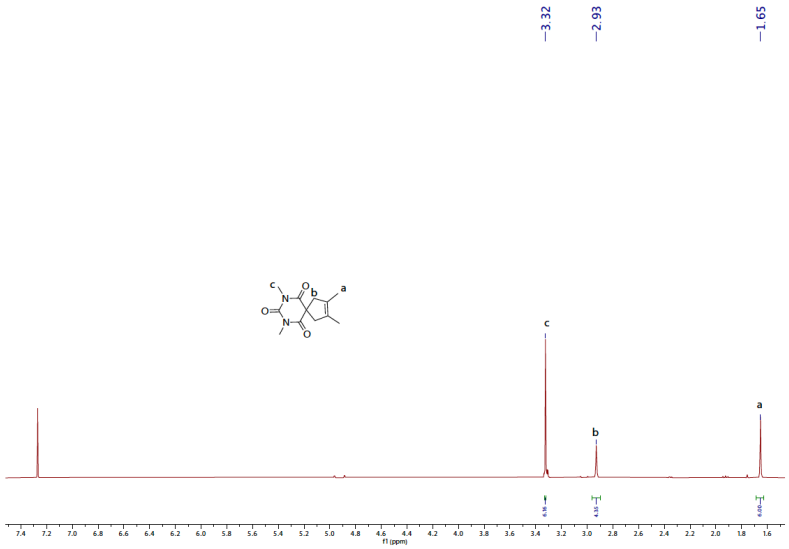

Figure 4-6. ^{1}H NMR spectrum of product **11′c** in $CDCl_3$.

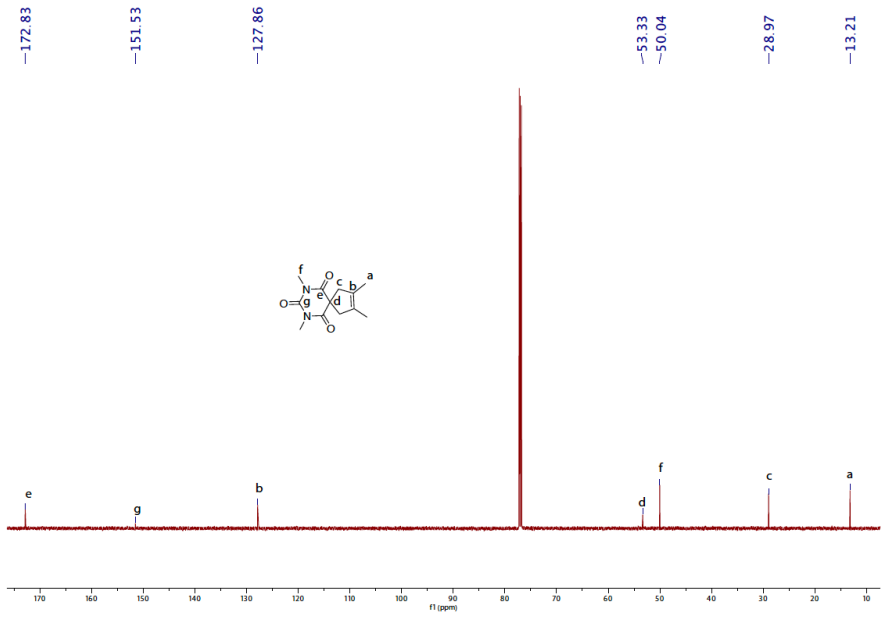

Figure 4-7. $^{13}C\{^{1}H\}$ NMR spectrum of product **11′c** in $CDCl_3$.

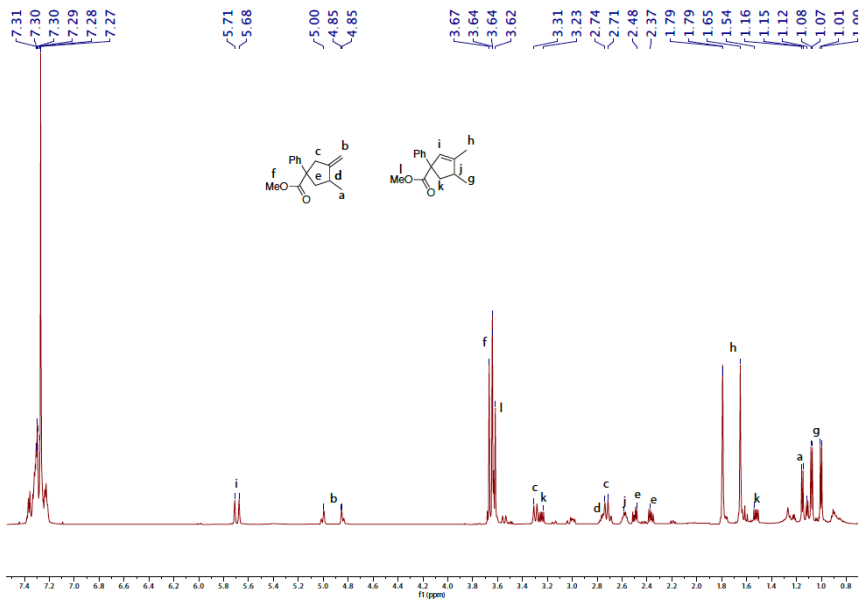

Figure 4-8. ^{1}H NMR spectrum of product **15′a** and **15′b** in $CDCl_3$.

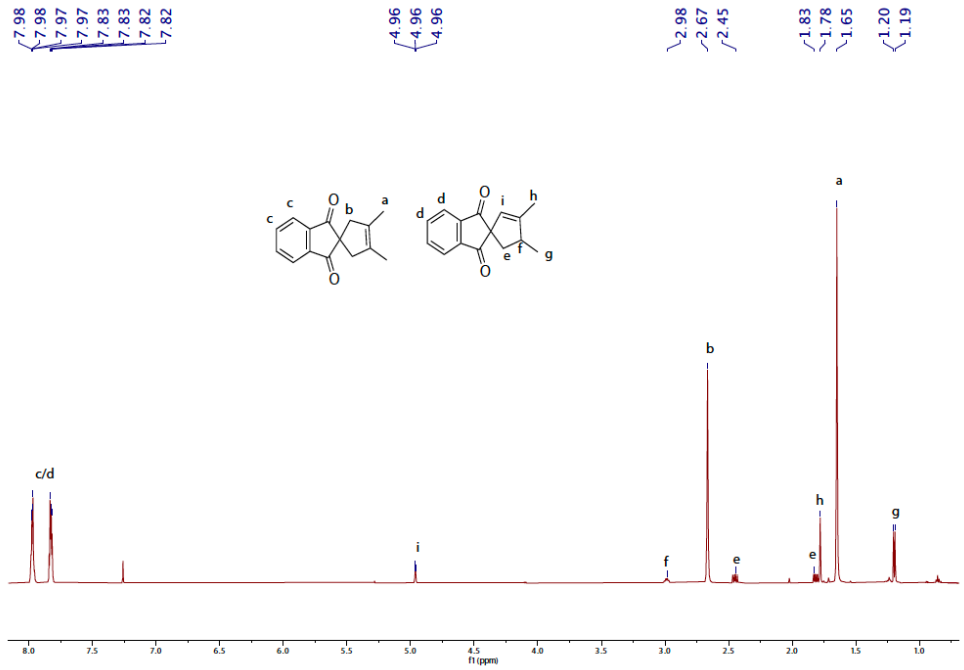

Figure 4-9. ^{1}H NMR spectrum of product **12′b** and **12′c** in $CDCl_3$.

References

1. Fráter, G.; Schröder, F., Cyclization of 1,5-Dienes: An Efficient Synthesis of β-Georgywood. *The Journal of Organic Chemistry* **2007,** *72* (4), 1112-1120.

2. Molander, G. A.; Hoberg, J. O., Organoyttrium-catalyzed cyclization of substituted 1,5- and 1,6-dienes. *Journal of the American Chemical Society* **1992,** *114* (8), 3123-3125.

3. Yamada, C.; Pahk, M. J.; Liu, R. S. H., Photosensitized cyclization reaction of 2-phenylhexa-1,5-diene. *Journal of the Chemical Society D: Chemical Communications* **1970,** (14), 882-882.

4. Adrian, J.; Gross, L. J.; Stark, C. B. W., The direct oxidative diene cyclization and related reactions in natural product synthesis. *Beilstein Journal of Organic Chemistry* **2016,** *12*, 2104-2123.

5. Muraoka, T.; Matsuda, I.; Itoh, K., Rhodium-Catalyzed Silylative Cyclization of 1,6-Heptadiyne Derivatives: A Versatile Route for the Synthesis of a 1,2-Dialkylidenecyclopentane Skeleton. *Organometallics* **2002,** *21* (17), 3650-3660.

6. Hong, F.-L.; Wang, Z.-S.; Wei, D.-D.; Zhai, T.-Y.; Deng, G.-C.; Lu, X.; Liu, R.-S.; Ye, L.-W., Generation of Donor/Donor Copper Carbenes through Copper-Catalyzed Diyne Cyclization: Enantioselective and Divergent Synthesis of Chiral Polycyclic Pyrroles. *Journal of the American Chemical Society* **2019,** *141* (42), 16961-16970.

7. Qian, D.; Hu, H.; Liu, F.; Tang, B.; Ye, W.; Wang, Y.; Zhang, J., Gold(I)-Catalyzed Highly Diastereo- and Enantioselective Alkyne Oxidation/Cyclopropanation of 1,6-Enynes. *Angewandte Chemie International Edition* **2014,** *53* (50), 13751-13755.

8. Abrams, J. N.; Zhao, Q.; Ghiviriga, I.; Minaruzzaman, Palladium(II)-catalyzed enyne cyclization strategies toward the podophyllotoxin ring system. *Tetrahedron* **2012,** *68* (2), 423-428.

9. Ma, S.; Yu, S.; Gu, Z., Gold-Catalyzed Cyclization of Enynes. *Angewandte Chemie International Edition* **2006,** *45* (2), 200-203.

10. Teng, Q.; Thirupathi, N.; Tung, C.-H.; Xu, Z., Hydroalkynylative cyclization of 1,6-enynes with terminal alkynes. *Chemical Science* **2019,** *10* (28), 6863-6867.

11. Ojima, I.; Tzamarioudaki, M.; Li, Z.; Donovan, R. J., Transition Metal-Catalyzed Carbocyclizations in Organic Synthesis. *Chemical Reviews* **1996,** *96* (2), 635-662.

12. Sato, F.; Urabe, H.; Okamoto, S., Synthesis of Organotitanium Complexes from Alkenes and Alkynes and Their Synthetic Applications. *Chemical Reviews* **2000,** *100* (8), 2835-2886.

13. Ma, K.; Martin, B. S.; Yin, X.; Dai, M., Natural product syntheses via carbonylative cyclizations. *Natural Product Reports* **2019,** *36* (1), 174-219.
14. Sow, B.; Bellavance, G.; Barabé, F.; Barriault, L., One-pot Diels–Alder cycloaddition/gold(I)-catalyzed 6-endo-dig cyclization for the synthesis of the complex bicyclo[3.3.1]alkenone framework. *Beilstein Journal of Organic Chemistry* **2011,** *7*, 1007-1013.

15. Zhang, Z.; Zhu, G.; Tong, X.; Wang, F.; Xie, X.; Wang, J.; Jiang, L., Transition Metal-Catalyzed Intramolecular Enyne Cyclization Reaction. *Current Organic Chemistry* **2006,** *10* (12), 1457-1478.

16. Aubert, C.; Buisine, O.; Malacria, M., The Behavior of 1,n-Enynes in the Presence of Transition Metals. *Chemical Reviews* **2002,** *102* (3), 813-834.

17. RajanBabu, T. V., Asymmetric Hydrovinylation Reaction. *Chemical Reviews* **2003,** *103* (8), 2845-2860.

18. Hu, Y.; Bai, M.; Yang, Y.; Zhou, Q., Metal-catalyzed enyne cycloisomerization in natural product total synthesis. *Organic Chemistry Frontiers* **2017,** *4* (11), 2256-2275.

19. Lee, Y.-C.; Kumar, K., Gold(I) Catalyzed Enyne Cycloisomerization – A Roadmap to Privileged Heterocyclic Scaffolds. *Israel Journal of Chemistry* **2018,** *58* (5), 531-556.

20. Molander, G. A.; Nichols, P. J., Organoyttrium-Catalyzed Sequential Cyclization/Silylation Reactions of 1,5-Dienes and 1,6-Dienes. *Journal of the American Chemical Society* **1995,** *117* (15), 4415-4416.

21. Radetich, B.; RajanBabu, T. V., Catalyzed Cyclization of α,ω-Dienes: A Versatile Protocol for the Synthesis of Functionalized Carbocyclic and Heterocyclic Compounds. *Journal of the American Chemical Society* **1998,** *120* (31), 8007-8008.

22. Yamamoto, Y., Transition-Metal-Catalyzed Cycloisomerizations of α,ω-Dienes. *Chemical Reviews* **2012,** *112* (8), 4736-4769.

23. Trost, B. M.; Lautens, M.; Chan, C.; Jebaratnam, D. J.; Mueller, T., Annulation via alkylation-Alder ene cyclizations. Palladium-catalyzed cycloisomerization of 1,6-enynes. *Journal of the American Chemical Society* **1991,** *113* (2), 636-644.

24. Bogdanović, B.; Henc, B.; Karmann, H.-G.; Nüssel, H.-G.; Walter, D.; Wilke, G., Olefin Transformations Catalyzed by Organonickel Compounds. *Industrial & Engineering Chemistry* **1970,** *62* (12), 34-44.

25. Bogdanovlć, B.; Stone, F. G. A.; West, R., Selectivity Control in Nickel-Catalyzed Olefin Oligomerization. In *Advances in Organometallic Chemistry*, Academic Press: 1979; Vol. 17, pp 105-140.

26. Grigg, R.; Malone, J. F.; Mitchell, T. R. B.; Ramasubbu, A.; Scott, R. M., Palladium- and rhodium-catalysed cyclisation of 1,6-, 1,7- and 1,8-dienes to cyclopentenes and

methylenecyclopentenes. Crystal structure of dichloro(4,4-diacetylhepta-1,6-diene)platinum(II). *Journal of the Chemical Society, Perkin Transactions 1* **1984,** (0), 1745-1754.

27. Böing, C.; Hahne, J.; Franciò, G.; Leitner, W., Stereoselective Nickel-Catalyzed Cycloisomerization of 1,6-Dienes. *Advanced Synthesis & Catalysis* **2008,** *350* (7-8), 1073-1080.

28. Diez-Holz, C. J.; Böing, C.; Franciò, G.; Hölscher, M.; Leitner, W., Phosphoramidite quinaphos-Type Ligands for Highly Selective Ni-Catalysed Asymmetric C–C Bond Forming Reactions. *European Journal of Organic Chemistry* **2007,** *2007* (18), 2995-3002.

29. Çetinkaya, B.; Demir, S.; Özdemir, I.; Toupet, L.; Sémeril, D.; Bruneau, C.; Dixneuf, P. H., η6-Mesityl,η1-Imidazolinylidene–Carbene–Ruthenium(II) Complexes: Catalytic Activity of their Allenylidene Derivatives in Alkene Metathesis and Cycloisomerization Reactions. *Chemistry – A European Journal* **2003,** *9* (10), 2323-2330.

30. Terada, Y.; Arisawa, M.; Nishida, A., Cycloisomerization Promoted by the Combination of a Ruthenium–Carbene Catalyst and Trimethylsilyl Vinyl Ether, and its Application in The Synthesis of Heterocyclic Compounds: 3-Methylene-2,3-dihydroindoles and 3-Methylene-2,3-dihydrobenzofurans. *Angewandte Chemie International Edition* **2004,** *43* (31), 4063-4067.

31. Yamamoto, Y.; Nakagai, Y.-i.; Ohkoshi, N.; Itoh, K., Ruthenium(II)-Catalyzed Isomer-Selective Cyclization of 1,6-Dienes Leading to exo-Methylenecyclopentanes: Unprecedented Cycloisomerization Mechanism Involving Ruthenacyclopentane(hydrido) Intermediate. *Journal of the American Chemical Society* **2001,** *123* (26), 6372-6380.

32. Fairlamb, I. J. S.; McGlacken, G. P.; Weissberger, F., Ruthenium(ii)-catalysed cycloisomerization of 1,6-dienes by focused microwave dielectric heating: improved rates and selectivities leading to exo-methylenecyclopentanes. *Chemical Communications* **2006,** (9), 988-990.

33. Kang, S.-K.; Ko, B.-S.; Lee, D.-M., Ru-Catalyzed cycloisomerization of δ-enallenes to form cyclic 1,3-dienes or 1,4-dienes. *Tetrahedron Letters* **2002,** *43* (38), 6693-6696.

34. Okamoto, S.; Livinghouse, T., Titanium(IV) Aryloxide Catalyzed Cyclization Reactions of 1,6- and 1,7-Dienes. *Journal of the American Chemical Society* **2000,** *122* (6), 1223-1224.

35. Okamoto, S.; Livinghouse, T., Titanium-Catalyzed Cycloisomerization of 1,6-Dienes. Regio- and Stereoselective Synthesis of exo-Methylenecycloalkanes. *Organometallics* **2000,** *19* (8), 1449-1451.

36. Yue, C. J.; Liu, Y.; He, R., Olefins isomerization by hydride-complexes of ruthenium. *Journal of Molecular Catalysis A: Chemical* **2006,** *259* (1), 17-23.

37. Leigh, G. J.; Sanders, J. R.; Hitchcock, P. B.; Fernandes, J. S.; Togrou, M., The use of trimethylsilyl iodide as a synthon in coordination chemistry. *Inorganica Chimica Acta* **2002,** *330* (1), 197-212.

38. Johnson, B. F. G.; Lewis, J.; Ryder, I. E., Some reactions of co-ordinated cycloheptatriene and cyclo-octa-1,5-diene in ruthenium (d6) complexes. *Journal of the Chemical Society, Dalton Transactions* **1977,** (7), 719-724.

39. Ho, H.-A.; Dunne, J. F.; Ellern, A.; Sadow, A. D., Reactions of Tris(oxazolinyl)phenylborato Rhodium(I) with C−X (X = Cl, Br, OTf) Bonds: Stereoselective Intermolecular Oxidative Addition. *Organometallics* **2010,** *29* (18), 4105-4114.

40. Yamamoto, Y.; Nakagai, Y.-i.; Itoh, K., Ruthenium-Catalyzed One-Pot Double Allylation/Cycloisomerization of 1,3-Dicarbonyl Compounds Leading to exo-Methylenecyclopentanes. *Chemistry – A European Journal* **2004,** *10* (1), 231-236.

41. Senthilkumar, S.; Thangapriya, C.; Alagumurugayee, R.; Kumarraja, M., MMZNiY-Catalyzed Tsuji–Trost Type of Reaction: A Selective Mono/Bis Allylation of Dicarbonyl Compounds. *Catalysis Letters* **2017,** *147* (11), 2755-2763.

42. Kimura, M.; Mukai, R.; Tanigawa, N.; Tanaka, S.; Tamaru, Y., Triethylborane as an efficient promoter for palladium-catalyzed allylation of active methylene compounds with allyl alcohols. *Tetrahedron* **2003,** *59* (39), 7767-7777.

43. Vasil'ev, A. A.; Kuchurov, I. V.; Zlotin, S. G., Tsuji–Trost allylation of CH acids in supercritical carbon dioxide: advantages and problems. *Mendeleev Communications* **2013,** *23* (2), 84-85.

44. Manick, A.-D.; Berhal, F.; Prestat, G., Development of a One-Pot Four C–C Bond-Forming Sequence Based on Palladium/Ruthenium Tandem Catalysis. *Organic Letters* **2018,** *20* (1), 194-197.

45. Thaharn, W.; Soorukram, D.; Kuhakarn, C.; Reutrakul, V.; Pohmakotr, M., Synthesis of C2-Symmetric gem-Difluoromethylenated Angular Triquinanes. *The Journal of Organic Chemistry* **2018,** *83* (1), 388-402.

46. Ribierre, J.-C.; Zhao, L.; Inoue, M.; Schwartz, P.-O.; Kim, J.-H.; Yoshida, K.; Sandanayaka, A. S. D.; Nakanotani, H.; Mager, L.; Méry, S.; Adachi, C., Low threshold amplified spontaneous emission and ambipolar charge transport in non-volatile liquid fluorene derivatives. *Chemical Communications* **2016,** *52* (15), 3103-3106.

47. Nečas, D.; Turský, M.; Kotora, M., Catalytic Deallylation of Allyl- and Diallylmalonates. *Journal of the American Chemical Society* **2004,** *126* (33), 10222-10223.

48. Zieliński, G. K.; Majtczak, J.; Gutowski, M.; Grela, K., A Selective and Functional Group-Tolerant Ruthenium-Catalyzed Olefin Metathesis/Transfer Hydrogenation Tandem Sequence Using Formic Acid as Hydrogen Source. *The Journal of Organic Chemistry* **2018,** *83* (5), 2542-2553.

49. Liu, J.; Mu, X.; Yang, Y.; Chen, F.; Wang, J.; Li, Y.; Wang, B., Construct 3D Pd@MoS_2-conjugated polypyrrole framworks Heterojunction with unprecedented photocatalytic activity for Tsuji-Trost reaction under visible light. *Applied Catalysis B: Environmental* **2019,** *244*, 356-366.

50. Autenrieth, B.; Frey, W.; Buchmeiser, M. R., A Dicationic Ruthenium Alkylidene Complex for Continuous Biphasic Metathesis Using Monolith-Supported Ionic Liquids. *Chemistry – A European Journal* **2012,** *18* (44), 14069-14078.

51. Ramesh, R.; Reddy, D. S., Zinc mediated allylations of chlorosilanes promoted by ultrasound: Synthesis of novel constrained sila amino acids. *Organic & Biomolecular Chemistry* **2014,** *12* (24), 4093-4097.

52. O'Brien, R. A.; West, C. W.; Hollingsworth, B. E.; Stenson, A. C.; Henderson, C. B.; Mirjafari, A.; Mobarrez, N.; West, K. N.; Mattson, K. M.; Salter, E. A.; Wierzbicki, A.; Davis, J. H., A simple and rapid route to novel tetra(4-thiaalkyl)ammonium bromides. *RSC Advances* **2013,** *3* (46), 24612-24617.

53. Nečas, D.; Turský, M.; Tišlerová, I.; Kotora, M., Nickel-catalyzed cyclization of α,ω-dienes: formation vs. cleavage of C–C bonds. *New Journal of Chemistry* **2006,** *30* (5), 671-674.

54. Feng, L.; Gan, Z.; Nie, X.; Sun, P.; Bao, J., Highly regioselective synthesis of N-acyl-2,3-dihydropyrrole or N-sulfonyl-2,3-dihydropyrrole derivatives by nano-palladium catalyzed cycloisomerization of 1,6-dienes. *Catalysis Communications* **2010,** *11* (6), 555-559.

55. Kwiatkowski, M. R.; Alexanian, E. J., Nickel-Catalyzed Mizoroki–Heck-Type Reactions of Unactivated Alkyl Bromides. *Angewandte Chemie International Edition* **2018,** *57* (51), 16857-16860.

CHAPTER 5. CONCLUSION

General conclusion

Photochemical oxidative addition of Si–H to metal carbonyl complexes follows a standard pathway involving a CO dissociation to create an empty reactive side on the metal center. In contrast, our study shows that under thermal condition (in presence of a strong donor ligand) rhodium dicarbonyl compound undergoes oxidative addition of the Si–H bond followed by CO dissociation. Also, the presence different substituent on Si affects the rate of oxidative addition as aromatic silanes reacts significantly faster compared to aliphatic silane.

Functionalized silica materials are powerful tools for different chemical, semiconductor, and medical industries. Successful surface modification via ruthenium-catalyzed dehydrocoupling with primary and secondary silanes produced a new functionalized silica material containing chemically active Si–H bonds. Also, utilization of the surface Si–H bonds in dehydrocoupling reactions with external amines produced a unique surface silazane material containing Si–O–Si–N bonding.

Finally, the ruthenium tris(oxazolinyl)borato complex showed excellent catalytic activity for cycloisomerization of 1,6-heptadienes with moderate selectivity towards *exo*-methylene isomer. Further, a significant solvent towards product selectivity is also observed.